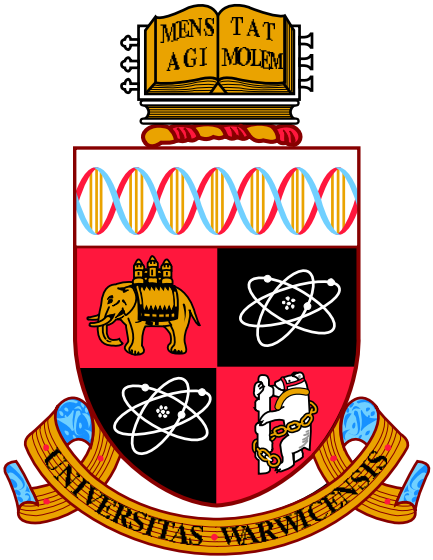

Chemical and biological approaches to enhance the bacteriophage as a probe in molecular recognition

Daniela P. Lobo

A thesis submitted to the University of Warwick for the degree of Doctor of Philosophy

Department of Chemistry

August 2017

Contents

List of figures

List of tables

List of abbreviations

Ab antibody

ABTS 2,2'-Azinobis (3-ethylbenzothiazoline-6-sulfonic acid)-diammonium

AF647 Alexa Fluor 647 dye

BSA bovine serum albumin

CD circular dichroism

DAPI 4',6-diamidino-2-phenyindole

DIT digital integration time

DLS dynamic light scattering

DMSO dimethyl sulfoxide

DNA deoxyribonucleic acid

DTNB 5,5-dithio-bis-(2-nitrobenzoic acid)

DTT dithiothreitol

EDTA ethylenediaminetetraacetic acid

ELISA enzyme-linked immunosorbent assay

Fab fragment antigen-binding

Fc fragment crystallisable region

FDLD fluorescence detected linear dichroism

FITC fluorescein isothiocyanate

GEnCs glomerular endothelial cells

HRP horseradish peroxidase

HUVEC human umbilical vein endothelial cell

IPTG isopropyl β-D-1-thiogalactopyranoside

kb kilobase (pair)

kDa kilodalton

LB lysogeny broth

LD linear dichroism

LED light emitting diode

M13 M13 bacteriophage

MALDI-TOF matrix-assisted laser desorption/ionisation time-of-flight

MDCC 7-Diethylamino-3-((((2-maleimidyl)ethyl)amino)carbonyl)coumarin

MWCO molecular weight cutoff

NHS-CBA 4-formyl succinimidyl benzoate

OD optical density

p3 p3 protein, minor coat protein of filamentous phage

p8 p8 protein, major coat protein of the filamentous phage

PBS phosphate buffer saline

PCR polymerase chain reaction

PEDOT poly(3,4-ethylenedioxythiophene)

PEG polyethylene glycol

PFU plaque forming units

PIV particle image velocimetry

p-NBA 4-nitrobenzaldehyde

PVDF polyvinylidene difluoride

ROI region of interest

RNA ribonucleic acid

SANH succinimidyl 6-hydrazinonicotinamide acetone hydrazine

SATA N-succinimidyl S-acetylthioacetate

SDS-PAGE sodium dodecyl sulfate polyacrylamide gel electrophoresis

SEC size exclusion chromatography

SERS surface-enhanced Raman spectroscopy

SMCC succinimidyl 4-(N-maleimidomethyl)cyclohexane-1-carboxylate

TCEP tris-(2-carboxyethyl)phosphine

TEM transmission electron microscopy

THAP trihydroxyacetophenone

TRITC tetramethylrhodamine isothiocyanate

UV ultraviolet

WGA wheat germ agglutinin

WSS wall shear stress

WT wild-type

X-gal 5-bromo-4-chloro-3-indoyl-β-D-galactopyranoside

Acknowledgements

I would like to thank my supervisors Professor Alison Rodger, Professor Timothy Dafforn and Dr. Matthew Hicks. Alison not only helped me establish the collaborations necessary to explore the areas of research we were interest on, she also allowed me to do so on areas outside the experience of her lab. Also, I am very thankful for her approach to academic life – it didn't seem to matter how busy she was, Alison always made time for her students. Tim's contagious enthusiasm constantly encouraged open discussions of new ideas and future directions, providing me with a fresh take on science every time we met. Matt always made time to discuss ideas, while sketching complex experiment designs at a coffee table. His experienced advise and thoughtful criticism was, without a doubt, essential for this work. I am grateful I had the opportunity to do a secondment at Linear Diagnostics, which gave me some level of understanding on working outside academia.

I would like to acknowledge the members of the Rodger's lab, particularly Dr. Alan Wemyss, Dr. Claire Broughton, Dr. Nikola Chmel, for the insightful exchange of ideas and helpful discussions. I would like to thank Dr. Anne Straube at University of Warwick, for her patience on the long hours attaining imaging data and help setting up experiments. I would like to thank members of the Dafforn's lab, especially Dr. Haydn Little from University of Birmingham, who was the first person to introduce me to the bacteriophage and so often helped me tackle the challenges it presented. Also, former and current Linear Diagnostics' research technicians, Rachael Lloyd and Lorea Orueta, for their guidance and practical help around the lab. Finally, I would like to thank C10 and Professor David Roper, at School of Life Sciences, for providing a link to a biological laboratory and facilitating space for part of this work.

This work would have not been possible without all the collaborations set up along the way, across different universities. My brief visit to University College London hosted by Professor John Ward and his student, Henry Malmanche, gave me an entirely different take on bacteriophage research. The experiments on wall shear stress were a constant search for resources, which involved work at University of Warwick, Birmingham, Bristol and Nottingham. Dr. Kenton Arkill, so full of brilliant ideas, showed me how physics and biology can work together. I am grateful he always tried to convert complex physics concepts into a more approachable language. I would also like to thank Professor David Bates and his group at University of Nottingham, especially to Dr. Maria Machado and Dr. Andrew Benest, for providing both material support and thoughtful discussions concerning this work. Professor Jennifer Cha, at University of Colorado Boulder, kindly opened the doors to her lab, where I worked alongside Dr. Michael Brasino and Dr. Dylan Domaille. This was an incredible experience, which allowed me to considerably expand my knowledge on chemical and genetic modifications to the bacteriophage.

I was lucky to have done my doctoral studies while being part of a cohort of 12 other Marie Curie fellows, from diverse backgrounds and cultures. I could have not asked for a greater group of people, for their scientific expertise and, most of all, for their friendship. I would like to especially thank Greg, for his seemly unlimited patience and encouragement.

Thank you to my parents, for always offering a loving place to recharge and reconnect despite the distance. Thank you for the gentle push, every single time, no matter how hard it was to part ways. This would not have been possible without you.

Declaration

This thesis is submitted to the University of Warwick for the degree of Doctor of Philosophy. Unless otherwise stated, the work presented was carried out by the author and it has not been submitted for any degree at this or any other University.

The content has not been previously published, except in the publication below:

- Lobo, D. *et al.* Direct detection and measurement of wall shear stress using a filamentous bionanoparticle. *Nano Res.* **8,** 3307–3315 (2015).

Summary

The aim of the work presented in this thesis was to explore the structural and molecular features of a filamentous bacteriophage for incorporation in biosensing platforms. To tune the bacteriophage surface as a scaffold for molecular recognition, chemical and biological protocols aimed at controlling and enhancing its intrinsic properties were developed. A key part of the work was aimed at anchoring bacteriophage particles by one-end to surfaces, and on labelling its viral capsid with dyes, antibodies and DNA molecules. The tolerance of the bacteriophage for modifications, as well its simplicity and robustness, makes it an attractive probe for biosensors. Furthermore, the filamentous structure of the bacteriophage was demonstrated to be a valuable feature in both microscopy- and spectroscopy-based biosensors. The ability of the bacteriophage to align under flow was considered as a simple, yet efficient approach for the detection of wall shear stress and pathogenic bacteria.

A novel method to detect wall shear stress (WSS) was developed by using a fluorescently decorated bacteriophage particle anchored by one-end to a surface. The response of this filamentous nanosensor to flow variations was tracked under a microscope, and gave valuable information on the shear flow of a fluid passing over a surface. Using a custom-made analysis tool and an algorithm, we were able to derive the wall shear stress on the point of attachment of the nanosensor, using endothelial cells as a model system. The proof-of-concept to this work highlighted how a simple bacteriophage construct can be use as a nanosensor for imaging and mapping flow.

Linear dichroism (LD) spectroscopy also explores the high aspect ratio of the filamentous bacteriophage. Linear Diagnostics Ltd., a startup company in Birmingham, exploits the natural LD properties of the bacteriophage and integrated it with a biosensing platform targeting pathogenic bacteria. The work reported in this thesis mainly focused on developing alternative approaches that could improve the biosensor sensitivity and simplicity, by modifying the bacteriophage scaffold, further demonstrating its versatility.

CHAPTER 1 – Introduction

1.1 Historical overview of bacteriophage research

The word "bacteriophage" means bacteria eater – bacteriophages, or simply phages, are a type of virus that infect bacteria. These ancient and diverse biological machines are one of the most abundant microbes in the biosphere and are ubiquitous in nature [1]. A large number of phage particles have been found in the sea, soil, and human gastrointestinal systems. For example, it has been reported that phages are the most abundant entity in seawater, exceeding the number of bacteria present by 5–25 fold [2,3]. Since their discovery, in the early decades of the twentieth century, phages have been of great interest to the scientific community as tool for the understanding of molecular biology and as powerful biomaterial.

During the World War I, the newly established hospital of the Institut Pasteur, an institution primarily dedicated to the study of infectious diseases, was investigating a devastating outbreak of dysentery in Paris [4]. The microbiological studies were assigned to Félix d'Hérelle, a biologist at the Institut, because of his interest in gastrointestinal diseases and experience on enteric bacteriology. By analysing stool samples from dysentery patients, d'Hérelle discovered "an invisible microbe antagonistic to the dysentery bacillus" [5]. He named this "invisible microbe" a bacteriophage, and, during his experiments, he established a correlation between the amount of bacteriophage in a stool sample and the stage of dysentery infection – bacteriophage titers peaked just as the patient started to recover. This led him to suspect that the bacteriophage has a biological protective role against the pathogenic bacteria, and therefore, the recovery of the patients might have been bacteriophage-mediated. D'Hérelle continued his studies on dysentery in humans, and carried identification and characterisation of the bacteria. While doing so, he discovered that something on these samples was causing lysis of the dysentery bacillus.

D'Hérelle, intrigued about this seemly antimicrobial substance, developed novel experimental protocols and devised theories to explain the nature of this material. His two-page paper, published in September 1917, described the necessary procedures to isolate the "invisible microbe" from stool samples of humans infected with dysentery bacillus. In a creative leap, d'Hérelle discovered that adding a few drops of the isolated "invisible microbe" to a fresh bacterial culture clears the culture solution, and that a few drops of this cleared culture has the same effect on another fresh bacterial culture. To d'Hérelle, this was evidence that the bacteriophage was destroying the bacteria [6].

D'Hérelle is commonly considered the father of bacteriophage research, and indeed he actively recognised the importance of this new biological entity. However, there is some controversy on who discovered it first [7]. Two years earlier (1915), independently from d'Hérelle's initial findings, a British microbiologist named Twort, documented a "patchy and glassy" dissolution on some bacterial cultures he was experimenting on. Twort published his observations on the "transmissible bacterial lysis" [8], similarly to d'Hérelle, but did not pursuit this line of investigation any further. Indeed, phage therapy (term referred to the use of phage to treat bacterial infectious) was an idea uniquely initiated by d'Hérelle. Moreover, his work was the seed to many of the future advancements in molecular biology.

Although d'Hérelle recognised the potential of the bacteriophage as an antibacterial agent, the basic ecology of the phage has poorly understood at the time, and the results obtained were conflicting and subjected to criticism. Phage therapy was later eclipsed by the discovery of effective antibiotics, such as penicillin. Recently however, phage therapy was been revived as a potential method to circumvent antimicrobial resistance. The Eliava Institute, in Georgia, is one of the major centres in bacteriophage research currently developing phage-based treatments for various bacterial pathogens. The main application of the Eliava phages is directed for the treatment of gastrointestinal, gynaecological, respiratory and dermatological problems. A different group of researchers, from

University of California, recently communicated that they have developed an intravenous phage cocktail that successfully treated a terminally-ill patient infected with a multi-drug resistant bacteria [9].

It was not until around the 1940s that scientists across laboratories began to understand the usefulness of the bacteriophage biology. The phage was recognised as an appropriate model for a number of experimental systems, leading to breakthrough discoveries in molecular biology. It started with a collaboration between Emory Ellis and Max Delbrück, responsible for the early findings on phage growth conditions [10]. Soon, several others merged with Ellis and Delbrück, forming the "phage group". The 40's and the 50's were the golden age for molecular biology, in large part due to the collaborative interactions between members of the "phage group". Until 1943, it was unknown that bacteria had genetic material. It was Delbrück and Salvador Luria who, in 1943, explained that bacterial resistance to phages (and antibiotics) are genetically inherited mutations, revealing that natural selection principles are applicable to bacteria [11]. It was also Luria who, in 1946, pioneered the concepts of genetic recombination and DNA repair, by discovering that phage can repair damages inflicted by UV irradiation [12]. James Watson, one of the Nobel Prize winners for the Watson-Crick DNA molecular structure, was in fact one of Luria's graduate students working at the time on phage genetic recombination. In 1952, a series of experiments from Alfred Hershey and Martha Chase supported previous and subsequent claims that it is the DNA, and not the proteins, that carry genetic information, by showing that the DNA of the phage enters the host bacterial cell [13]. Restriction enzymes, essential in genetic engineering, originated from studies on a phage system. The phenomenon was first identified in the early 1950's by Luria and Giuseppe Bertani, and further explored in the 1960's by Werner Arber and Matthew Meselson [14-17]. In 1954, François Jacob and Elie Wollman at Institut Pasteur established the relationship between prophage and the genetic material in bacterium. Building from that success, François Jacob, jointly with Jacques Monod and André Lwoff, proposed the concepts of messenger RNA, operons and regulator genes, developing the field

of transcriptional regulation [18-20]. In 1961, at the Cavendish Laboratory in Cambridge, Sydney Brenner, Francis Crick and others demonstrated the basic nature of the genetic code, unveiling its triplet nature, by using a phage gene [21].

Bacteriophages have laid the foundation for molecular biology, helping to understand the building blocks and the molecular basis of life itself. Molecular biology gave rise to the synthetic biology and biotechnology movement, which envisions integrating fundamental, but complex, biological concepts into simple designs, to address bioengineering challenges. As explored in section 1.3, the bacteriophage became preeminent as a programmable scaffold, originating unique biomaterials with multiple nanotechnology applications.

1.2 Bacteriophage classification

Bacteriophages are composed of nucleic acids (DNA or RNA) and a protein capsid, with diverse morphologies. Some are tailed with an isometric capsid, while others have a filamentous capsid and do not possess a tail. Colloquially, phages can be organised in three major categories, based on their life cycle and morphology [22-25]:

i) lytic or productive phages, such as T7, T4 and MS2 phages, which cause bacteria cell lysis and death upon release of the newly synthesised virion particles;

ii) temperate or lysogenic phages, such as λ phage, which can either multiply via a lytic cycle or by lysogeny, incorporating their genetic material into the bacterial genome and producing a latent state phage (prophage);

iii) filamentous phages, such as f1, fd and M13 phages, which are commonly considered lysogenic phages that do not lyse their host cells.

A more comprehensive and detailed classification is done by the International Committee on Taxonomy of Viruses (ICTV), which organises phages primarily based on the nature of their genomes – single or double stranded, circular or

linear, with varying sizes ranging from 5 kilobases to 725 kilobases [26,27]. As of 2017, there are 19 recognised families of bacteriophage. The *Myoviridae*, *Siphoviridae* and *Podoviridae* families are composed of double-stranded DNA tailed virions, and represent 96% of all identified bacteriophages [28]. The seven T phages (denoted T1-T7) belong to these families, and are complex and large biological assemblies, often used as a biotechnology tool. Indeed, most of the discoveries by the "phage group" derived from these phages. Phages from the *Microviridae* and *Inoviridae* families are composed of single-stranded circular DNA. The *Microviridae* have an icosahedral capsid, while the *Inoviridae* are filamentous. All the work presented in this thesis is done in phages from the *Inoviridae* family.

1.2.1 Filamentous bacteriophage

Over the past 50 years, the structure and life cycle of the filamentous phages has been extensively investigated, as reviewed here [29,30]. The interest in filamentous phages grew from recognising the potential of their unique structural and biological properties – it was noticed that filamentous phage could display peptides on their surface when their genome was modified. This technology, invented in the 80's by Smith and colleagues, was named phage display [31,32]. The link between genetic material and display of a functional protein allowed for the design of screening libraries platforms [33-36], currently widely used for studying protein-protein interactions.

Compared to tailed phages, whose DNA is over 200 kilobases long, filamentous phages are fairly simple structures. All filamentous phage strains have a similar structure and life cycle. They are composed of a few different proteins assembled into ordered arrays that encapsulate the viral genome, forming a long thread-shaped particle. Contrary to most tailed phages, which have on average a 50/50 ratio of protein and nucleic acid, filamentous phages have a higher proteic content with only 6–21% (by weight) of its components being from DNA [27]. The first discovered filamentous phage, f1, was isolated in the 1960's [37] and characterised as being part of the Ff phage class, which also includes the best-

studied M13 and fd phages. These phages, sharing a > 98% genome homology [38], are non-lytic and specific for the *Escherichia coli* conjugative F episome [39-42]. It was later discovered the existence of filamentous phages, If and Ike, that do not need the F pilus to infect the bacterial host [43,44]. The list of discovered filamentous phages keeps growing and it includes more than 60 different virions [45]. In this thesis, all experimental work will be carried on the M13 and fd phages.

The M13 and fd bacteriophages have similar architectures and biophysical properties – a thin and long cylindrical particle (Fig. 1.1) with a diameter of approximately 6 nm and length of 900 nm, encapsulating a 6407 nucleotides viral genome containing eleven protein-coding sequences [30]. Five of these are structural proteins; the remaining six proteins are fundamental for the life cycle of the phage, but are not present in the viral capsid. The viral capsid is made of 2700 copies of the major coat protein (p8) capped at both ends by 3-5 copies of each minor coat protein (p3 and p6; p7 and p9) (depending on the reference, these proteins can be denoted as gp8/gp3/gp6/gp7/gp9, or pVIII/pIII/pVI/pVII/pIX) [46-48]. Each p8 protein is a helical 50 amino acid long peptide, with the C-terminus interacting with the viral genome and the N-terminal end exposed to the surface. Neighbouring p8 subunits are connected by hydrophobic interactions, and packed in an approximately 20 ° orientation along the long axis. The p8 proteins assembly forms a hollow tube, which encloses the single-stranded circular DNA [49,50]. The p3 minor protein is the largest protein of the viral capsid – a 406 amino acid peptide – and it is responsible for the infectivity of the phage. It is composed of three domains, separated by glycine-rich linkers, which are involved in the binding of the phage to the bacteria surface [38,51-53]. Each p3 protein, containing cysteine residues, is stabilised by disulfide bridges [54,55].

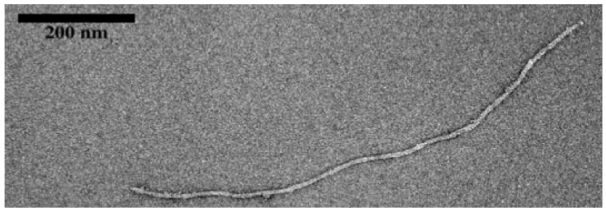

Figure 1.1: Transmission electron microscopy (TEM) image of a filamentous bacteriophage [56].

As mentioned above, phages from the Ff class can only infect *E. coli* bacteria that express the F pilus, essential for bacterial conjugation. Although filamentous phages are not lytic, they hijack the bacterial host machinery during their lifecycle [38]. The p3 protein binds to the F pilus, anchoring the phage particle closer to the bacterial cell surface. This binding promotes depolymerisation of the phage coat proteins, which gather in the bacterial inner membrane, and mediates the entry of the phage genomic material into the cytoplasm of the bacteria. The viral DNA is replicated and additional phage coat proteins are synthesised – the single-stranded viral DNA gets converted into an intermediate double-stranded template (termed RF, replicative form), and it is replicated by rolling-circle amplification. This produces several new strands of viral DNA that are then packed into new phage particles at the inner membrane. The p7 and p9 coat proteins start the extrusion of the phage particle from the bacteria through a phage-created pore, and in a screw-like motion, the phage is coated with p8 proteins along its length. The p3 and p6 terminate the assembled viral capsid, and the newly created phage progeny gets released from the *E. coli* cell to the surrounding environment, ready to attack a new host cell [38]. Typically, wild-type Ff filamentous phages lifecycles are very efficient, reaching titers of up to 10^{13} phage particles per mL of culture.

1.3 Filamentous phages and nanotechnology

In recent decades, multiple groups have taken advantage of the filamentous phages' structural, chemical and biological features for the development of nanotechnology platforms. Their i) stability to a wide range of pH values,

elevated temperatures, proteolytic enzymes, and non-aqueous media; ii) straightforward and cost-effective large-scale production; iii) tolerance for bioconjugation and surface chemistry manipulation; and iv) simple genetic tunability, enable the use of filamentous phages as a powerful scaffold with numerous applications [25,57-59].

Perhaps, filamentous phages are best known for their biological role on phage display, which has been summarised in several reviews [60-62] and books [24,63,64]. In essence, phage display consists of genetically inserting a random DNA sequence encoding for a peptide into the phage genome, resulting in the expression and display of the peptide onto the phage surface. After several biopanning rounds, a target-specific binding peptide will be identified and selected from screening a random library. Using this technique, several target-specific binding peptides have been discovered, which contributed for the development of vaccines and antibodies, and protein engineering [45,60,63]. Despite its irrefutable impact in modern biotechnology, the applications of filamentous bacteriophages go beyond phage display. The use of phages in bioassays has been reviewed before [25,65-68]; a brief overview with a few examples of phage-based materials integrated in biosensing platforms will be shown here.

1.3.1 Filamentous phage-based biosensors

In the era of personalised medicine, there is a clear demand for early diagnostic platforms, meaning there is a constant need for smarter, smaller, faster and inexpensive biosensors, which ideally provide both qualitative and quantitative information. Biosensors are analytical devices that integrate a biological sensing entity with sophisticated physicochemical transducers [69]. Escalating healthcare costs allied with consumers demand continuously catapults the biosensors market, further promoting the ever-increasing search for novel biomarkers, measuring techniques and molecular recognition elements. An essential element for any biosensing assay is the probe that binds to a target of interest. Traditionally, these probes are antibodies. However, functionalised filamentous

phage particles may be used as a substitute, by acting as molecular recognition elements in immunoassays sensing for a diverse class of analytes, from single molecules to whole cells [70]. The phage surface can be genetically programmed and chemically modified with functional molecules, such as peptide motifs [71], optical labels [72], antibodies [73], nanoparticles [74], and chemical coupling tags [75], and incorporated in conventional analytical methods, for example spectroscopy or enzyme-linked immunosorbent assay (ELISA). Commonly, functionalised phages can participate in biosensing platforms as biorecognition elements for target probing (section 1.3.1.1), or as structural templates for the controlled synthesis of nanostructures (section 1.3.1.2).

1.3.1.1 Phage as a biorecognition element

The phage anti-immunocomplex assay (PhAIA) [76,77] is an example of a modified ELISA method in which filamentous phages replace detection antibodies. Due to their size, small analyte molecules are generally precluded from non-competitive two-site sandwich immunoassays, which propelled the development of anti-immunocomplex antibodies [78-80]. However, these antibodies are difficult to produce, and often result in high cross-reactivity with the primary antibody [76]. PhAIA uses phage particles functionalised with an anti-analyte peptide fused to its p8 proteins, instead of anti-immunocomplex antibodies, to detect the formation of the analyte-antibody immunocomplex. A plate is coated with the immunocomplex (*i.e.* analyte molecules bound to anti-analyte antibodies) to which the peptide-functionalised phages are added. The peptide on the phage binds to the analyte-antibody immunocomplex, which can then be detected and visualised by using anti-phage/HRP-conjugated antibodies. The authors of the PhAIA work claim that the large surface area of the phage increases the overall sensitivity of the assay, as the phage can incorporate a larger number of labels compared to single antibodies on a regular ELISA [76]. PhAIA has been successfully employed to detect several small molecule pesticides, such as molinate [76,81], clomazone [82], phenoxybenzoic acid (PBA) [77,83,84], and brominated diphenyl ether 47 (BDE 47) [85], and properly integrated with

other analytical methods, for instance, polymerase chain reaction (PCR) [84], magneto-electrochemical immunoassay [81], and magnetic beads immunoassays [83].

Phage particles displaying target-binding motifs have also been used in biosensors for detection and imaging of cancer cells and associated biomarkers. Zhang and co-workers designed a peptide-functionalised phage particle capable of detecting metastatic cells. These modified phages were immobilised onto the surface of a light-addressable potentiometric sensor (LAPS) [86] chip, and were shown to detect and distinguish between metastatic and non-metastatic cells in a blood sample [87]. In another example, researchers at University of California, Berkeley engineered a phage displaying antibodies for epidermal growth factor receptor (EGFR), which was used as a probe in a NMR sensor [88] and as an imaging agent for flow cytometry [89], to detect EGFR-positive cancer cells. Ghosh *et al.* constructed a phage-templated magnetic nanoparticles engineered to display a peptide that targets a glycoprotein overexpressed in various cancers. This phage scaffold was used for *in vivo* imaging of cancer cells in mice [90]. To expand the versatility of phage-based probes in oncology, functionalised phages could be designed to simultaneously target and deliver an antineoplastic agent to tumor cells. To explore this dual modality, a group in MIT built an *in vitro* phage-based platform for targeting prostate cancer cells, as an imaging and drug delivery probe [91].

Detection and identification of food-borne pathogens is another emerging application of biosensors. Pacheco-Gomez *et al.* developed a simple immunoassay combining an engineered antibody-binding phage scaffold with linear dichroism (LD) spectroscopy, targeting the pathogenic *Escherichia coli* O157 [92]. This LD-based biosensor exploited the differences in the phage scaffold optical properties when *E. coli* cells were present in a sample, generating a spectroscopic measurable signal. Another common food-poisoning culprit, *Salmonella typhimurium,* is the target to phage-based magnetoelastic (ME) biosensors. Genetically engineered phages displaying *Salmonella*-binding

peptides were immobilised on the ME platform and tested on food samples, such as fresh tomatoes [93], spinach leaves [94], milk and apple juice [95]. The phage-based ME biosensors showed specificity for *Salmonella*, and were reported to be stable even when exposed to harsh environments [96]. In the near future, these low-cost, wireless phage-based ME screening devices could be used *in situ* and integrated at multiple points of the food supply chain to monitor for bacterial contamination.

1.3.1.2 Phage as a scaffolding element

As explored above, phages can serve as a biological template to display probes for target recognition. Moreover, the filamentous structure of these phage particles is a unique platform for controlled nanosynthesis and assembly [97,98]. The large surface area of the phage scaffold can generate amplified signals – the minor proteins (generally the 3–5 copies of p3 proteins) are involved in antigen-binding, while the whole structure of the phage (the ~ 2700 copies of p8 proteins) are supplemented with functional groups and nanomaterials. Phage-based ordered nanostructured materials can be exploited for nanotechnology. For example, phage nanofibers were modified to build semiconductor nanowires [99-101], lithium ion batteries [102,103], photovoltaic cells [104] and as a matrix for tissue engineering and regenerative medicine [105-109].

Hybrid phage-based macromolecular structures, forming films, matrixes and nanowires, can be incorporated with analytical methods for the detection of antigens. Researchers at University of California, Irvine built a "virus electrode", consisting of a self-assembled monolayer of phage particles, genetically engineered for recognition of an antigen, covalently attached to a gold electrode surface [110,111]. Building on this success, the same group grafted the antigen-specific phages into an array of a conducting polymer named poly(3,4-ethylenedioxythiophene) (PEDOT). This formed a virus-PEDOT biocomposite material for electrochemical detection of prostate cancer biomarkers [112-115]. This bio-inorganic hybrid material bridged the electronic applicability of a

polymeric backbone with the biorecognition versatility of engineered phage particles, into a biosensor platform. Magnetic beads and quantum dots have also been used as nanomaterials for constructing phage-based bionanostructures. For example, Wang *et al.* engineered a viral scaffold made of phage particles decorated with magnetic nanoparticles for the rapid detection of *Candida albicans* [116]. Jin and co-workers designed a quantum dot-phage template to build a hybrid composite film on a biosensing platform for 2,4,6-Trinitrotoluene (TNT) [117].

A network of gold nanoparticles and phages is another example of a nanoengineering material [74]. Engineered phages coated with gold nanoparticles can be explored as a signal reporter in optical methods, including spectroscopy and microscopy techniques, and also as a replacement of specialised detection enzymes, such as horseradish peroxidase (HRP), in ELISAs. For example, Guo *et al.* tailored bifunctional phages displaying a gold-binding peptide on its p8 proteins and an antibody (as a biorecognition element) on its p3 proteins [118]. The formation of an immunoaffinity complex, between the phage and an antigen, can be optically visualised by adding gold nanoparticles. This phage-based immunoassay was designed to identify *Bacillus anthracis* spores, but could be easily adapted to target other antigens by changing the biorecognition element on the bifunctional probe. The antigen-binding and signal-generating capacity of the bifunctional phage eliminates the need to use secondary antibodies with HRP molecules [118]. Another example of the use of gold nanoparticles as signalling motifs in phage-based biosensors is given in [119].

Without the need for any specialised detection apparatus, Lee *et al.* built a phage-based sensing platform for protein detection. First, engineered antigen-binding phages (*i.e.* containing antigen-binding motifs on its p3 proteins) were chemically modified to append thiol groups along its surface. Next, the antigen-binding thiolated phage was mixed with the antigen and then captured using magnetic beads. After elution of the phage-antigen complex from the beads, gold nanoparticles are added. A visible, by naked eye, colour change from red to blue,

associated with the aggregation of the gold nanoparticles, suggests the presence of the antigen. The authors stated that, although a single phage only interacts with a few antigen molecules, the multiple binding groups can amplify the resulting signal by promoting the aggregation effect of a large number of gold nanoparticles. The same researchers later designed a similar optical biosensor using chemically DNA-conjugated phages loaded with DNA-coated gold nanoparticles [120], and developed a colorimetric bioassay using the DNA conjugated to an antigen-binding phage as a probe for the presence of the antigen [121]. Surface-enhanced Raman scattering (SERS) spectroscopy can also be integrated with phage-based biosensors. This was successfully demonstrated here [122], in which DNA-modified phage particles were coupled with DNA-conjugated SERS nanoparticles. In this set up, SERS nanoparticles cover the phages surface as a result of DNA hybridization, creating a phage-templated SERS nanoprobe for antigen sensing. Target antigen molecules were first captured onto silica microbeads. Next, the DNA-modified phages, which display an antigen-binding motif on its p3 proteins, were conjugated to the silica microbeads. The DNA-conjugated SERS nanoparticles were then mixed with the phage-loaded silica beads. Individual silica beads loaded with the phage-SERS nanoparticles were later analysed on the Raman instrument, detecting as low as 10 pM of the tested antigen. A similar design [123] was tested using gold nanocubes, labelled with Raman reporters, and bifunctional phage particles, displaying an antibody at one end and gold nanoparticle binding peptides along its surface. First, the bifunctional phage was conjugated with the gold nanocubes – an average of 10-15 50 nm gold nanocubes were aligned along each phage. Next, the target antigen was captured and immobilised on magnetic beads. This immunocomplex-bead was then conjugated with the phage-SERS probes, and later analysed by SERS spectrometry.

Another interesting property of the filamentous phages is their ability to form self-templating supramolecular structures, creating materials with unique optical and photonic properties [124-127]. By mechanically pulling substrates from a phage suspension at controlled speeds, assembled phage films with different

morphologies and levels of hierarchical organisation were generated. Professor Seung-Wuk Lee and researchers from his lab pioneered and tuned this self-templating process building a bio-inspired colorimetric sensor, coined "Phage litmus" [125]. This sensing platform is designed to detect volatile organic compounds, TNT and humidity levels.

1.4 Scope of work

As illustrated above, due to its structural and biological simplicity, it is possible to chemically and genetically modify the filamentous bacteriophage, and adapt it for a template on novel biosensing methods. The research presented here mainly focused on the development of innovative bacteriophage-based biosensors. Particularly, this thesis focus on work done in two biosensors:

i) A proof-of-concept platform for imaging and monitoring flow, targeting cardiovascular diseases. For this, we developed novel strategies for immobilisation of phage particles onto surfaces, enabling a successful integration of a biological scaffold and microfluidics with biosensors. This new methodology was adapted for *in vitro* experiments in endothelial cells, further demonstrating the versatility and validity of the system.

ii) Develop new experimental set-ups for a biotech startup (Linear Diagnostics Ltd.) diagnostic platform. Linear Diagnostics' product is a biosensor that detects the presence of a target of interest (*e.g.* pathogenic bacteria) by exploiting a spectroscopy phenomenon. While collaborating with Linear Diagnostics, we developed new chemical and biological protocols attempting to make their technology simpler, cheaper and more sensitive.

1.5 References

1. Kutter, E., Sulakvelidze, A. *Bacteriophages: Biology and Applications.* (CRC Press, 2005). ISBN: 9780849313363
2. Fuhrman, J. A. Marine viruses and their biogeochemical and ecological effects. *Nature* **399,** 541–8 (1999).
3. Suttle, C. Viruses of biological control agents for booms of marine phytoplankton. *Proc. Brown Tide Summit, New York Sea Grant Institute.* 71–6 (1996).
4. Summers, W. *Félix d'Hérelle and the Origins of Molecular Biology.* (Yale University Press, 1999). ISBN: 0300071272
5. d'Hérelle, F. Sur un microbe invisible antagoniste des bacilles dysentériques. *Comptes rendus Hebd. des séances l'Académie des Sci.* **165,** 373–5 (1917).
6. Summers, W. In the beginning. *Bacteriophage* **1,** 50–51 (2011).
7. Duckworth, D. Who discovered bacteriophage? *Bacteriol. Rev.* 793–802 (1976).
8. Twort, F. An investigation on the nature of ultra-microscopic viruses. *Lancet* 1241–3 (1915).
9. Outbreak News Today, Press release (2017). *Bacteriophage therapy treats patient near death with MDR Acinetobacter baumannii.* Available at: http://outbreaknewstoday.com/bacteriophage-therapy-treats-patient-near-death-mdr-acinetobacter-baumannii-45488/ [Accessed: 27th May 2017].
10. Ellis, L., Delbrück, M. The growth of bacteriophage. *J. Gen. Physiol.* **3,** 365–384 (1939).
11. Luria, E., Delbrück, M. Mutations of bacteria from virus sensitivity to virus resistance. *Genetics* **28,** 491–511 (1943).
12. Luria, E. Reactivation of irradiated bacteriophage by transfer of self-reproducing units. *Proc. Natl. Acad. Sci.* **33**, 253–64 (1947).
13. Hershey, A., Chase, M. Independent functions of viral protein and nucleic acid in growth of bacteriophage. *J Gen Physiol* **36,** 39–56 (1952).
14. Arber, W., Linn, S. DNA modification and restriction. *Annu. Rev. Biochem.* **38,** 467–500 (1969).
15. Meselson, M., Yuan, R. DNA restriction enzyme from E. coli. *Nature* **217,** 1110–4 (1968).
16. Dussoix, D., Arber, W. Host specificity of DNA produced by Escherichia coli. II. Control over acceptance of DNA from infecting phage lambda. *J. Mol. Biol.* **5,** 37–49 (1962).
17. Lederberg, S., Meselson, M. Degradation of non-replicating bacteriophage DNA in non-accepting cells. *J. Mol. Biol.* **8,** 623–8 (1964).
18. Jacob, F., Perrin, D., Sánchez, C., Monod, J. L'opéron : groupe de gènes à expression coordonnée par un operateur. *C. R. Hebd. Seances Acad. Sci.* **250,** 1727–1729 (1960).
19. Jacob, F. The Birth of the Operon. *Science.* **332,** 767–767 (2011).
20. *Morange, M.* "François Jacob (1920–2013) – French freedom fighter who helped to uncover how genes are regulated". *Nature* **497** (2013).
21. Crick F., Barnett L., Brenner S, Watts-Tobin R. General nature of the genetic code for proteins. *Nature* **192,** 1227–32 (1961).

22. McGrath, S., van Sinderen, D. *Bacteriophage: genetics and molecular biology*. (Caister Academic Press, 2007). ISBN: 9781904455141
23. Mao, C., Liu, A., Cao, B. Virus-based chemical and biological sensing. *Angew. Chemie - Int. Ed.* **48,** 6790–6810 (2009).
24. Barbas, C., Burton, D., Scott, J., Silverman, G. *Phage display: a laboratory manual*. (Cold Spring Harbor Laboratory Press, 2001). ISBN: 9780879697402
25. Peltomaa, R., López-Perolio, I., Benito-Peña, E., Barderas, R., Moreno-Bondi, M. C. Application of bacteriophages in sensor development. *Anal. Bioanal. Chem.* **408,** 1805–1828 (2016).
26. Fauquet, C., Mayo, M., Maniloff, J., Desselberger, U., Ball, L. *Virus Taxonomy. 8th report of the International Committee on the Taxonomy of Viruses.* (Elsevier/Academic Press, 2005). ISBN: 9780122499517
27. Sharp, R. Bacteriophages: Biology and history. *J. Chem. Technol. Biotechnol.* **76,** 667–672 (2001).
28. Ackerman, H. Tailed bacteriophages: the Caudovirales. *Adv. Virus Res* **51,** 135–201 (1998).
29. Marvin, D. Filamentous phage structure, infection and assembly. *Curr. Opin. Struct. Biol.* **8**, 150–158 (1998).
30. Rakonjac, J. *Filamentous bacteriophages: biology and applications*. Encyclopaedia of Life Sciences (2012). John Wiley & Sons, Ltd.
31. Smith, G. Filamentous fusion phage: novel expression vectors that display cloned antigens on the virion surface. *Science* **228**, 1315–1317 (1985).
32. Parmley, S., Smith, G. Antibody-selectable filamentous fd phage vectors: affinity purification of target genes. *Gene* **73**, 305–318 (1988).
33. Barbas, C., Kang, A., Lerner, R., Benkovict, S. Assembly of combinatorial antibody libraries on phage surfaces: The gene III site. *Proc. Natl. Acad. Sci.* **88,** 7978–7982 (1991).
34. Kang, A., Barbas, C., Janda, K., Benkovic, S., Lerner, R. Linkage of recognition and replication functions by assembling combinatorial antibody Fab libraries along phage surfaces. *Proc. Natl. Acad. Sci.* **88,** 4363–4366 (1991).
35. Pande, J., Szewczyk, M., Grover, A. Phage display: Concept, innovations, applications and future. *Biotechnol. Adv.* **28,** 849–858 (2010).
36. Bratkovič, T. Progress in phage display: Evolution of the technique and its applications. *Cell. Mol. Life Sci.* **67,** 749–767 (2010).
37. Loeb, T. Isolation of a bacteriophage specific for the F plus and Hfr mating types of Escherichia coli K-12. *Science.* **131,** 932–933 (1960).
38. Rakonjac, J., Bennett, N., Spagnuolo, J., Gagic, D., Russel, M. Filamentous bacteriophage: biology, phage display and nanotechnology applications. *Curr. Issues Mol. Biol.* **13,** 51–76 (2011).
39. Hofschneider, P., Mueller-Jensen, K. On infectious substructures from E. coli bacteriophages. Demonstration and properties of 'Ht2' particles. *Z Naturforsch B.* **18,** 922–927 (1963).
40. Marvin, D., Hoffmann-Berling, H. A fibrous DNA phage (Fd) and a spherical RNA phage (Fr) specific for male strains of E. coli. Physical characteristics. *Z. Naturforsch. B* **18,** 884–893 (1963).

41. Zinder, D., Valentine, R., Roger, M., Stoeckenius, W. f1, a rod-shaped male-specific bacteriophage that contains DNA. *Virology* **20**, 638–640 (1963).
42. Salivar, W., Tzagoloff, H., Pratt, D. Some physical-chemical and biological properties of the rod-shaped coliphage M13. *Virology* **24**, 359–371 (1964).
43. Meynell, G., Lawn, A. Filamentous phages specific for the sex factor. *Nature* **217**, 1184–1186 (1968).
44. Khatoon, H., Iyer, R., Iyer, V. A new filamentous bacteriophage with sex-factor specificity. *Virology* **48**, 145–155 (1972).
45. Henry, K. A., Arbabi-Ghahroudi, M., Scott, J. K. Beyond phage display: Non-traditional applications of the filamentous bacteriophage as a vaccine carrier, therapeutic biologic, and bioconjugation scaffold. *Front. Microbiol.* **6,** 1–18 (2015).
46. Marvin, D. Filamentous phage structure, infection and assembly. *Curr. Opin. Struct. Biol.* **8**, 150–158 (1998).
47. Hemminga, M. *et al.* Viruses: Incredible nanomachines. New advances with filamentous phages. *Eur. Biophys. J.* **39,** 541–550 (2010).
48. Wang, Y. *et al.* The Structure of a Filamentous Bacteriophage. *J. Mol. Biol.* **361,** 209–215 (2006).
49. Webster, R., Lopez, J. Structure and assembly of the class I filamentous bacteriophage. In "Virus structure and Assembly", 235–268 (Jones and Bartlett, 1985).
50. Marvin, D., Hale, R., Nave, C., Helmer-Citterich, M. Molecular models and structural comparisons of native and mutant class I filamentous bacteriophages Ff (fd, f1, M13), If1 and IKe. *J. Mol. Biol.* **235,** 260–286 (1994).
51. Holliger, P., Riechmann, L., Williams, R. Crystal structure of the two N-terminal domains of g3p from filamentous phage fd at 1.9 Å: evidence for conformational liability. *J. Mol. Biol.* **288,** 649–657 (1999).
52. Lubkowski, J., Hennecke, F., Pluckthun, A., Wlodawer, A. The structural basis of phage display elucidated by the crystal structure of the N-terminal domains of g3p. *Nat Struct Biol.* **5**,140-147 (1998).
53. Lubkowski, J., Hennecke, F., Plückthun, A., Wlodawer, A. Filamentous phage infection: Crystal structure of g3p in complex with its coreceptor, the C-terminal domain of TolA. *Structure* **7,** 711–722 (1999).
54. Kather, I., Bippes, C., Schmid, F. A stable disulfide-free gene-3-protein of phage fd generated by in vitro evolution. *J. Mol. Biol.* **354,** 666–678 (2005).
55. Fuh, G., Sidhu, S. Efficient phage display of polypeptides fused to the carboxy-terminus of the M13 gene-3 minor coat protein. *FEBS Lett.* **480,** 231–234 (2000).
56. Lobo, D. *et al.* Direct detection and measurement of wall shear stress using a filamentous bio-nanoparticle. *Nano Res.* **8,** 3307–3315 (2015).
57. Reiss, B. D. *et al.* Biological routes to metal alloy ferromagnetic nanostructures. *Nano Lett.* **4,** 1127–1132 (2004).
58. Huang, Y. *et al.* Programmable assembly of nanoarchitectures using genetically engineered viruses. *Nano Lett.* **5,** 1429–1434 (2005).

59. Lee, J. W., Song, J., Hwang, M. P. & Lee, K. H. Nanoscale bacteriophage biosensors beyond phage display. *Int. J. Nanomedicine* **8,** 3917–3925 (2013).
60. Smith, G., Petrenko, V. Phage display. *Nucleic Acids Res.* **97,** 5–9 (1985).
61. Katz, B. Structural and mechanistic determinants of affinity and specificity of ligands discovered or engineered by phage display. *Annu. Rev. Biophys. Biomol. Struct.* **26,** 27–45 (1997).
62. Kehoe, J., Kay, B. Filamentous phage display in the new millennium. *Chem. Rev.* **3824,** 4056–4072 (2005).
63. Sidhu, S. *Phage display in Biotechnology and Drug Discovery.* (CRC Press, 2005). ISBN: 9780824754662
64. Clackson, T., Lowman, H. *Phage display: a practical approach.* (Oxford University Press, 2004).
65. Singh, A., Poshtiban, S., Evoy, S. Recent advances in bacteriophage based biosensors for food-borne pathogen detection. *Sensors* **13,** 1763–1786 (2013).
66. Smartt, A., Ripp, S. Bacteriophage reporter technology for sensing and detecting microbial targets. *Anal. Bioanal. Chem.* **400,** 991–1007 (2011).
67. Smartt, A. *et al.* Pathogen detection using engineered bacteriophages. *Anal. Bioanal. Chem.* **402,** 3127–3146 (2012).
68. Petrenko, V. Landscape phage as a molecular recognition interface for detection devices. *Microelectronics J.* **39,** 202–207 (2008).
69. Turner, A. Biosensors: sense and sensibility. *Chem. Soc. Rev.* **42**, 3184–3196 (2013)
70. Huang, J., Bishop-Hurley, S., Cooper, M. Development of anti-infectives using phage display: Biological agents against bacteria, viruses, and parasites. *Antimicrob. Agents Chemother.* **56,** 4569–4582 (2012).
71. Sorokulova, I. *et al.* Landscape phage probes for Salmonella typhimurium. *J. Microbiol. Methods* **63,** 55–72 (2005).
72. Wang, Q. *et al.* Chemical modification of M13 bacteriophage and its application in cancer cell imaging. *Bioconjug. Chem.* **21,** 1369–77 (2010).
73. Brasino, M. *et al.* Real-time femtomolar detection of cancer biomarkers from photoconjugated antibody–phage constructs. *Analyst* **142,** 91–97 (2017).
74. Souza, G. *et al.* Networks of gold nanoparticles and bacteriophage as biological sensors and cell-targeting agents. *Proc. Natl. Acad. Sci.* **103,** 1215–1220 (2006).
75. Chung, W., Lee, D. Chemical modulation of M13 bacteriophage and its functional opportunities for nanomedicine. *Int. J. Nanomedicine* **9,** 5825–5836 (2014).
76. González-Techera, A., Vanrell, L., Last, J., Hammock, B., González-Sapienza, G. Phage anti-immune complex assay: General strategy for noncompetitive immunodetection of small molecules. *Anal. Chem.* **79,** 7799–7806 (2007).
77. González-Techera, A. *et al.* Polyclonal antibody-based noncompetitive immunoassay for small analytes developed with short peptide loops isolated from phage libraries. *Anal. Chem.* **79,** 9191–9196 (2007).

78. Towbin, H., Motz, J., Oroszlan, P., Zingel, O. Sandwich immunoassay for the hapten angiotensin II a novel assay principle based on antibodies against immune complexes. *J. Immunol. Methods* **181,** 167–176 (1995).
79. Self, C., Dessi, J., Winger, L. High-performance assays of small molecules: Enhanced sensitivity, rapidity, and convenience demonstrated with a noncompetitive immunometric anti-immune complex assay system for digoxin. *Clin. Chem.* **40,** 2035–2041 (1994).
80. Ullman, E. *et al.* Anti-immune complex antibodies enhance affinity and specificity of primary antibodies. *Proc. Natl. Acad. Sci.* **90,** 1184–1189 (1993).
81. Arévalo, F., González-Techera, A., Zon, M., González-Sapienza, G., Fernández, H. Ultra-sensitive electrochemical immunosensor using analyte peptidomimetics selected from phage display peptide libraries. *Biosens. Bioelectron.* **32,** 231–237 (2012).
82. Rossotti, M. A. *et al.* Phage anti-immunocomplex assay for clomazone: Two-site recognition increasing assay specificity and facilitating adaptation into an on-site format. *Anal. Chem.* **82,** 8838–8843 (2010).
83. Kim, H. *et al.* Magnetic bead-based phage anti-immunocomplex assay (PhAIA) for the detection of the urinary biomarker 3-phenoxybenzoic acid to assess human exposure to pyrethroid insecticides. *Anal. Biochem.* **386,** 45–52 (2009).
84. Kim, H., McCoy, M., Gee, S., González-Sapienza, G., Hammock, B. Noncompetitive Phage Anti-Immunocomplex Real-Time Polymerase Chain Reaction for Sensitive Detection of Small Molecules. *Anal. Chem.* **83,** 246–253 (2010).
85. Kim, H. *et al.* Development of a noncompetitive phage anti-immunocomplex assay for brominated diphenyl ether 47. *Anal. Biochem.* **401,** 38–46 (2010).
86. Hafeman, D., Parce, J., Mcconnell, H. Light-addressable potentiometric sensor for biochemical systems. Science **240**, 1182–1185 (1988).
87. Zhang, H. *et al.* Metastatic cell detection using phage-peptide modified light addressable potentiometric sensor. *Biotechnol Appl Biochem* **192,** 185–192 (2008).
88. Palaniappan, K. *et al.* Molecular imaging of cancer cells using a bacteriophage-based ^{129}Xe NMR biosensor. *Angew. Chemie - Int. Ed.* **52,** 4849–4853 (2013).
89. Carrico, Z. *et al.* N-terminal labelling of filamentous phage to create cancer marker imaging agents. *ACS Nano* **6,** 6675–6680 (2012).
90. Ghosh, D. *et al.* M13-templated magnetic nanoparticles for targeted in vivo imaging of prostate cancer. *Nat. Nanotechnol.* **7,** 677–682 (2012).
91. Ghosh, D., Kohli, A., Moser, F., Endy, D., Belcher, A. Refactored M13 bacteriophage as a platform for tumor cell imaging and drug delivery. *ACS Synth. Biol.* **1,** 576–582 (2012).
92. Pacheco-Gomez, R. *et al.* Detection of pathogenic bacteria using a homogenous immunoassay based on shear alignment of virus particles and linear dichroism. *Anal. Chem.* **84,** 91–97 (2012).

93. Li, S. *et al.* Direct detection of *Salmonella typhimurium* on fresh produce using phage-based magnetoelastic biosensors. *Biosens. Bioelectron.* **26,** 1313–1319 (2010).
94. Wang, F. *et al.* Detection of *Salmonella typhimurium* on spinach using phage-based magnetoelastic biosensors. *Sensors* **17,** 1–9 (2017).
95. Lakshmanan, R. *et al.* Detection of *Salmonella typhimurium* in fat free milk using a phage immobilized magnetoelastic sensor. *Sensors Actuators, B Chem.* **126,** 544–550 (2007).
96. Bhunia, A., Moon, S., Taitt, C. High throughput screening for food safety assessment. (Elsevier, 2015). ISBN: 9780857098016
97. Huang, Y. *et al.* Programmable assembly of nanoarchitectures using genetically engineered viruses. *Nano Lett.* **5,** 1429–1434 (2005).
98. Nam, K., Reelle, B., Lee, S., Belcher, A. Genetically driven assembly of nanorings based on the M13 virus. *Nano Lett.* **4,** 23–27 (2004).
99. Whaley, S., English, D., Hu, E., Barbara, P., Belcher, A. Selection of peptides with semiconductor binding specificity for directed nanocrystal assembly. *Nature* **405,** 665–8 (2000).
100. Mao, C. *et al.* Virus-based toolkit for the directed synthesis of magnetic and semiconducting nanowires. *Science* **303,** 213–217 (2004).
101. Mao, C. *et al.* Viral assembly of oriented quantum dot nanowires. *Proc. Natl. Acad. Sci.* **100,** 6946–6951 (2003).
102. Oh, D. *et al.* M13 Virus-directed synthesis of nanostructured metal oxides for lithium–oxygen batteries. *Nano Lett.* **14,** 4837–4845 (2014).
103. Lee, Y. *et al.* Fabricating genetically engineered high-power lithium-ion batteries using multiple virus genes. *Science.* **324,** 1051–1055 (2009).
104. Dang, X. *et al.* Virus-templated self-assembled single-walled carbon nanotubes for highly efficient electron collection in photovoltaic devices. *Nat. Nanotechnol.* **6,** 377–384 (2011).
105. Yoo, S., Oh, J., Lee, S. Phage-chips for novel optically readable tissue engineering assays. *Langmuir* (2011).
106. Wang, J., Wang, L., Li, X., Mao, C. Virus activated artificial ECM induces the osteoblastic differentiation of mesenchymal stem cells without osteogenic supplements. *Sci. Rep.* **3,** 1242 (2013).
107. Zhu, H. *et al.* Controlled growth and differentiation of MSCs on grooved films assembled from monodisperse biological nanofibers with genetically tunable surface chemistries. *Biomaterials* **32,** 4744–4752 (2011).
108. Wang, J. *et al.* Phage nanofibers induce vascularized osteogenesis in 3D printed bone scaffolds. *Adv. Mater.* **26,** 4961–4966 (2014).
109. Wang, J. *et al.* Untangling the effects of peptide sequences and nanotopographies in a biomimetic niche for directed differentiation of iPSCs by assemblies of genetically engineered viral nanofibers. *Nano Lett.* **14,** 6850–6856 (2014).
110. Yang, L. *et al.* Virus electrodes for universal biodetection. *Anal. Chem.* **78,** 3265–3270 (2006).
111. Yang, L., Diaz, J., McIntire, T., Weiss, G., Penner, R. Covalent virus layer for mass-based biosensing. *Anal. Chem.* **80,** 933–943 (2008).
112. Donavan, K. *et al.* Virus - Poly(3,4-ethylenedioxythiophene) composite films for impedance-based biosensing. *Anal. Chem.* **83**, 2420–2424 (2011).

113. Arter, J. *et al.* Virus-polymer hybrid nanowires tailored to detect prostate-specific membrane antigen. *Anal. Chem.* **84,** 2776–2783 (2012).
114. Arter, J., Taggart, D., McIntire, T., Penner, R., Weiss, G. Virus-PEDOT nanowires for biosensing. *Nano Lett.* **10,** 4858–4862 (2010).
115. Mohan, K., Donavan, K., Arter, J, Penner, R., Weiss, G. Sub-nanomolar detection of prostate specific membrane antigen in synthetic urine by synergistic, dual ligand phage. *J. Am. Chem. Soc.* **135**, 7761–7767 (2013).
116. Wang, Y. *et al.* Ultrasensitive rapid detection of human serum antibody biomarkers by biomarker-capturing viral nanofibers. *ACS Nano* **9,** 4475–4483 (2015).
117. Jin, H. et al. Quantum dot-engineered M13 virus layer-by-layer composite films for highly selective and sensitive turn-on TNT sensors. *Chem. Commun.* **49,** 6045–6047 (2013).
118. Guo, Y. *et al.* Construction of bifunctional phage display for biological analysis and immunoassay. *Anal. Biochem.* **396,** 155–157 (2010).
119. Lee, J., Cha, J. Amplified protein detection through visible plasmon shifts in gold nanocrystal solutions from bacteriophage platforms. *Anal. Chem.* **83,** 3516–3519 (2011).
120. Lee, J., Domaille, D., Cha. J. Amplified protein detection and identification through DNA-Conjugated M13 bacteriophage. *ACS Nano* **6,** 5621–5626 (2012).
121. Domaille, D., Lee, J., Cha, J. High density DNA loading on the M13 bacteriophage provides access to colorimetric and fluorescent protein microarray biosensors. *Chem. Commun* **49,** 1759–1761 (2013).
122. Lee, J. *et al.* M13 bacteriophage as materials for amplified surface enhanced Raman scattering protein sensing. *Adv. Funct. Mater.* **24,** 2079–2084 (2014).
123. Lee, H. *et al.* Virus templated gold nanocube chain for SERS nanoprobe. *Small* **10,** 3007–3011 (2014).
124. Chung, W., Oh, J., Kwak, K., Lee, B., Meyer, J. Biomimetic self-templating supramolecular structures. *Nature* **478,** 364–368 (2011).
125. Oh, J. *et al.* Biomimetic virus-based colourimetric sensors. *Nat. Commun.* **5,** 1–8 (2014).
126. Lee, J. *et al.* Phage-based structural color sensors and their pattern recognition sensing system. *ACS Nano* **11,** 3632–3641 (2017).
127. Kim, W. *et al.* Biomimetic self-templating optical structures fabricated by genetically engineered M13 bacteriophage. *Biosens. Bioelectron.* **85,** 853–859 (2016).

CHAPTER 2 – Materials and methods

2.1 General production of bacteriophage

M13 phage was produced as per the method of Pacheco-Gomez *et al.* [1], fd phage and mosaic phage were produced following Brasino *et al.* [2]. Typically, a 250 mL flask containing 40 mL of an aliquot of an overnight *E. coli* culture (TOP10 F', Invitrogen, or *E. coli* strain K91Kan, provided by Brasino; see Table 2.2) in LB broth with tetracycline (5 μg/mL) was inoculated with ~ 10 μL of a concentrated phage stock (~ 10 mg/mL), and incubated between 5 and 12 hours at 37 °C, 200 rpm. To grow the mosaic phage, IPTG (between 0.1–1 mM) was also added to the culture broth.

2.2 Purification of bacteriophage

2.2.1 PEG/NaCl precipitation

Following incubation (method 2.1), the phage/bacteria culture was centrifuged (Avanti series or Allegra X-22R, Beckman Coulter) at 10,000 × *g* for 15 minutes. The supernatant, containing the phage particles, was collected and a 20% (w/v) polyethylene glycol (PEG, M_w= 6000 or 8000), 2.5 M NaCl solution was mixed at a 1/5th volumetric ratio to precipitate the phages [3]. This mixture was left at 4 °C overnight. The next day, the mixture was centrifuged at 10,000 × *g* for 20 minutes. The supernatant containing *E. coli* cells was removed and discarded, and the phage pellet was resuspended in 1 mL of buffer (generally PBS, but it depends on the intended experiment) and spun at 22,000 × *g* for 5 minutes to precipitate cellular debris. This step was sometimes repeated one more time. The ~ 1 mL supernatant was transferred to a fresh eppendorf and mixed with 200 μL of the PEG/NaCl stock. The mixture was left at 4 °C for ~ 2 hours. This was centrifuged at 22,000 × *g* for 15 minutes and the phage pellet was resuspended in buffer.

2.2.2 Caesium chloride purification

To further purify the bacteriophage, the phage sample was mixed with caesium chloride (CsCl) powder to give a final concentration of 0.4 mg/mL of CsCl [4,5]. The samples were centrifuged for 24 hours at 35,000 rpm at 15 °C. After extraction, the samples were dialysed using 3500 MWCO dialysis tubing (Sigma) in 50 mM potassium phosphate buffer pH 8 for 24 hours. This purification step was not performed in all phage samples.

2.2.3 Size exclusion chromatography purification

The M13-Antibody-TRITC and M13-WGA-TRITC constructs (Chapter 4) were purified using a size exclusion chromatography (SEC) purification system (ÄKTA Explorer 10, GE Healthcare), fitted with a Superdex 200 (120 mL column volume) HiLoad 16/60 prepacked column. The column was equilibrated with 1 column volume of water and 1.2 column volumes of elution buffer (50 mM potassium phosphate buffer, 150 mM NaCl, pH 8) before sample injection. Three wavelengths were recorded simultaneously (269, 280 and 555 nm). 2 mL fractions were collected using a Frac-950 fraction collector (Amersham Pharmacia Biotech). These samples were then typically concentrated by PEG precipitation.

2.2.4 Desalting columns

Desalting spin columns (Zeba column, 7K MWCO, 0.5 mL, Thermo Fisher Scientific) or gravity flow PD-10 desalting columns (Sephadex G-25, 1 mL–2.5 mL, GE Healthcare) were used to desalt and remove excess reagents from phage samples.

2.3 Estimating bacteriophage concentration

2.3.1 Bacteriophage plaque assay for phage titer

Plaque assays measure the ability of a single phage particle to form a plaque on a monolayer of susceptible host cells. The turbid plaque is developed as part of the

infection of a bacterial cell by one phage, followed by rapid replication of that phage. Each formed plaque on a bacterial lawn in a LB/agar plate (method 2.3.1.1) represents an area of bacteria growth inhibition started by a viral particle. Agar restricts movement of the phage particles so that a phage can only infect adjacent bacterial cells. There are two commonly used methods for assessing phage plaque formation:

- Double agar overlay method (Fig. 5.4, Chapter 5) [6]

A lawn of susceptible/host bacterial cells (*i.e. E. coli* expressing F' pilus, method 2.11.3) is mixed with serial dilutions of a phage suspension and grown on the surface of a "soft" agar layer (with a "hard" agar layer on the bottom of the plate, method 2.11.1). The plates are incubated overnight at 37 ˚C. This method is the most commonly used to determine phage titer in pfu/mL (see below) by counting the number of visible phage plaques.

- Droplet method (Fig. 5.4, Chapter 5), adapted from [7]

10 μL drops of diluted phage suspensions are spotted onto a bacterial lawn (method 2.3.1.1). The plates are allowed to dry on a laminar flow hood, and then incubated overnight, at 37 ˚C.

2.3.1.1 Preparing a bacterial lawn plate

Bacterial lawns [6] were prepared by adding plating cells (*E. coli* expressing F' pilus) to a LB/agar plate. These plates are made of two layers: ~ 8 mL of a "hard" bottom layer (1.5%) and ~ 4 mL of a "soft" top layer (0.7%) (method 2.11.1).

2.3.1.2 Counting and calculating titer in pfu/mL

The viral activity of the constructed phage particles can be measured in plaque forming units (pfu) per mL. For this, one has to count the number of cloudy patches (plaques) that formed on the surface of the LB/agar plate. The assumption is that each isolated plaque represents one phage particle. A plate with between 30 and 300 plaques is selected and the number of plaques is manually counted. The titer is determined by dividing the number of plaques

with the used dilution factor and the volume of diluted phage stock added to the plate.

2.3.2 UV-Vis spectrophotometric phage quantification

Phage concentration was determined from its absorption spectrum, measured using a UV-Visible absorption spectrophotometer (Jasco V-550). The concentration of phage (in mg/mL) was then calculated using the Beer-Lambert law, based on absorbance at 269 nm, arising from a combination of peptide and DNA absorbance [8], and the extinction coefficient, which was experimentally determined to be 3.84 cm^2 mg^{-1} for the wild-type phage [9]. The molecular weight of the wild-type phage is ~ 17×10^6 Da [10]. The concentration of phage in number of virions/mL was calculated from the formula as per [11].

2.4 Bioconjugation protocols

2.4.1 p3 chemical modifications

2.4.1.1 Bioconjugation with antibody

Anti-collagen antibodies were selectively conjugated to the ~ 5 copies of p3, at one end of the M13, by using reducing conditions to break the disulfide bonds of the p3 proteins. 2000× molar excess of tris(2-carboxyethyl)phosphine hydrochloride (TCEP, Sigma) in 100 mM phosphate buffer pH 7.5 was added to an initial mass of M13 (5.8×10^{-8} mmoles) in order to reduce p3 proteins (2.9×10^{-7} mmoles). The sample was incubated for 1 hour at room temperature. The reduced M13 samples were purified by using a PD-10 column (Sephadex G-25, GE Healthcare) and eluted in conjugation buffer (50 mM potassium phosphate buffer, 150 mM NaCl, 5 mM EDTA buffer, pH 7). The anti-collagen antibody (abcam, ab19808) was then derivatised with maleimide. Succinimidyl-4-(N-maleimidomethyl cyclohexane-1-carboxylate (SMCC, Thermo Scientific Pierce) was added to the anti-collagen antibody in a 25× molar excess. The modified anti-collagen antibody was added in a 1:1 ratio over the p3 proteins. The sample was incubated for 2 hours and eluted in the conjugation buffer using a PD-10 column. Finally, the maleimide-derivatised

anti-collagen antibodies and the reduced M13 bacteriophage were mixed and left to react overnight at 4 °C. The resulting sample was then purified using PD-10 column. After conjugation with TRITC dye molecule (method 2.4.2.1), the sample was purified by size exclusion chromatography (method. 2.2.3).

2.4.1.2 Bioconjugation with WGA-FITC

The p3 proteins of the phage were conjugated to wheat germ agglutinin fluorescein-conjugated (WGA-FITC), similarly to method 2.4.1.1. The disulfide bonds of the p3 protein were reduced using TCEP in 100 mM phosphate buffer pH 7.5, and added to an initial mass of M13 phage (5.8×10^{-8} mmoles). The sample was incubated for 1 hour at room temperature. The reduced M13 was purified using a PD-10 column (Sephadex G-25, GE Healthcare), with a conjugation buffer (50 mM potassium phosphate buffer, 150 mM NaCl, 5 mM EDTA buffer, pH 7) as eluent. Wheat germ agglutinin conjugated with FITC (WGA-FITC, lectin from *Triticum vulgaris*, lyophilized powder, Sigma) was used at molar equivalents to the p3 proteins. The WGA was maleimide-derivatised with SMCC, in a 25× molar excess. The sample was incubated for 2 hours and eluted in the conjugation buffer using a PD-10 column. The p3-modified phage and the maleimide-derivatised WGA were then mixed and left to react overnight at 4 °C. The resulting sample was then purified using PD-10 columns. After conjugation with TRITC dye molecule (method 2.4.2.1), the sample was purified by size exclusion chromatography (method. 2.2.3).

2.4.1.3 Bioconjugation with magnetic bead

Following manufacturer's instructions, 50 nm protein A functionalised magnetic beads (Ocean NanoTech) were conjugated with antibodies. Typically, 8 μg of anti-p3 antibody (mouse isotype IgG_{2a}, NEB) in PBS-T (PBS + 0.1% Tween-20) was mixed with ~ 3×10^{11} magnetic beads, and rotated for 1 hour at room temperature. The mixture was placed on a N40 neodymium magnet (12.7×12.7×3.2 mm, from Power Magnet Store on Amazon) overnight (~ 10

hours). The following day, holding the eppendorf so it would not be displaced from the magnet, the supernatant was carefully removed. The beads were resuspended in PBS-T buffer, gently vortexed, and captured on the magnet for another 10 hours. The supernatant was then carefully discarded. A sample containing ~ 2×10^{10} wild-type phage particles was pipetted into the beads-antibody complex, and incubated overnight, while rotating. The eppendorf was placed on the magnet to capture the beads complex and magnetised for 10 hours. The supernatant was carefully collected. PBT-T buffer was slowly added and the sample were briefly vortexed, and the beads were magnetised overnight. This washing step was repeated three more times. The phage-bead construct samples were then stored in the fridge until analysis (TEM, method 2.5.7).

2.4.2 p8 chemical modifications

2.4.2.1 Fluorescent labelling with dye molecules

The p8 proteins of the phage were labeled with tetramethylrhodamine-isothiocyanate (TRITC, Invitrogen Thermo Fisher Scientific), Alexa Fluor 647 (AF647, Invitrogen Thermo Fisher Scientific), or 7-Diethylamino-3-((((2-maleimidyl)ethyl)amino)carbonyl)coumarin (MDCC, Invitrogen Thermo Fisher Scientific) [12]. TRITC is an amine-reactive dye that produced a bright orange bioconjugate with excitation/emission maxima at 555/580 nm. AF647 and MDCC are maleimide-derivatised dyes producing red (extinction/emission maxima at 650/665 nm) and blueish (extinction/emission maxima at 420/470 nm) bioconjugates, respectively. Dye stock solutions were prepared in dimethyl sulfoxide (DMSO), typically to a stock concentration of 10 mg/mL, and slowly added to 1–2 mg of phage in buffer (pH 7–8, depends on experiment as defined in the main body of the thesis), in order to provide a 1:1 molar ratio over the p8 proteins. Usually, the sample was incubated at room temperature, with continuous stirring, for 2 to 8 hours, however longer incubation times seem not to present an issue. Phage-dye constructs were separated from unreacted dye molecules either by using PD-10 columns, size exclusion chromatography or by multiple rounds of PEG/NaCl precipitation.

To estimate the degree of labelling of the phage particles with TRITC dye (Fig. 3.13, Chapter 3) the following steps were carried out. After removing excess TRITC dye from the phage-dye sample, the coverage (%) of the phage surface with TRITC molecules was estimated. This was done by measuring the absorbance of the phage-dye conjugate at 269 nm on a UV-Vis spectrometer (Jasco, V-550). However, dyes generally also absorb in the 260–280 nm range, contributing to the absorbance at 269 nm. A correction factor (CF) is then required. The CF for TRITC was calculated to be ~ 0.34 (by dividing the absorbance of the free dye at 269 nm with the maximum absorbance of the free dye at 555 nm). The phage concentration in the phage-dye sample was corrected by subtracting the absorbance at 269 nm to the absorbance at 555 nm multiplied by the CF of TRITC. The degree of labelling of the phage surface with TRITC dye was then determined by dividing the molar concentration of TRITC (ε = 65,000 M^{-1} cm^{-1}) with the corrected molar concentration of phage (method 2.3.2), in the phage-dye sample.

2.4.2.2 Chemically introducing antibodies

2.4.2.2.1 Linear Diagnostics' protocol

The first step of this bioconjugation protocol is to modify the primary amines of the p8 proteins by adding thiol groups. A phage aliquot (1–2mg) was diluted in 50 mM potassium phosphate buffer pH 8. N-succinimidyl S-acetylthioacetate (SATA, Thermo Fisher Scientific) was dissolved in DMSO and added to the phage sample in order to make a 20× molar excess over p8 proteins. This reaction was incubated for 1 hour at room temperature. Hydroxylamine (Sigma) dissolved in potassium phosphate buffer and 250 mM EDTA was then added to the SATA-modified phage and left to react for 20 minutes at room temperature. Next, the thiolated phage was purified using PD-10 columns and eluted in 50 mM potassium phosphate, 150 mM NaCl, 5 mM EDTA pH 7. The second step of this protocol is to maleimide-derivatise the antibodies. Antibody (*e.g.* anti-*E. coli* or anti-*Salmonella*, BioRad) was first purified on a PD10 column and eluted in 100 mM potassium phosphate buffer pH 7.5. Succinimidyl 4-(N-

maleimidomethyl)cyclohexane-1-carboxylate (SMCC, Thermo Fisher Scientific) was dissolved in DMSO, and added in a 25× molar excess over the initial amount of antibody. This reaction was incubated for 1 hour at room temperature. Next, the maleimide-derivatised antibody was purified using PD-10 columns and eluted in 50 mM potassium phosphate, 150 mM NaCl, 5 mM EDTA pH 7. The thiolated-phage and maleimide-derivatised antibody samples were mixed and reacted for at least 2 hours at room temperature. If dye labelling of the p8 proteins was intended, the method in section 2.4.2.1 would be followed. Finally, the antibody-phage conjugate was purified by PEG/NaCl precipitation (2 hours at 4 ˚C) and the resulting phage pellet resuspended in 100 mM phosphate buffer pH 7.5.

2.4.2.2.2 Aldehyde-hydrazine bioconjugation

The protocol was adapted from [13]. First, the amines on the p8 proteins were modified with hydrazine groups. For this, phage particles were reacted with the crosslinker reagent succinimidyl 6-hydrozinonicotinate (SANH, Solulink). Stocks of SANH were prepared in PBS buffer, and the appropriate amount was added to typically 1 mg of phage, ensuring the desired molar ratio over protein (usually 10-fold molar excess). This mixture was left to stir overnight at 4 ˚C. The next day, phage was purified by PEG/NaCl precipitation (2 hours at 4 ˚C). The phage pellet was then resuspended in 100 mM potassium phosphate buffer, pH 6. An aliquot of this sample was saved for quality control experiments, such as LD measurements of the SANH-modified phages and the p-NBA test (method 2.9.1). The second step of this protocol involved introducing aldehyde moieties to glycosylated antibodies (*e.g.* anti-*E. coli*, BioRad #4329-4906). Sodium periodate ($NaIO_4$, Sigma) was dissolved in water (usually 1 mM was used) and immediately added to the antibody sample (diluted in PBS buffer; amounts used ranging from 1 mg to 250 µg of antibody). This reaction was incubated for 30 minutes at room temperature. The oxidised antibodies were then purified using desalting columns (Zeba columns, Thermo Fisher Scientific) and eluted in 100 mM potassium phosphate buffer pH 6. An aliquot of the oxidised antibody was saved for quality control (Purpald test, method 2.9.2).

Finally, the aldehyde-modified antibody sample was mixed with the hydrazine-modified phage sample. Immediately after, 10 µL, of a 1 M aniline stock in acetate buffer pH 4.6 solution was added to catalyse the reaction. This was incubated overnight at 35 ˚C, while mixing at an eppendorf thermomixer at 650 rpm. The following day, the phage-antibody conjugate was purified by PEG/NaCl precipitation (overnight at 4 ˚C) or by using Zeba columns. The phage pellet was resuspended in PBS buffer and stored in the fridge until used in the LD-based immunoassay (method 2.8.2.2). Observation – when the phage pellet looked like a transparent-gel rather than the usual white compacted pellet, this was thought to suggest crosslinking between phage particles.

2.4.2.2.3 DNA-conjugated phage

The p8 proteins of the phage were modified to facilitate conjugation with short DNA strands [14]. Two phage-DNA probes, conjugated with different DNA strands, were designed for this (see Chapter 3, Table 3.2). First, the primary amines of the p8 proteins were modified with 4-formyl succinimidyl benzoate (NHS-CBA), to introduce aldehydes groups on the phage surface. This was done by adding 5 µL of a 10 mM NHS-CBA stock (in DMSO) to 1 mg/mL phage in 100 mM $NaHCO_3$ pH 8.3 buffer (sodium bicarbonate (Sigma) in water). This mixture was then left to react overnight at 4 ˚C. PEG/NaCl was added to the aldehyde-modified phage and this mixture was split in two fractions – half to produce the phage-DNA probe 1 and the other half to produce phage-DNA probe 2. Each fraction of the aldehyde-modified phage was PEG/NaCl precipitated (for 1-2 hours at 4 ˚C) and the phage pellet resuspended in 200 mM NH_4OAc pH 5 buffer (ammonium acetate (Sigma) in water, pH-adjusted with glacial acetic acid (Sigma)).

- Phage-DNA probe 1 conjugate

62.5 µL of 200 µM I-Link DNA (hydrazine-modified DNA, from Integrated DNA Technologies) was mixed with an equal volume of aldehyde-modified phage, and left to react at room temperature for 24 hours. After incubation, the phage-DNA conjugate was purified by PEG/NaCl precipitation, and

resuspended in PBS buffer. Phage concentration was determined by UV spectrophotometry.

- Phage-DNA probe 2 conjugate

9.15 µL of a 42 mM SANH (Solulink) stock was added to 10 µL of 1.3 mM DNA-NH_2 (NH_2-modified DNA, from Integrated DNA Technologies) in a total of 30 µL made up with 300 mM $NaHCO_3$ buffer, and left to react overnight at 4 °C. This step was necessary to modify the amines on the DNA with hydrazine groups (IDT does not produce 3' I-Link modifications of the DNA). After cleaning the SANH-modified DNA in a NAP-5 column (GE Healthcare) and lyophilizing the eluted product, the DNA was resuspended in 200 mM NH_4OAc pH 4.5, and added to the aldehyde-modified phage for a 24 hours reaction at room temperature. Finally, the phage-DNA conjugate was purified by PEG/NaCl precipitation, and resuspended in PBS buffer. Phage concentration was determined by UV spectrophotometry.

2.5 Microscopy and imaging experiments

2.5.1 Imaging on collagen-coated slides

Images were acquired at 10 frames per second using a spinning disk confocal microscope (PerkinElmer Ultraview ERS) with a 1.4 NA, 100× oil immersion objective, 561 nm laser, TRITC filter sets (Croma) and an ORCA R^2 camera (Hamamatsu) under control of Volocity 6.3 (Perkin-Elmer).

2.5.2 Imaging on endothelial cells-coated slides

Cultures of endothelial cells were grown using standard cell biology procedures. The cells were then split and seeded into µ-Slide I $Luer^{0.8}$ collagen-coated slides (ibidi) and incubated until confluence. GEnC cells were cultured and seeded by Dr. Hesham Elhegni, from University of Bristol. HUVEC cells were cultured and seeded by Dr. Maria Machado, from University of Nottingham. The phage constructs on the cells were visualised using a Nikon Ti Eclipse inverted microscope through 60× oil immersion objective 1.4 (Nikon Plan Apo VC 60x Oil DIC N2). Cells within the imaging window were illuminated at 535 nm

using a wide-field fluorescent light emitting diode (Precise Excite Cool LED) and emitted light was filtered through a 620 nm filter block and detected on a high resolution monochromatic camera (Photometric's CoolSnap HQ2). Images were collected using Nikon's NIS Elements software.

2.5.3 Flow experiments on the collagen-coated slides

A chamber flow slide with a collagen coating (ibidi, µ-Slide I Luer$^{0.8}$) was used. The channel was carefully filled with the M13-Antibody-TRITC construct sample and left to incubate for 1 hour at room temperature. The slide was linked to the tubing ('white' perfusion set, #10963) of the pump system, and the reservoirs were filled with sterile PBS. The experiments were performed at 35 °C, on the temperature-controlled system box of the microscope. The reservoirs and tubing were left inside the box for 1 hour to equilibrate the temperature of the buffer. The software allows varying the pressure/flow rate/shear stress to the desired testing values. A defined nominal shear stress (WSS on a flat surface due to the bulk flow rate) profile was applied, ranging from –3.5 to +3.5 dyn/cm^2, each cycle lasting 20 seconds.

2.5.4 Flow experiments on the endothelial cells-coated slides

The apparatus used for the collagen antibody constructs was also used for the cells experiments. Endothelial cells were seeded onto the same type of flow collagen-coated slide (ibidi, µ-Slide I Luer$^{0.8}$) and the M13-WGA-TRITC construct was added to the chamber and left to react for 1 hour in an incubator at 37 °C/5% CO_2. The slide was linked to the pressure pump and the reservoir of the fluidic unit was filled with sterile PBS buffer. A defined nominal wall shear stress profile was applied, from –3.5 to +3.5 dyn/cm^2, each cycle lasting 20 seconds.

2.5.5 *In vitro* labelling of glycocalyx on endothelial cells

Endothelial cells, previously seeded and grown until confluence onto the microfluidic chamber of an ibidi µ-Slide, were rinsed three times with pre-

warmed PBS buffer. The cells were incubated for 1 hour at 37 °C with FITC-conjugated wheat germ agglutinin (WGA-FITC, Sigma), at a 1:200 dilution. The endothelial cells were rinsed again three times with PBS, and then fixed with ~ 100% methanol for 15 minutes. To label the nucleus of the cells, these were incubated for 3 minutes with 4',6-diamidino-2-phenylindole (DAPI, Thermo Fisher Scientific) at a 1:500 dilution, and then rinsed three times with PBS. Labelled endothelial cells were immediately visualised under a confocal laser scanning microscope (Leica TCS SPE), and a Z-stack was collected (Chapter 4, Fig. 4.2).

2.5.6 Imaging the M13+WGA-FITC+TRITC phage construct

A 10 μL drop of M13+WGA-FITC+TRITC phage construct was immobilised under a 5% agarose flat pad. A cover slip was gently fixed on top, and sample was imaged using a confocal microscope beam splitter (Leica TCS SP8) for the TRITC and FITC dye molecules conjugated to the phage.

2.5.7 Transmission Electron Microscopy (TEM)

TEM grids (Formvar/Carbon on 200 Mesh Copper, Agar Scientific) were treated by glow discharge (E200 Auto sputter coater) for 30 seconds. Phage samples were prepared (5 μL, typically at concentrations ranging from 0.1 mg/mL to 0.05 mg/mL) and added onto the TEM grid. The liquid was removed by wicking with filter paper after 60 seconds. 1% uranyl acetate (5 μL) was added and wicked off with filter paper after 60 seconds. A JEM-2200FS TEM (Joel, Japan) was used to visualise the grids, typically at a 10000×, 15000× or 25000× magnification. ImageJ/Fiji software was used to analyse and process TEM images.

2.6 Enzyme-Linked Immunosorbent Assay (ELISA)

2.6.1 ELISA protocol in maleimide-coated microplates

A maleimide-activated microplate (Pierce, Thermo Fisher Scientific #15150) was used for this ELISA [15]. The wells were washed three times with 200 μL

of 100 mM sodium phosphate buffer, 150 mM NaCl, 0.05% Tween-20, pH 7.2. A phage sample (2 mg) was reduced with 5 mM TCEP (Pierce, Thermo Fisher Scientific, #20491) for one hour at room temperature, and eluted on a PD-10 column (GE Healthcare) in 100 mM sodium phosphate buffer, 150 mM NaCl, 10 mM EDTA, pH 7.2. Phage not reduced with TCEP was used as a control. A serial dilution of the phage samples was added to the wells, sealed with an adhesive lid and incubated for 3 hours at room temperature. The wells were emptied by flicking the microplate and tapping it onto a paper towel, and adding 200 µL of wash buffer in each well. This process was repeated four times. 1:5000 diluted HRP/anti-M13 antibody conjugate (GE Healthcare #27-9421-01) was added to each phage-coated well, and incubated for 1 hour at room temperature. The wells were then emptied and blotted on a paper towel, and filled with wash buffer. The microplate was blotted on paper towel to remove any remaining wash buffer. This process was repeated six times. A 2,2'-Azinobis (3-ethylbenzothiazoline-6-sulfonic acid)-diammonium solution (1-Step ABTS Substrate solution, Thermo Fisher Scientific #37615) was added to each well and incubated until a green colour has formed. The ABTS-HRP reaction absorbance was measured in a microplate reader set at 410 nm. Reactions were blanked against a well filled with ABTS.

2.6.2 Phage-binding ELISA

This ELISA was performed to test the MSal17 phage construct (*Salmonella*-binding peptide on phage). Several wells of a 96-well microplate (Nunc MaxiSorp™, flat-bottom/clear) were coated with gamma-irradiated *Salmonella* or *E. coli* bacteria, typically in the range of 10^7–10^5 cells/mL, in PBS buffer. The plate was cover with adhesive plastic and incubated for 12-18 hours at 4 °C. The next day, the wells were emptied, by vigorously flicking the plate over a sink, and washed three times with 200 µL of PBS. The plate was gently blotted on paper towel between washes. 200 µL of a blocking buffer (1% BSA in PBS) was added to each well and left to incubate for two hours at room temperature. The plate was then washed three times with PBS buffer. ~ 100 µL (0.5 mg/mL for ELISA on Fig. 5.25, and 0.2 mg/mL for ELISA on Fig. 5.26) samples of MSal17 and

wild-type phage in PBS buffer were added to the wells, and incubated at room temperature for approximately 3 hours. The plate was then washed four times with PBS buffer. 200 µL of diluted (1:5000) anti-phage/HRP conjugate antibody in blocking buffer was added, and incubated for one hour at room temperature. Each well was washed six times with 200 µL of PBS buffer as described above, and 200 µL of 1-step ABTS solution was added. Absorbance at 410 nm was then measured on a plate reader. The blank in this experiment was considered to be the absorbance (at 410 nm) of a bacterial-coated well filled with ABTS solution.

2.6.2.1 Gamma-irradiated bacteria

An important consideration for the MSal17 phage construct assays was the sterilisation method to which the bacteria were subjected prior to use in the immunoassay. Since *Salmonella* species and some *E. coli* are pathogenic, most commercially available bacterial batches on the market are "dead", commonly destroyed by heat, to accommodate for the standard Bio Safety level 1 laboratories. The high temperatures that heat-killed bacteria are exposed to can denature the tertiary structure of the proteins expressed on its surface, which may be essential for some binding-peptides recognition. Exposure to gamma radiation presumably only damages bacterial DNA, incapacitating bacteria to multiply, without compromising the outer structure morphology and the antigen characteristics of the whole cell [16]. *Salmonella* and *E. coli* bacteria were inactivated by gamma irradiation at 10 kGy in a Gammabeam 650 irradiator (Atomic Energy of Canada Limited), to render them safe to use outside a CAT II level laboratory. No special precautions, other than usual aseptic technique, were required for working with these microorganisms. These bacterial cultures were kindly provided by Dr. Irene Grant, at the Agri-Food and Biosciences Institute of Northern Ireland.

2.7 Gel electrophoresis

2.7.1 Agarose gel electrophoresis

For agarose gel electrophoresis [17], an agarose suspension (1%–2%, depending on the purpose of the gel) was prepared by adding agarose powder to 50 ml of tris/borate/ethylenediaminetetraacetic acid (TBE) buffer. The suspension was heated in a microwave until the agarose was fully dissolved. The suspension was briefly left to cool down, while occasionally swirling the flask, at which point ~ 4 µl of ethidium bromide laboratory stock was added. The gel was poured into a casting tray and a comb was introduced to position the wells. Once the gel had solidified, the comb was removed. The gel was placed into a gel tank filled with TBE buffer. Loading dye (NEB) was added to each sample, and loaded into the wells, along with the DNA ladder (2-log or 1 kb ladder, NEB). Typically, the gel was run for approximately 60 minutes at 100 V, and later visualised on a gel doc imaging system (Syngene or AlphaImager) under a UV lamp.

2.7.2 Sodium dodecyl sulphate polyacrylamide gel electrophoresis

Samples were separated and visualised under denaturing conditions by a 12% sodium dodecyl sulphate polyacrylamide gel electrophoresis (SDS-PAGE, [18]). A 10 mL resolving gel – 3.2 mL of water, 4 mL of acrylamide/bis-acrylamide (30%/0.8% w/v), 2.6 mL of 1.5 M Tris pH 8.8, 0.1 mL of 10% (w/v) SDS, polymerised with 100 µL of 10% (w/v) ammonium persulfate (APS) and 10 µL of *N,N,N',N'*-tetramethylethylenediamine (TEMED) – was cast using a Hoefer Mighty Small kit, and allowed to set. The stacking gel – 2.975 mL of water, 1.25 mL of 0.5 M Tris-HCl pH 6.8, 0.05 mL of 10 % (w/v) SDS, 0.67 mL of acrylamide/bis-acrylamide (30%/0.8% w/v), polymerised with 50 µL 10% (w/v) APS and 5 µL TEMED – was immediately poured on top of the solidified resolving gel. A well comb was inserted, and the gel was left to set. Typically, 20 µL samples were mixed with 5 µL 1× loading buffer (5×; 0.2 M Tris pH 6.8, 20% (v/v) glycerol, 10% (w/v) SDS, 0.05% (w/v) bromophenol blue, 10 mM dithiothreitol (DTT)) and denatured for 10 minutes at 95 °C. When running the gel under non-reducing conditions, DTT was not added to the samples. The

samples were then pipetted into the wells, alongside the molecular weight marker (10 μL) (ColourPlus Prestained protein ladder, NEB) in a separate well. Electrophoresis occurred in SDS-PAGE running buffer (25 mM Tris pH 8.3, 200 mM glycine, 0.1% (w/v) SDS) at 180 V and allowed to run until loading dye ran off the bottom of the gel. The gel was then stained with Instant Blue stain (Expedeon) for 15–30 minutes, briefly washed with water, and imaged (Syngene).

2.7.2.1 Silver staining

For silver staining the gel [19], the SDS–PAGE (method 2.7.2) was firstly prefixed in ~ 200 mL 50% (v/v) methanol, 10% acetic acid at 37 ˚C for 30 minutes, and then prefixed in ~ 200 mL 50% (v/v) methanol, 7% acetic acid at 37 ˚C for 30 minutes. The gel was washed briefly in deionised water and, in the fume hood, carefully placed in 150 mL gluteraldehyde for 30 minutes at 37 ˚C. The gel was rinsed again and excess gluteraldehyde was removed by soaking it in deionized water overnight at 37 ˚C. The following day, the gel was rinsed and washed at 37 ˚C in 5 μg/mL DTT for 30 minutes. The DTT was poured off and, without rinsing, 0.1% (w/v) $AgNO_3$ was added (150 mL). The gel was shaken at 37 ˚C for 30 minutes. The gel was rinsed briefly in deionised water and then developed with 150 mL 3% (w/v) Na_2CO_3 containing 75 μL 37% formaldehyde. Staining was stopped once the appropriate density had been reached with 7.5 mL of 2.3 M citric acid. The gel was washed six times with deionised water, soaked for another 10 minutes in 0.3% (v/v) Na_2CO_3 and then rinsed again in deionised water.

2.7.3 10–20% Tris-Tricine precast gel

A 10–20% Tris-Tricine precast gel was acquired from BioRad. The buffers were prepared as followed: Loading sample buffer recipe (×6) – 100 mM Tricine pH 8.8, 40% glycerol, 4% SDS, ~ 2% bromophenol blue. Anode buffer recipe – 100 mM Tris pH 8.8. Cathode buffer recipe – 100 mM Tricine, 100 mM Tris, 0.1 % SDS. After adding the loading buffer to the samples, these were heated at 92 ˚C

for 5 minutes, following manufacturer instructions. 10 μL of Prestained Colourplus ladder (NEB) was loaded, and ~ 25 μL of each sample was loaded per well. The gel was run at 100 V for 90 minutes, or until dye front leaves the bottom of the gel.

2.7.3.1 Fluorescent imaging

Before staining, the 10–20% Tris-Tricine precast gel (method 2.7.3) was imaged using a Typhoon FLA 9500 (GE). Parameters: laser – 635 nm; Filter – LPR; Channel – standard Alexa Fluor 647.

2.7.4 4–12% Bis-Tris precast gel

A gradient 4–12% Bis-Tris precast gel (NuPAGE, Thermo Fisher Scientific, catalog #NP0322BOX) was used to analyse the His-tagged phage on the pull-down assay (Chapter 3, Fig. 3.13), and the DNAzyme experiments (Chapter 3, Fig. 3.18). Samples were diluted in LDS sample buffer (NuPAGE, Thermo Fisher Scientific, catalog #NP0007), and denatured at 90 °C for 10 minutes, following manufacturers' instructions. Typically, ~ 10 μL of diluted samples were added per well, along with 10 μL of pre-stained protein standard (Novex, Thermo Fisher Scientific, catalog #LC5800). The gels were resolved in MES SDS running buffer (NuPAGE, Thermo Fisher Scientific, #NP0002) for approximately 35 minutes at 200 V. After electrophoresis, gels were placed in deionized water and microwaved for about a minute until solution almost started to boil, and left to shake for 2 minutes. This process was repeated 2 more times. ~ 30 mL of SimplyBlue SafeStain (Thermo Fisher Scientific, catalog #LC6060) was then added, and the gels microwaved for ~ 1 minute until solution almost boils. The gels were shaken for 10 minutes, and then washed with water for 10 minutes. Finally, a solution of 20% NaCl was added to the gels for 10 minutes. The gels were then visualised under white light, and pictures were collected.

2.7.5 Western blot

A 4-20% Criterion TGX Stain-Free precast gel was run for ~ 50 minutes at 170 V (until dye front has reached the bottom of the gel). The gel was then imaged on ChemiDoc MP (Stain-free enabled) and Image Lab Software with settings for 'best sensitivity' and 'faint bands' (~ 5 minutes exposure). For the Western blot [20], the gel was transferred onto a PVDF membrane (Trans-Blot Turbo Midi PVDF Transfer Packs, 1704157) using the Trans-Blot Turbo Transfer System with the appropriate settings. The membrane was blocked overnight in 10% milk in PBS buffer. The following day, the membrane was incubated overnight in 0.1% milk in PBS with 0.2 μg primary antibody (anti-his_6, Roche, 1922416). The membrane was washed in 1x PBS-Tween, three times every 20 minutes for 1 hour, followed by a 2 hours incubation with 0.1% milk in PBS with 1:2500 dilution of secondary antibody (anti-mouse IgG, HRP conjugate, W402B). The membrane was successively washed 1x PBS-Tween, three times every 20 minutes for 1 hour. The blot was incubated for 5 minutes in a 1:1 mix of Clarity Western ECL Blotting Substrates, and image on Image Quant LAS4000 (auto exposure time). Markers: 10 μL Amersham Low Molecular Weight Calibration Kit for SDS Electrophoresis (17-0446-01); 4 μL BenchMark His-tagged Protein Standard (Catalog #LC5606).

2.8 Spectroscopy techniques

2.8.1 MALDI-TOF mass spectrometry

Matrix-assisted laser desorption/ionisation time-of-flight (MALDI-TOF, [21]) spectra were taken on a Voyager DE-STR system (Applied Biosystems) on linear mode, and data was collected and analysed with support from Dr. Brasino. Phage samples were denatured at 95 ˚C for 5 minutes, and some of the samples were also desalted (Zeba Spin columns, Thermo Fisher Scientific). Not desalting the samples would result in less resolved spectra. Typically, 5 μL of trihydroxyacetophenone (THAP) matrix was mixed with 5 μL of phage sample, and 2 μL of this was loaded onto the MALDI-TOF plate. The sample-matrix droplet was allowed to completely dry before measurements. THAP matrix is

made of 18 mg trihydroxyacetophenone, 5 mg ammonium citrate dibasic, in acetonitrile:water (50:50), made up to 1 mL.

2.8.2 Linear dichroism and fluorescence detected linear dichroism

Linear dichroism (LD) and fluorescence detected linear dichroism (FDLD) experiments were carried out using Jasco J-720, Jasco J-815 and Jasco J-1500 spectropolarimeter. Typically, 60–80 μL samples were pipetted into a quartz Couette cell, assembled with the quartz capillary rod, and placed inside the LD chamber. A baseline was recorded in a non-spinning mode and the resultant spectrum was subtracted from the measured samples. Samples were measured in spinning mode at ~ 3000 rpm. The FDLD experiments had a similar design, except for a cut-off filter (Semrock) which is added in from of the apparatus detector, as described in the main body of the thesis. Table 3.1 (Chapter 3) highlights the main parameters used for these measurements.

2.8.2.1 Thermostability of phage particles

The effect of temperature on the structural stability of mutant and wild-type phage particles was evaluated by LD (Chapter 5, Fig. 5.7). Several phage aliquots in PBS buffer were incubated at increasing temperatures on a thermocycler for 5 minutes, from 20 ˚C to 100 ˚C with 10 ˚C increments. While collecting the spectra, the LD cell apparatus was kept at the temperature being tested.

2.8.2.2 Linear dichroism-based immunoassay

Typically, 40 μL of functionalised phage sample was diluted in 60 μL of buffer; 80 μL of this mix was then transferred into the LD quartz cell. The immunoassay was performed by carefully mixing 10 μL of a bacterial stock (*E. coli* and *Salmonella* (Insight Biotechnology, #50-95-90 and #50-74-01) or gamma-irradiated bacteria (method 2.6.2.1)) diluted to the intended concentration, with 40 μL of phage sample and 50 μL of buffer. This was left to incubate at room temperature for 5 minutes, and 80 μL of this mixture was measured. Alternatively, phage samples were diluted to LD_{225} ~ 0.01-0.02 prior

to performing the immunoassay (for example, when comparing different phage samples across independent LD immunoassays (Chapter 5, Fig 5.11)). When indicated, the phage LD spectra was normalised at a single wavelength (225 nm) to simplify comparison between samples in another region of the spectra.

2.8.2.3 Phage induced alignment on a quartz window

A sample of phage was induced to align on a quartz window for LD measurements. For this, two layers of a 20 μL drop (5 mg/mL wild-type phage stock on water) were dried on a circular quartz window. The first drop was added onto the middle of the window, and then, with a pipette tip, induced to orient/dry in one direction (*i.e.* horizontally dragging the drop with the tip, from left to right, until the surface of the window looked dry); a second 20 μL drop was added and the procedure repeated. The quartz window was then attached in front of the detector and LD was measured. A blank (*i.e.* the quartz window with nothing on it) was previously recorded, and subtracted from the measured LD. This same quartz window with dried phage was manually rotated by 90 ° to measure the LD data named as "90 degrees rotation", given on Fig. 3.21 (Chapter 3).

2.8.3 Circular dichroism

0.1 mg/mL of FITC-conjugated wheat germ agglutinin (WGA-FITC) in phosphate buffer before and after reaction with SMCC were analysed by circular dichroism (CD) spectroscopy. CD experiment was carried out on a Jasco J-1500 spectropolarimeter using a 1 cm quartz cuvette. A baseline was recorded using phosphate buffer and subtracted from the sample spectra. Parameters – Range: 200–260 nm, Response: 1s, Data pitch: 0.5 nm, Scanning mode: Continuous, Scan speed: 100 nm/min, Band width: 1 nm, Number of accumulations: 3.

2.8.4 Dynamic light scattering

Dynamic light scattering (DLS) measurements were obtained with a Malvern Zetasizer Nano-series Range. A 600-seconds equilibration time at 20 °C was set before starting measurements, using ~ 100 μL of each phage sample pipetted into

disposable cuvettes. Eight measurements over ten runs were recorded, and the results were averaged and plotted.

2.9 Colorimetric tests

2.9.1 p-nitrobenzaldehyde test

The p-nitrobenzaldehyde (p-NBA) test [13] was used to confirm the presence of hydrazine moieties to the phage surface (Chapter 5). A 0.5 mM p-nitrobenzaldehyde stock was prepared by initially dissolving the compound at a higher concentration in organic solvent (DMSO) and then adding the appropriate aliquot to 100 mM acetate buffer, pH 5 to result in the final concentration. An aliquot of the SANH-modified phage was added to the p-nitrobenzaldehyde solution, and incubated for 2 hour at 37 ˚C. Absorbance spectra was collected, and signal measured at 390 nm, against a blank prepared by addition of an equal aliquot of buffer in p-NBA solution. The p-NBA test was used to check for the modifications of the phage surface with SANH. The hydrazine modification level of the phages can be estimated quantitatively. The absorbance of the chromophore was measured at 390 nm and concentration calculated using the molar extinction coefficient. The ratio hydrazine/phage can then be estimated by dividing the hydrazine concentration by the phage concentration (mol/L).

2.9.2 Purpald test

The presence of aldehydes on a drop of $NaIO_4$–treated antibody was confirmed by a colorimetric change to purple, upon adding a freshly prepared solution of 4-amino-3-hydrazino-5-mercapto-1,2,4-triazole (Purpald, Alfa Aesar) in sodium hydroxide [13].

2.9.3 Ellman's reagent test

5,5-dithio-bis-(2-nitrobenzoic acid) (DTNB, Ellman's reagent, Thermo Fisher Scientific) was used to confirm the presence of cysteines on the surface of the V31C phage (Chapter 5). 25 µL of 1 mg/mL V31C phage was diluted in 25 µL

of 100 mM phosphate 1 mM EDTA buffer, and mixed with 50 µL of a 4 mg/mL Ellman's reagent. In a few seconds, the solution turned into a bright yellow, indicating the presence of thiol groups on the V31C phage. This colorimetric change was not noticeable in wild-type phage.

2.10 Magnetic beads-based protocols

2.10.1 Pull-down assay using nickel-chelating beads

This assay tested the ability of the His-tagged phage to bind to nickel ions-coated surfaces. Nickel-chelating magnetic beads (HIS-select nickel magnetic agarose beads, Sigma #H9914) were used to capture His-tagged phage, following manufacturer's instructions. ~ 150 µg of untagged phage (control) and His-tagged phage were added to 20 µL of an uniformly dispersed beads suspension, and incubated for approximately 30 minutes. The mixture of phage and beads was placed in a magnetic separator, and the supernatant was collected and saved for gel analysis (Chapter 3, Fig. 3.13, labelled as "Supernatant"). The beads were briefly washed with washing buffer (50 mM sodium phosphate, 300 mM NaCl, 10 mM imidazole) and collected with the magnetic separator. 100 µL of elution buffer (50 mM sodium phosphate, 300 mM NaCl, 250 mM imidazole) was added to the beads-phage, and incubated for 15 minutes. Finally, the beads-phage samples were placed in the magnetic separator and the supernatant was collected and saved for gel analysis (Chapter 3, Fig, 3.13, labelled as "250 mM imidazole elution").

2.10.2 Magnetic beads purification of LD immunoassay samples

100 µL of protein A magnetic beads (SureBeads, Biorad) were resuspended and briefly washed in 500 µL of PBS-T (PBS + 0.1% Tween-20) buffer. The beads were magnetised using a magnetic separator rack, and the supernatant was discarded. This step was repeated two more times. 300 µL of an immunoassay sample was mixed to the beads, and this mixture was rotated for 1 hour at room temperature. The beads were then captured using the magnetic separator, and the supernatant (the immunoassay sample) was collected to re-test on the LD

immunoassay. The magnetic beads were kept for further analysis on a silver stained SDS-PAGE.

2.11 General cloning techniques

2.11.1 Recipe for LB medium and LB/agar plates

To prepare 500 mL of lysogeny broth (LB), 5 g of tryptone (Oxoid), 2.5 g of yeast extract (Sigma), and 2.5 g of NaCl (Sigma) were added to deionised water. After autoclaving and cooling down the medium, the appropriate antibiotic was added. Plates were prepared by adding either 15 g/L or 7 g/L of agar (Difco) to the LB medium, to make 1.5% "hard" agar plates or 0.7% "soft" agar plates (commonly used in phage techniques, method 2.3.1). The LB/agar solution was then autoclaved, briefly cooled down, and the appropriate antibiotic was added (generally, tetracycline or kanamycin). When using XL-1 blue competent cells, plates also contained isopropyl β-D-1-thiogalactopyranoside (IPTG, Sigma) to a final concentration of 20 mM, and 5-bromo-4-chloro-3-indoyl-β-D-galactopyranoside (X-gal, Bioline) to a final concentration of 80 μg/mL. The LB/agar/antibiotic solution was immediately poured into sterile petri dishes and left to solidify on a laminar flow cabinet. Plates were wrapped in parafilm and stored in the fridge for up to a week.

2.11.2 Making competent cells

The protocol was followed as per [4]. One mL of a 5 mL overnight *E. coli* culture was added to 100 mL of LB media and incubated at 37 ˚C until OD_{600}~ 0.4. The bacterial culture was split into two 50 mL Falcon tubes and incubated on ice for 30 minutes. The incubated cells were centrifuged at 2700 × *g* for 10 minutes at 4 ˚C, the supernatant was discarded and tubes were inverted and set a paper towel to dry for 1 minute. The bacterial pellet was resuspended with gentle vortexing in 30 mL of chilled 0.08 M $MgCl_2$/0.02 M $CaCl_2$. The resuspended cells solution was spun at 2700 × *g* for 10 minutes at 4 ˚C, decanted and dried as before. The bacterial pellet was resuspended in 2 mL of 0.1 M $CaCl_2$. 70 μL of DMSO was then added and the bacterial solution was gently swirled, and left on

ice for 15 minutes. Another 70 μL of DMSO was added and the tubes were again gently swirled to mix. 200 μL of the bacterial solution was then dispensed in pre-chilled eppendorfs, and frozen in liquid nitrogen. The competent cells were stored at the –80 ˚C freezer.

2.11.3 Preparing *E. coli* cultures

A liquid culture of *E. coli* was streaked onto a LB/agar plate supplemented with the appropriate antibiotic (method 2.11.1) and incubated overnight at 37 ˚C. A single colony was then picked (method 2.11.4.5) and grown in LB medium supplemented with the appropriate antibiotic, overnight at 37 ˚C, shaking at 200 rpm. A final concentration of 20% (v/v) glycerol was added to the *E. coli* culture. Stock cultures were stored at the –80˚C freezer. Working cultures were prepared by inoculating LB medium with an aliquot (10–100 μL) of the stock culture, and incubated overnight at 37 ˚C, 200 rpm.

2.11.4 Cloning on a fd phage vector

Genetic engineering the p3 and p8 proteins of the phage was explored, to build phage mutants (Chapter 5). Standard molecular techniques were employed [4]. The cloning illustrated in Table 2.1 was done on a phage cloning vector derived from the fd-tet phage (termed f8 when the display of the foreign peptide was done on every copy of the p8 protein, or mosaic f88 when the display of the foreign peptide was done on the synthetic p8 proteins), containing a tetracycline resistance gene and restriction sites within the phage proteins. Therefore, the term “wild-type” or “control” used on the experiments presented on the main body of the thesis refers to the non-mutated fd phage.

Phage constructs	Phage protein	Primers set	Restriction Enzymes
His-tagged phage	WT p3	R: 5′ GGCCGCATGGTGATGATGGTGGTGCATGGCCACGT 3′ F: 5′ TGGCCATGCACCACCATCATCACCATGC 3′	NotI SfiI
TRP mutant phage	WT p8	R: 5′ GATCCTCTCCTCCCCACTCTTGCA 3′ F: 5′ GAGTGGGGAGGAGAG 3′	BamHI PstI
V31C phage	WT p8	R: 5′ TGCGCCGACAATGCAAACAACCATCGC 3′ F: 5′ GCGATGGTTGTTTGCATTGTCGGCGCA 3′	–
MSal17 phage	Synthetic p8	R: 5′ GGGCCGCCGCCGTGGTGAAGCCAGAATTGTGCCGAATCGGGGCGGTTGGCAA 3′ F: 5′AGCTTTGCCAACCGCCCCGATTCGGCACAATTCTGGCTTCACCACGGCGGCGGCCCTGCA 3′	HindIII PstI

Phage plasmids	Source	Reference
M13mp18	New England Biolabs	[4]
f8 and f88	Cha's lab bacteriophage collection (Boulder, USA)	[2, 24]

Table 2.1: List of primers and restriction enzymes, and of phage plasmids. Oligonucleotide set of primers and restriction enzymes used for cloning on the synthetic p8, wild-type (WT) p8 and p3 proteins of the phage, to build the His-tagged, extra tryptophan (TRP), *Salmonella*-binding (MSal17) and V31C mutant phages. Phage plasmids were used for the cloning work described below.

Bacteria strains	Genotype	Source	Reference
Escherichia coli TOP10 F'	F′{*lac*Iq, Tn*10*(TetR)} *mcr*A Δ(*mrr-hsd*RMS-*mcr*BC) Φ80*lac*ZΔM15 Δ*lac*X74 *rec*A1 *ara*D139 Δ(*ara leu*) 7697 *gal*U *gal*K *rps*L (StrR) *end*A1 *nup*G	Thermo Fisher Scientific	–
Escherichia coli K91Kan	Hfr-C lacZ mkh thi	Cha's lab bacteria culture collection (Boulder, USA)	[2, 22]
Escherichia coli DH5α	F^- Φ80*lac*ZΔM15 Δ(*lac*ZYA-*arg*F) U169 *rec*A1 *end*A1 *hsd*R17 (rk^-, mk^+) *pho*A *sup*E44 λ^- *thi*$^-$1 *gyr*A96 *rel*A1	Thermo Fisher Scientific	–
Escherichia coli XL1-blue	recA1 endA1 gyrA96 thi-1 hsdR17 supE44 relA1 lac [F′ proAB lacIqZΔM15 Tn10 (TetR)]	Stratagene (Agilent Technologies)	–
Salmonella enterica spp.	–	Collection from the Agri-Food and Bioscience Institute (Belfast, UK)	[16, 23]

Table 2.2: List of bacterial strains. These bacteria were used for growing bacteriophage cultures and for the cloning work described in this thesis.

2.11.4.1 Annealing oligomers

This method was carried out to construct the His-tagged, extra tryptophan (TRP) and MSal17 mutant phages. 1 μL of each oligomer/primer (reverse and

forward, with the restriction cutting sites, Table 2.1) were diluted in 18 µL of annealing buffer (10 mM Tris, 50 mM NaCl, 1 mM EDTA pH 7.3). This was briefly incubated at 95 ˚C for 5 minutes, and left to anneal at room temperature for approximately 1 hour.

2.11.4.2 Cloning vector digestion and extraction

The f8 or f88 cloning vector (derived from the fd-tet phage) was digested with the appropriate restriction enzymes for approximately 1 hour at 37 ˚C, and the product was run on a 2% agarose gel (method 2.7.1). The digested vector was excised from the gel under a UV lamp and extracted using a gel extraction kit (Qiagen, QIAquick #28704), following suppliers' recommendations.

2.11.4.3 DNA ligation

Ligation reactions were conducted following protocols provided by the enzyme suppliers (New England Biolabs, NEB). Typically, 1 µL of T4 ligase enzyme and 2 µL of ligation buffer were added per 20 µL of total volume of ligation reaction. Molar ratio of vector to DNA insert varied, but generally 7 µL of DNA fragment (annealed product from method 2.11.4.1) was mixed with 10 µL of cloning vector (method 2.11.4.2), and incubated for 6 hours at 16 ˚C, followed by inactivation of the enzyme at 65 ˚C for 10 minutes.

2.11.4.4 Transformation of competent *E. coli* cells

An aliquot of competent cells (DH5α from Thermo Fisher Scientific, or *E. coli* K91Kan cells, method 2.11.2) was gently thawed on ice. 3-5 µL of ligation reaction (method 2.11.4.3) was mixed to 100–200 µL of cells, and left on ice for 30 minutes. The cells were then subjected to a heat shock of 42 ˚C for 45 seconds. The transformed cells were chilled on an ice bath for 5 minutes, and 800–900 µL of super optimal broth (SOC, NEB) medium was added. The cells were incubated at 37 ˚C for one hour. Then, 200 µL of the incubated cells were plated on previously set 1.5% LB/agar/antibiotic plate, and allowed to grow overnight at 37 ˚C.

2.11.4.5 Picking single *E. coli* colonies

Each isolated *E. coli* colony, infected with the replicative form dsDNA of the phage, was picked from the LB/agar/tetracycline plate with a sterile loop, transferred to 5 mL of LB/tetracycline medium, and allowed to grow for 20 hours at 37 ˚C, 200 rpm.

2.11.4.6 Miniprep

The miniprep procedure was done using a Qiagen kit, following manufacturers' instructions. Briefly, an overnight *E. coli* culture (method 2.11.4.5) was centrifuged and the resulting cell pellet was resuspended in Qiagen P1 buffer with ribonuclease. P2 buffer was then added to the cell suspension and the tube was gently inverted several times. This mixture was centrifuged and the supernatant was applied to a miniprep column (Qiagen). The columns were centrifuged and the flow through was discarded. PB buffer was applied to the column and centrifuged. PE buffer with ethanol was applied to the column and centrifuged. The flow through was discarded and the column was centrifuged again to remove any residual ethanol. 30-40 μL of water was applied directly to the center of the column membrane and left to stand for 2 minutes before undergoing centrifugation. The eluted sample, containing the plasmid phage DNA, was collected, and the DNA concentration was determined using a Nanodrop. If necessary, the DNA product was sent to sequencing, to confirm the success of the cloning protocol.

2.11.4.7 Growing the mutant phage constructs

If sequencing confirmed successfully mutagenesis, the minipreped DNA was again transformed into competent cells (method 2.11.4.4) and plated on LB/agar/antibiotic plates. A few colonies were then picked (method 2.11.4.5) and grown in ~ 40 mL of LB/antibiotic medium for 20 hours at 37 ˚C, 200 rpm. Phages were subsequently purified by PEG/NaCl precipitation as before (method 2.2.1), and stored in fridge in the desired buffer. Perhaps, the yield of

mutant phages production would benefit from optimising the growing conditions, however this was not explored in this thesis.

2.11.4.8 Site directed mutagenesis

Site directed mutagenesis by polymerase chain reaction (PCR) was conducted to replace a valine of the wild-type p8 protein for a cysteine, originating the V31C phage (Chapter 5). The oligo-primers were designed following QuikChange (Stratagene) guidelines. A PCR reaction was set using: 1 µL of a 1:40 dilution of each primer (Table 2.1), 0.5 µL of deoxynucleotide triphosphates mix (dNTPs, NEB), 5 µL of 5× red buffer (NEB), 2 µL of template DNA (phage vector, 2 ng/µL), 0.5 µL of Phusion HF polymerase (NEB), made up to a total of 25 µL in water. The cycling program instructed into the thermocycler (GeneAmpPCR System 9700) was 5 minutes at 95 ˚C, followed by 50 seconds at 95 ˚C, 50 seconds at 60 ˚C, 1 minute per kb of template at 68 ˚C, for 18 cycles, and then extension time at 68 ˚C for 7 minutes. Methylated DNA was digested with 0.5–1 µL DpnI enzyme (NEB) for 1 hour at 37 ˚C. The digested PCR product was then transformed into competent cells (method 2.11.4.4), and a few colonies were picked (method 2.11.4.5). Minipreps of phage DNA (method 2.11.4.6) were sequenced to check if clones contained the desired mutation, and the successful clones were grown into the V31C phage (as in method 2.11.4.7).

2.11.5 Cloning on a M13mp phage vector

2.11.5.1 Longer mutant phage constructs

The pQR226 plasmid (from the Ward lab collection, at UCL) was utilised as a source plasmid for the generation of sticky-end DNA fragments by restriction digestion. The pQR226 plasmid was cut with KpnI (2 sites) or with BamHI (2 sites) restriction enzymes (NEB) which generates two fragments, one of approximately 1 kb and another of 4 kb, respectively. After digesting the source plasmid with the restriction enzymes for 1 hour at 37 ˚C, the DNA fragments were run and excised from a 2% agarose gel (method 2.7.1). The digested

fragments were excised from the gel under a UV lamp and extracted using a gel extraction kit (Qiagen, QIAquick #28704), following suppliers' recommendations. Similarly, the cloning vector (M13mp18 plasmid, NEB) was digested with restriction enzymes, ~ 1 µL KpnI for the "+ 1kb" construct and ~ 1 µL BamHI for the "+ 4kb" construct, and extracted from a 2% agarose gel (method 2.7.1). The 1 kb and 4 kb fragments were then ligated with the digested M13mp18 cloning vector (as in method 2.11.4.2) and transformed into XL-1 blue competent cells (Agilent). For this, 50 µL of XL-1 bue competent cells were mixed with ~ 5 µL of the ligation mixture for transformation. This mixture was left on ice for 20 minutes, and was then subjected to a heat shock at 42 ˚C for 45 seconds. The transformed cells were then left on ice for 3 minutes. 200 µL of LB medium was added to the transformed cells and briefly mixed. 100 µL of this mixture was added to ~ 4 mL of 0.7% LB/agar (containing 200 µL of *E. coli* cells, IPTG, and X-gal), and gently mixed. Immediately after, the mixture was poured onto a 1.5% LB/agar plate, and quickly but gently swirled clockwise to evenly distribute the LB/agar over the surface. The plate was left to set on a laminar flow hood, and incubated for 16 hours, at 37 ˚C. The following day, the recombinant plasmids were selected by blue-white colour screening. Single isolated white plaques were picked from the plates using a sterile loop or a pipette tip, and transferred into 5 mL of LB/tetracycline medium inoculated with an overnight culture of *E. coli* cells, and allowed to grow overnight at 37 ˚C, 200 rpm. The cultures were then miniprep (method 2.11.4.6). The collected plasmids were run on a diagnostic digestion gel and sequenced, to confirm the phage plasmids contained the inserted DNA fragments. If cloning was successful, a ~ 100 µL aliquot of the cultured mutant phage (used for the miniprep) was added to 40 mL of LB/tetracycline medium inoculated with ~ 200 µL of *E. coli* cells, and incubated overnight at 37 ˚C, 200 rpm. The next day, the phage was purified by PEG/NaCl precipitation (method 2.2.1).

2.12 References

1. Pacheco-Gomez, R. *et al.* Detection of pathogenic bacteria using a homogenous immunoassay based on shear alignment of virus particles and linear dichroism. *Anal. Chem.* **84,** 91–97 (2012).
2. Brasino, M., Lee, J., Cha, J. Creating highly amplified enzyme-linked immunosorbent assay signals from genetically engineered bacteriophage. *Anal. Biochem.* **470,** 7–13 (2014).
3. Yamamoto, K. *et al*. Rapid bacteriophage sedimentation in the presence of polyethylene glycol and its application to large-scale virus purification. *Virology* **40,** 734–744 (1970).
4. Sambrook, J., Russel D. *Molecular cloning: A laboratory manual* (CSHL Press, 2001) ISBN: 0879695773
5. Monjezi, R. *et al.* Purification of bacteriophage M13 by anion exchange chromatography. *Journal of Chromatography B.* **878,** 1855–1859 (2010)
6. Kropinski, A. *et al*. Enumeration of bacteriophage by double agar overlay plaque assay. *Bacteriophages* in *Method in Molecular Biology* book series (Springer, 2009) ISBN: 9781588296825
7. Miles, A., Misra, S., Irwin, J. The estimation of the bactericidal power of the blood. *J. Hyg. (Lond).* **38,** 732–749 (1938).
8. Ikehara, K. *et al.* Studies on the structure of filamentous bacteriophage fd. Physicochemical properties of phage fd and its components. *Bull. Inst. Chem. Res.* **51**, 140-152 (1973)
9. Casadevall, A., Day, L. DNA packing in the filamentous viruses fd, Xf, Pfl and Pf3. *Nucleic Acids Res.* **10,** 2467–2481 (1982).
10. Henry, T., Pratt, D. The proteins of bacteriophage M13. *Proc. Natl. Acad. Sci.* **62,** 800–807 (1969).
11. Berkowitz, S., Day, Loren. Mass, length, composition and structure o the filamentous bacterial virus fd. *J. Mol. Biol.* **102**, 531-547 (1976).
12. Chung, W., Lee, D., Yoo, S. Chemical modulation of M13 bacteriophage and its functional opportunities for nanomedicine. *International Journal of Nanomedicine* **9**, 5825–5836 (2014).
13. Hermanson, G. *Bioconjugation techniques* (Academic Press, 2013) ISBN: 9780123822390
14. Domaille, D., Lee, J., Cha, J. High density DNA loading on the M13 bacteriophage provides access to colorimetric and fluorescent protein microarray biosensors. *Chem. Commun.* **49,** 1759–1761 (2013).
15. Engvall, E., Perlmann, P. Enzyme-Linked Immunosorbent Assay. *The Journal of Immunology **109***, 129–135 (1972).
16. Wang, J. *et. al.* Rapid detection of pathogenic bacteria and screening of phage-derived peptides using microcantilevers. *Anal. Chem.* **86**, 1671–1678 (2014).
17. Lee, P. *et al.* Agarose gel electrophoresis for the separation of DNA fragments. *Journal of Visualized Experiments* **62**, 1–5 (2012).
18. Laemmli, U. Cleavage of structural proteins during the assembly of the head of bacteriophage T4. *Nature* **227**, 680–685 (1970).

19. Morrissey, J. Silver stain for proteins in polyacrylamide gels: A modified procedure with enhanced uniform sensitivity. *Anal. Biochem.* **117**, 307–310 (1981).
20. Burnette, S. Western blotting: electrophoresis of protein from sodium dodecyl sulphate polyacrylamide gels to unmodified nitrocellulose and radiographic detection with antibody and radioiodinated protein A. *Anal. Biochem*. **112**, 195–203 (1982).
21. Singhal, N. *et al*. MALDI-TOF mass spectrometry: An emerging technology for microbial identification and diagnosis. *Frontiers in Microbiology* **6**, 1–16 (2015).
22. Smith, G., Scott, J. Libraries of peptides and proteins displayed on filamentous phage. *Methods Enzymol.* **217**, 228-257 (1993).
23. Morton, J. *et al.* Production and evaluation of the utility of novel phage display-derived peptide ligands to Salmonella spp. for magnetic separation. *J. Applied Microbiol.* **115**, 271–281 (2013).
24. Sidhu, S. *Phage display in Biotechnology and Drug Discovery.* (CRC Press, 2005). ISBN: 9780824754662

CHAPTER 3 – Filamentous bacteriophage as a scaffold for chemical and genetic modifications

3.1 Introduction

The simplicity of the filamentous bacteriophage, combined with its stability, allows for surface chemistry and genetic modulation. Most of its proteins can be chemically manipulated without compromising its functionality, making the phage an attractive platform for controlled and site-specific modifications [1]. The virus is also stable to a broad range of conditions unlike many other biological materials, being resistant to elevated temperatures and the presence of non-aqueous solvents [2]. Although the virus' genome tolerates mutations, this can be problematic as it may disrupt the correct assembly of the bacteriophage particle [2,3] – quite frequently, the only method to assess if the mutation of interest results in a viable phage is by trial-and-error. In that sense, genetic engineering is generally considered to be more time consuming than chemical approaches. In the long term, however, it may counterbalance. Bioconjugation protocols to chemically modify the phage have usually longer hands-on time as they need to be constantly repeated to replenish the used sample; if correctly handled, a genetically modified phage plasmid can be stored almost indefinitely, resulting in a homogeneous sample of the mutated phage particles. As with most things in science, it is a matter of trade-off.

In this chapter, chemical and genetic engineering methods to modify the p3 and p8 proteins of the filamentous phage are explored. Ultimately, some of these modifications will be integrated in phage-based biosensing platforms, as exemplified by the work in Chapter 4 and 5.

3.1.1 Filamentous bacteriophage structure and properties

Filamentous bacteriophages are a family of single-stranded DNA viruses that infect a variety of Gram-negative bacteria, including *Escherichia coli*, *Salmonella enterica*, *Xanthomonas campestris* and *Pseudomonas aeruginosa* [4]. The most well-studied and characterised of these filamentous phages belong to the Ff class, named after their method of host cell infection via the F pilus on the surface of *E. coli* cells. The Ff viruses include the M13, fd and f1 bacteriophages, which possess a > 98% homology at the DNA sequence level [2]. All experiments described in this thesis were done using the M13 and fd phages. The overall structure of these phages is identical, with their p8 protein sequence differing in a single amino acid (M13 has an asparagine at position 12 while the fd phage has an aspartic acid residue).

Ff viral particles are thin and long, semi-flexible filaments, with a diameter of about 6 nm and 800 nm to 1 μm long; interestingly however, the length of the bacteriophage can vary depending on the length of its encapsulated DNA [5] – this specific feature was explored in Chapter 5. Ff phages are not lytic, but opportunistic – the phage release does not result in bacterial cell death; yet, the infected cells grow and divide at a reduced rate [4], which is visible by a much less turbid (and hence, a lower optical density, OD) growth media solution, suggesting less bacterial cells present in the culture. Fig. 3.1 shows a picture of the sidewall of two flasks, one containing an *E. coli* culture not infected with phage, and the other containing an *E. coli* culture infected with the phage.

As described in Chapter 1, Ff phage genome encodes a total of eleven proteins, five of which are structural – 2700 copies of a major coat protein (p8) capped with 3–5 copies of four minor coat proteins (p3 and p6, p7 and p9, on the proximal and distal ends, respectively). An illustration of the filamentous bacteriophage is given in Fig. 3.2.

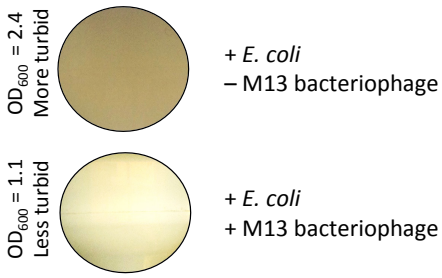

Figure 3.1: Differences in turbidity of a bacterial culture inoculated with phage. Cropped sidewall picture of flasks of a non-infected *E. coli* (TOP10 F') culture and of an *E. coli* culture infected with M13. Although the M13 is a non-lytic phage, it slows down *E. coli* bacterial growth. The decrease of turbidity, indicating fewer *E. coli* cells in solution, is obvious by eye. Both cultures were grown using the same conditions, in LB media, and incubated at 37 °C, for 5 hours. *E. coli* was infected with M13 at the zero hour time point.

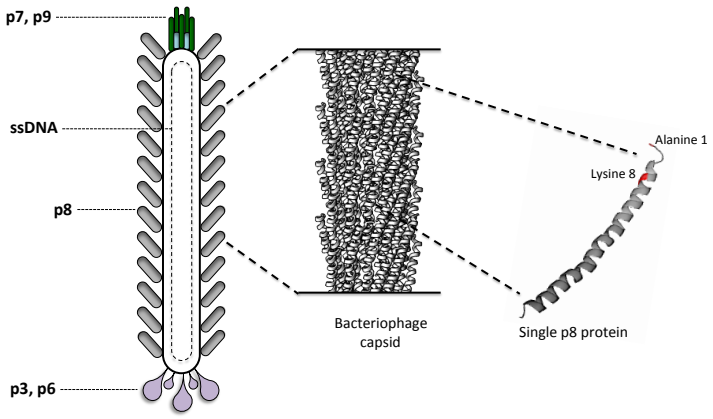

Figure 3.2: Scheme illustrating the structure of the filamentous bacteriophage. The ~ 900 nm filament has five structural proteins and a 6.4 kb single-stranded circular DNA (not drawn to scale). Section of the long axis of the filamentous bacteriophage (PDB entry: 2C0W) made of 2700 copies of assembled p8 proteins along its length. Structure of a single p8 protein, with lysine (Lys 8) and alanine (Ala 1) highlighted in red. Hydrophobic interactions between the adjacent copies of p8 protein are responsible for the packed capsid surrounding the bacteriophage. Bacteriophage illustration adapted from [4].

3.1.2 Filamentous phage as a versatile biomaterial

As illustrated in Chapter 1, multiple groups have taken advantage of the bacteriophage structural features, and also its tolerance to extreme conditions of temperature (> 80 °C), pH (pH 3 to pH 11), and presence of organic solvents [2, 7]. Filamentous phages have been reported as a scaffold in material sciences, such as nanowires and films for nanoelectronic applications [8–10], and in medical sciences, in both diagnostics and therapeutics, such as for bioimaging [11], drug delivery systems [12], as probes for detecting cancer biomarkers [13], and in biosensors for the detection of pathogenic targets [14]. The extensive list of nanotechnology applications relies on the development of methods to chemically and genetically modify the bacteriophages' surface. Furthermore, the filamentous structure of these phages also grants them with the ability to align under flow, which has also been exploited for diagnostic purposes [15].

3.1.2.1 LD and M13 alignment

M13 is a long and thin semi-rigid construct [16] and its alignment in flow on spectroscopy techniques has been investigated [15, 17]. Linear dichroism (LD) is an absorbance-based spectroscopy technique that informs on the orientation of the electronic transition moments of a sample, by using polarized light [18]. LD will be a technique used throughout this thesis, especially on Chapter 5, where different phage designs were integrated in a LD-based diagnostic platform.

The first example of a filamentous bacteriophage LD spectrum was shown by Clack and colleagues, in 1992 [19]. To obtain an LD spectrum, the sample must be induced to align, so ideally, these molecules should have a high aspect ratio. Fig. 3.3 illustrates LD spectroscopy main components and how they contribute to the alignment of filamentous structures.

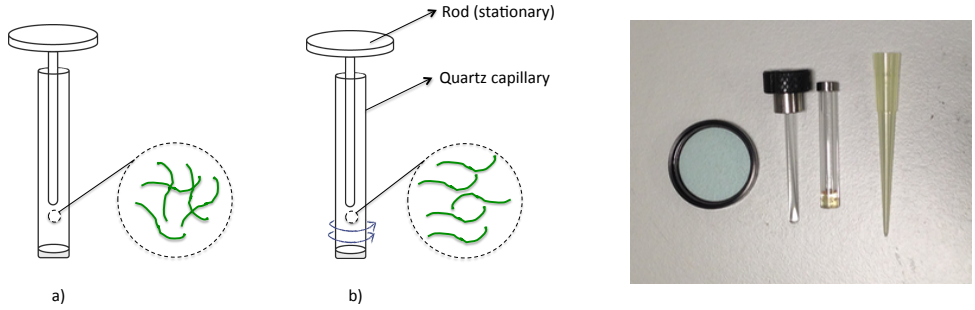

Figure 3.3: Linear dichroism principle and quartz components. (Left) Illustration of an LD quartz Couette flow cell and the principle of LD on the alignment of filamentous particles (green) when shear force is off (a) and on (b) by the rotation of the capillary (blue arrows). (Right) Photo of some of the components for LD and FDLD spectroscopy. From left to right: a filter, a rod and a quartz capillary. Disposable yellow tip for size reference.

LD is mathematically defined as the difference in absorption of light linearly polarized parallel and perpendicular to the orientation axis of a molecule [18]. When the transition moments within a sample are aligned more parallel than perpendicular with respect to its orientation axis, this results in a positive LD signal. A negative LD signal is observed when the transition moments are aligned more perpendicular than parallel in regards to the molecules' orientation axis. In simpler terms, a linear molecule, such as DNA or a filamentous bacteriophage, can align under flow and the degree of its alignment can be measured. Fig. 3.4 shows the M13 filamentous bacteriophage LD fingerprint spectra, using the parameters given in Table 3.1. The signal derived from the viral DNA and the p8 proteins dominates the LD spectrum over the minor coat proteins. The more concentrated the phage sample (hence, more phage particles in the sample), the more intense the LD signal will be – both due to the Beer-Lambert law and inter-particle interactions favouring the phage being parallel to each other. The largest peak detected is in the far-UV region and it corresponds to the electronic transitions from the peptide backbone. Throughout this thesis, the LD signal at 225 nm is tracked for modifications happening to the overall alignment of the phage, because it illustrates alterations to its long orientation axis. The broader peak in the near-UV region is from the absorbance of the aromatic amino acids tryptophan and tyrosine in the p8 protein.

Parameter	LD	FDLD
D.I.T.	1 s	1 s
Bandwidth	1 nm	1 nm
Data pitch	0.2 nm	0.2 nm
Scanning mode	Continuous	Continuous
Scanning speed	100 nm/min	100 nm/min
Accumulations	3	8
HT Voltage	Variable	Variable

Table 3.1: Parameters used for LD and FDLD experiments. All measurements made on Jasco J-815, Jasco J-1500 and Jasco J-720 spectropolarimeter.

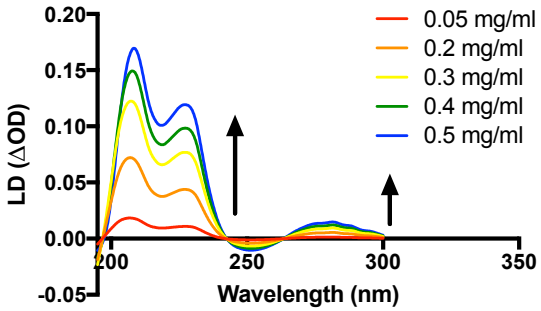

Figure 3.4: Filamentous bacteriophage LD spectra. Example of LD spectra at a range of M13 bacteriophage concentrations in phosphate buffer (Chapter 2, method 2.8.2). The peaks intensity at 225 nm and near-UV region increase with increasing phage concentrations. Measurements recorded using parameters given in Table 3.1.

3.1.2.2 FDLD and M13 intrinsic fluorescence

Fluorescence detected linear dichroism (FDLD) is a spectroscopy technique that follows the same principles as LD, except it detects fluorescence rather than absorbance of the aligned molecules. For this reason, it is considered to be a more sensitive technique [20,21]. This is observable when comparing the near-UV peak of the phage, illustrated in Fig. 3.4 and Fig. 3.5 – for example, at the same concentration of 0.2 mg/mL, the LD signal intensity at 280 nm is 0.0054 and the FDLD signal intensity at 280 nm is 0.0996, an almost 20-fold increase.

The near-UV peak in the phage originates from the two tyrosines and one tryptophan of the p8 protein [1]. This grants the phage with intrinsic fluorescence, which can be measured in a spectrofluorimeter (Fig. 3.5). An important consideration is that of tryptophan emission fluorescence strong dependency to the surrounding microenvironment [20]. The fluorescence properties of the phage were further discussed in Chapter 5, when constructing a longer mutant phage and a mutant phage with an extra tryptophan.

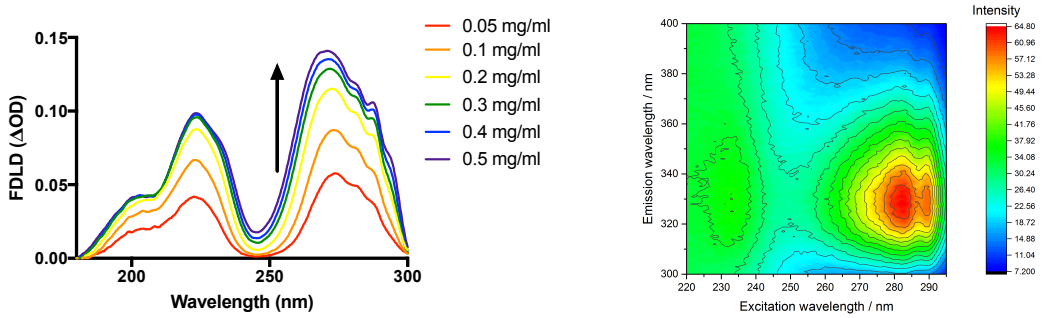

Figure 3.5: Filamentous bacteriophage intrinsic fluorescence. (Left) FDLD spectra of a range of concentrations of M13 bacteriophage (Chapter 2, method 2.8.2). The near-UV peak derives from the aromatic amino acids in the p8 protein, tryptophan and tyrosine. Measurements recorded using parameters given in Table 3.1. A Semrock 300 nm long-pass edge filter was used to block transmitted incident light. (Right) 3D plot illustrating the fluorescence emission intensity at a range of excitation wavelengths, of the aromatic amino acids on the phage surface. Data collected on a Jasco FP-6500 spectrofluorimeter.

3.2 Results and discussion

Chemical and biological approaches for manipulation of the bacteriophage surface were explored. More specifically, we describe modifications to the p3 proteins (section 3.2.1) and to the p8 proteins (section 3.2.2).

3.2.1 Anchoring the phage by one-end

Functionalised-phage particles immobilised onto a surface could be used on the design of M13-based microfluidics biosensing platforms. This type of set-up was

used to develop the work on Chapter 4. It could also be an interesting and useful feature to integrate in the spectroscopy-based biosensor described in Chapter 5.
Anchored phage particles have been previously used as detection elements in biosensing platforms [22–25]. The reported advantage of this set-up over standard immunoassays is that the large surface area of the anchored functionalised phage results in amplified output signals [25]. Anchoring the particle by its p3 protein allows for the surface of the phage, made of 2700 copies of p8 proteins, to be functionalised with molecular recognition elements, such as antibodies. Thus, for example, a biosensing platform using antibody-functionalised phages (*e.g.* anti-*E. coli* antibodies) anchored onto a surface, could be integrated with a microfluidics system for the detection of pathogenic bacteria (*e.g. E. coli*). Another application for the anchored phage particle could be to use it as a nanosensor to detect flow variations – the proof-of-concept to this biosensing platform, with envisioned application on vascular flow imaging, is explored in Chapter 4.

An approach to anchor the phage by one-end could be to chemically or biologically modify the p3 protein. In here, three methods were experimented – immobilising the phage onto a surface by an antibody, by a magnetic bead, and by a His-tag motif. The considerations were costs and overall simplicity of the protocol, time required to complete the protocol, and how easy would it be to transfer this system to a microfluidic biosensor set-up.

3.2.1.1 Anchoring the phage using an antibody

Anchoring the phage using an antibody was the approach chosen for the biosensing platform described in Chapter 4. Although the work in Chapter 4 was the only application in which this set-up was tested, it is believed that it could be easily integrated in different biosensing designs. This method exploited the eight cysteines present on the p3 protein, each of these being involved in disulfide bonds [26]. These disulfide bridges can be broken using a reducing agent, such as TCEP (tris-(2-carboxyethyl)phosphine). The exposed thiol groups can be then conjugated to maleimide groups. A reaction with a bifunctional

reagent, such as SMCC (succinimidyl 4-(N-maleimidomethyl)cyclohexane-1-carboxylate), would then crosslink the thiol groups from the p3 protein of the bacteriophage to the maleimide-modified amino groups of an antibody. Hence, the final product of this reaction is a bacteriophage with antibodies on the p3 protein (*i.e.* an antibody on the end of the phage). A detailed protocol is given in Chapter 2 (method 2.4.1.1), and illustrated in Fig. 3.6. To our knowledge, this was the first report of the cysteines on the p3 proteins being used for this purpose.

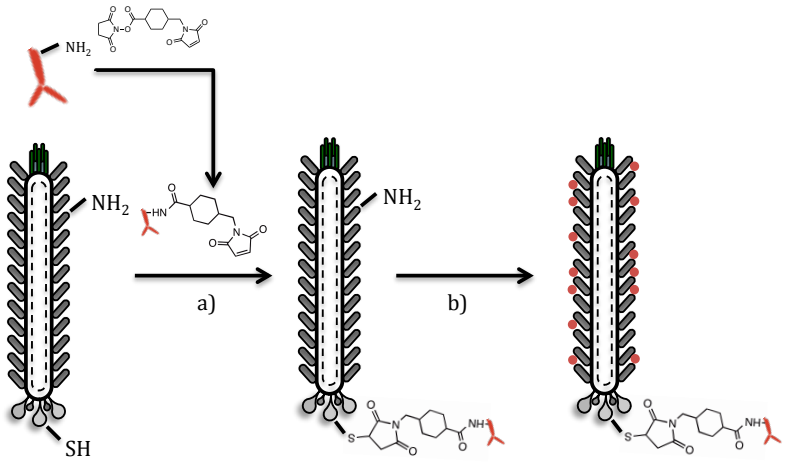

Figure 3.6: Schematic representation of the 2-steps modification of the bacteriophage to conjugate antibody (*i.e.* anti-collagen antibody) and fluorescent dye (*i.e.* TRITC). a) Conjugation of the maleimide-derivatised antibody (maleimide group introduced using SMCC) to the thiol groups (-SH) of the p3 protein. b) Conjugation of the dye (shown as red dots) to the primary amines (-NH_2) of p8 protein, as explored in section 3.2.2.1. Figure not drawn to scale.

It is known, from the M13 genome sequence, that wild-type phage has cysteines in the minor coat proteins – however, the p8 protein can be mutated to have thiol groups on its surface, as explored in Chapter 5. The presence of cysteines on the p3 protein of the bacteriophage was further confirmed by ELISA (enzyme-linked immunosorbent assay). For this, maleimide-coated 96 well-plates were used. The disulfide bonds of wild-type M13 bacteriophage were reduced using TCEP, to produce free sulfhydryls. The reaction was left to incubate for an hour at room temperature and excess reagent removed using a

PD-10 column. Wild-type M13 bacteriophage not reduced with TCEP was used as a control for this experiment. A standard ELISA protocol was then followed (Chapter 2, method 2.6.1), using a horseradish peroxidase (HRP) conjugated anti-M13 antibody to detect for the presence of phage. If the wells with reduced phage turned into a colourful product, we could confirm the coupling between the thiols of the phage and the maleimide molecules anchored to the microplate was successful. If the cysteines on the p3 protein are not reduced, and hence there are no thiol anchoring molecules to attach to the maleimide groups on the wells, the phage would be simply rinsed off the microplate and there would be no colour development. Indeed, these suppositions were observed during an ELISA, as shown in Fig. 3.7.

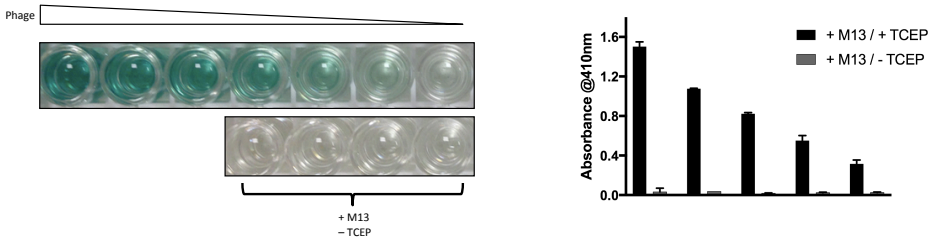

Figure. 3.7: Anchoring the phage onto a maleimide surface. (Left) ELISA picture of serial dilution of the wild-type phage with and without TCEP on a maleimide-coated plate, after adding 2,2'-Azino-bis(3-ethylbenzothiazoline-6-sulfonic acid) (ABTS) solution. (Right) Plot of the average absorbance at 410 nm at decreasing phage concentrations, preceded by a 5 mM TCEP reaction (black bars) or without a TCEP reaction (grey bars). Error bars represent standard deviation from two independent ELISA wells.

The wild-type M13 phage has cysteines residues on the p3 proteins. The ELISA confirmed there are sulfhydryl groups in the phage, as long as a reducing agent (such as TCEP) is added to the reaction. Hence, it was expected the phage was anchored to the surface of the wells by its p3 proteins, only by one end. This explored ability, to anchor the wild-type phage to surfaces by the existing cysteines, is important for the assay described on Chapter 4.

3.2.1.2 Anchoring the phage using a magnetic bead

Anchoring phage particles to a surface could also be achieved using magnetic beads. A seemly straightforward method to attach the phage by one-end to a magnetic bead would be to capture it using anti-p3 antibodies (reactive against p3 proteins of the phage) that have been conjugated to protein A-functionalised beads (the Fc region of antibodies binds to protein A [27, 28]). This final product, of a phage attached to the surface of a magnetic bead via an anti-p3 antibody, will be denominated as phage-bead immunocomplex. An illustration of this set-up is given in Fig. 3.8.

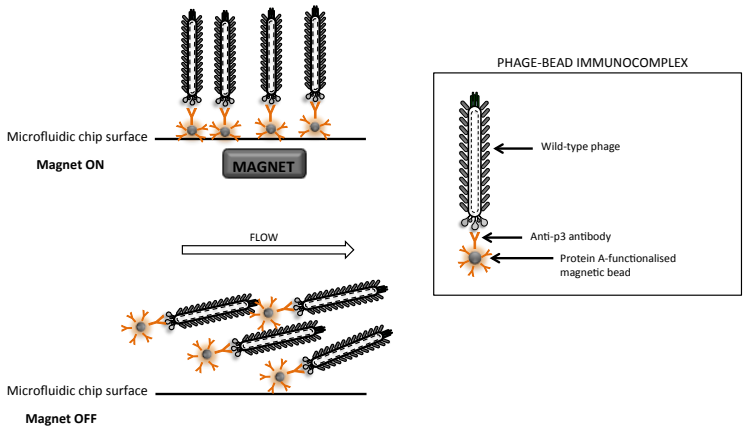

Figure 3.8: Schematics of the idealised phage-bead immunocomplex on a microfluidics set-up. In an ideal scenario, a monolayer of the phage-bead would cover the surface of a microfluidic slide. Not drawn to scale.

The set-up illustrated on Fig. 3.8, using a phage-bead immunocomplex anchored onto a microfluidics platform, was initially designed to integrate in the LD-based biosensor described in Chapter 5. It was hypothesised that this system could improve the range of detection and increase the versatility of the current biosensor. Immobilising the phage particles onto a surface using magnetic beads has the advantage of an easy switching on/off modality (*i.e.* a magnet would be enough to capture/release the phage-bead from the surface). The phage-bead immunocomplex illustrated in Fig. 3.8 would have to be created in a chemically controlled process. One phage per bead was the intended final product – this would cover the surface of a microfluidic set-up, ideally creating a monolayer of

phage-bead particles. The motivation for having only one phage rather than several phages anchored to a bead was simplicity – one phage per bead was believed to be an easier, more predictable system for the subsequent spectroscopy experiments.

In order to integrate the phage-bead immunocomplex into a spectroscopic-based biosensing platform, the size of the magnetic beads is a factor to consider, as large diameter beads would unfavorably increase the amount of light scattered during the spectroscopy measurements. From serial experimentation, it was concluded the commonly used 2.8–1 μm diameter magnetic beads were not compatible with our spectroscopy techniques. A more exhaustive market search revealed that the available magnetic beads that are simultaneously small and functionalised with protein A are limited. Ultimately, 50 nm diameter protein A functionalised magnetic beads were tested to conjugate with the phage. Although the observable effect of light scattering was indeed insignificant, smaller diameter beads were found to be much harder to work with, as they take much longer to sediment with a magnet.

Additionally to the properties of the chosen magnetic beads, the magnet used to capture these beads is another important consideration in the design. The main application of 50 nm magnetic beads is on magnetic-activated cell sorting (MACS), in which high-gradient magnetic field columns are used to capture cells that were tagged with the beads [29]. At a stage where the method was still being devised, these columns were considered to be prohibitively expensive. Standard neodymium magnets were tested instead. Because the application of the purchased magnets is not targeted for immunoprecipitation assays, an experiment was carried out to test whether the neodymium magnets could magnetise the 50 nm magnetic beads. Since these beads are functionalised with protein A, it is possible to label them with an amine-reactive fluorescent dye (such as TRITC, tetramethylrhodamine isothiocyanate). 20 μL of a stock solution of TRITC (10 mg/mL) was added to an aliquot of 10^{11} 50 nm magnetic beads in PBS buffer, and left to react for 2 hours at room temperature. The

labelled beads were then collected and the supernatant discarded. The labelled beads were washed two times with PBS buffer. 2 µL of the beads (in a total of 100 µL in PBS) were pipetted into the chamber of the microfluidic slide. This slide was fixed to the stage of a fluorescence microscope and the top wall of the microfluidics chamber was set on focus. A time-lapse was recorded before and after the N40 neodymium magnet was set on top of the microfluidic slide. As shown in Fig. 3.9, after approximately 1 minute, several of the fluorescently labelled magnetic beads were pulled to the surface, towards the magnet. Thus, it seemed the N40 neodymium magnet could pull the 50 nm magnetic beads out of solution, with some of the beads reacting instantly to the applied magnetic field.

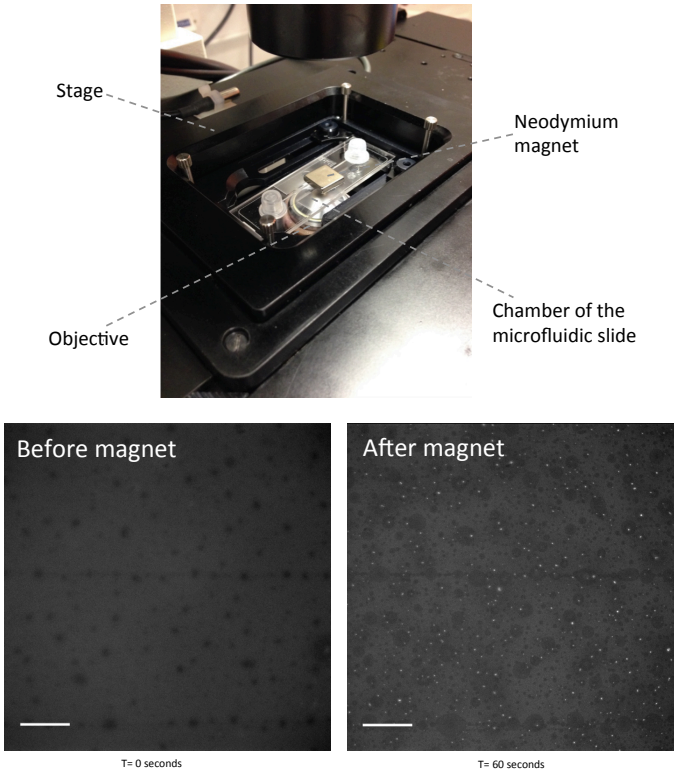

Figure 3.9: Neodymium magnet capturing 50 nm magnetic beads. (Top) For this experiment, a N40 neodymium magnet was fixed on top of a chambered microfluidic slide and then set on the stage of an inverted microscope (Bottom) Two snapshots of the top of the microfluidic slide, before and after the magnet was fixed to the surface of the slide. Several TRITC-coated 50 nm magnetic beads (bright spots) got pulled by the magnet after a few seconds. Time-lapses were collected using a 10x objective on an inverted wide-field microscope (Olympus, IX71). Focus was on the top wall of the microfluidics chamber. Scale bar: 100 µm.

The question of if and how long it takes to collect all the beads out of solution was left unanswered by this experiment. By naked eye, a suspension of approximately 10^{11} 50 nm beads in buffer became completely clear after leaving it on the magnet for approximately 10 hours.

The first part of the protocol consisted of conjugating anti-p3 antibodies to the magnetic beads. The second part was to immobilise the phage particles onto the surface of the antibody-coated magnetic beads. This protocol was set-up following manufacturer instructions, and as described in Chapter 2 (method 2.4.1.3). The antibodies were captured on the surface of the protein A-functionalised magnetic beads, and these were then added to the phage sample so that there are more beads than phage particles. The reaction was set at a roughly 10:1 bead-to-phage ratio, envisioning that the antibody-coated beads would capture a phage particle. TEM images of the samples were collected, in search of the phage-bead immunocomplex (Fig. 3.10).

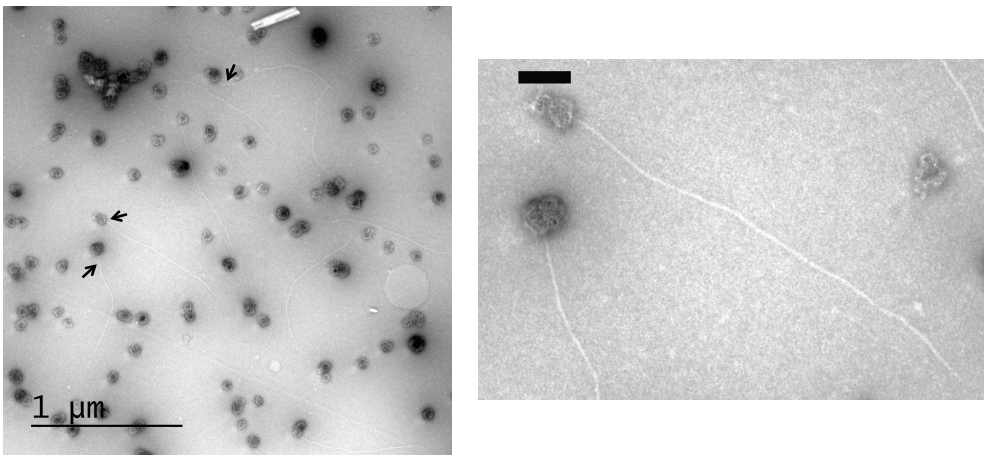

Figure 3.10: TEM image of the phage-bead immunocomplex. Micrograph of apparent single phages anchored by one-end to the surface of magnetic beads (examples indicated with arrows). TEM image zoomed at phage anchored by one-end to magnetic bead. Scale bar: 100 nm.

Fig. 3.10 shows TEM images of a single phage anchored by one-end to the surface of a magnetic bead. As observed, most of the magnetic beads did not

capture phage particles and remained phage-free. Based on eight TEM images, the apparent efficiency of the described conjugation protocol was approximately 5 %. This was calculated by counting the number of phage-free beads and the number of beads with a phage attached to it, in these eight micrographs. Nonetheless, the estimated yield is possibly an overestimation – it is challenging to measure this value based only on TEM, as the images might not be representative of the whole sample and it is difficult to confirm the phage is actually anchored to the bead. Further testing and complementary experiments would be necessary to investigate the phage-bead immunocomplex. An ELISA would not be suitable, as this would require the use of an anti-phage/HRP antibody to detect the phage – this antibody could simply bind to the protein A on the beads. Perhaps, labelling the phage with a fluorescent dye prior to its conjugation to the beads and measuring the fluorescence intensity of the sample after conjugation could provide some insight into the phage-bead immunocomplex. Using standard spectroscopy techniques, it may be challenging to measure the signal generated as it would be diffused in a large volume and may not be above background. Optical methods have been developed to detect single molecules, which confine samples to very low volumes ensuring a high local concentration of recognition molecules [30].

The ultimate goal of these experiments was to design and develop a method to anchor a phage particle onto a magnetic bead. This phage-bead construct was believed to have applications extendable to microfluidic biosensor, in a spectroscopy-based platform. Although in principle it appeared to be a simple design, several experimental components of this project were rather challenging. The small sized beads were difficult to work with, and capturing/washing the magnetic beads using a magnet was a rather lengthy protocol – on average, 6 days were needed to complete the whole protocol, mainly because of the number of washing/capturing steps required to remove unbound molecules (each taking approximately 10 hours). It was also noticed that the pellet resultant from the captured beads is delicate and unstable – any vibration on the working bench or even during pipetting could dislocate the pellet, making it necessary to wait

another several hours for the pellet to get compacted. Another limitation of this design is the cost of the reagents (the anti-p3 antibodies and the functionalised 50 nm magnetic beads). This would be especially obvious during early development stages and optimisation, which would require a trial-and-error approach, flagging a warning for its adoption as a proof-of-concept assay. To produce the 1-to-1 phage per bead complex in a robust method, it would be necessary to kinetically study the interaction between the beads and the phage, to understand, for example, the diffusion rate of the phage and capture efficiency of the beads. Although it is potentially feasible to integrate a phage-bead immunocomplex in a microfluidics set-up, these samples proved to be inadequate for the originally intended spectroscopy-based biosensing platform.

3.2.1.3 Anchoring the phage using a His-tag moiety

Since the previous method, using the 50 nm magnetic beads, was concluded to be challenging to integrate with the spectroscopy-based biosensing platform, His-tag motifs were considered as an alternative. Genetically inserted His-tag motifs on the p3 proteins [31] could be used to pull the phage particles onto nickel-coated surfaces, anchoring them by one-end.

A polyhistidine-tag, generally called His-tag, comprises six to fourteen histidine residues, fused to the N- or C-terminal of a protein. His-tags have a wide range of applications for binding assays and immobilisation protocols [32]. Polyhistidine-tags are a commonly used tool for affinity purification methods. Most His-tagged recombinant proteins can be effortlessly purified as the histidines on the His-tag have high affinity for divalent nickel ions. Nickel ions can be loaded over surfaces derivatised with chelating agents, such as nitrilotriacetic acid (NTA), covalently linked to a matrix. This way, nickel-coated surfaces can be used to immobilise the His-tagged proteins of interest. Bound proteins can be then released from the nickel surface using mild conditions. Imidazole, an analogue of histidine, is generally used to displace the His-tagged protein as it competes for the coordination bond between histidine and the nickel ions. Low pH buffers can alternatively be used to elute the

proteins, as they protonate the histidines on the His-tags, although care must be taken as exposure to low pH may damage the protein of interest [33]. The common drawback of using a polyhistidine affinity tags is the nonspecific binding of untagged proteins. Other anchoring tag motifs, such as biotinylation-accepting domain affinity tags, have shown to give higher yields and purity of tagged proteins [34].

A six histidines His-tag motif was cloned to the N-terminal of the p3 proteins of the phage (Chapter 2, method 2.11.4), and a western blot (Chapter 2, method 2.7.5) was set-up to confirm its expression. Two His-tagged phage cultures were checked – the 1st generation His-tagged phage and the 2nd generation His-tagged phage.

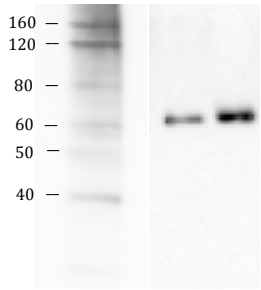

Figure 3.11: Western blot to confirm His-tag on the p3 proteins of the phage. Lane on the left, marker with respective protein molecular weight (kDa). Lanes on the right, two independent propagations of the His-tagged phage (1st and 2nd generation).

A 2nd generation His-tagged phage was grown directly from an aliquot of the 1st generation phage. This was to determine whether the p3 proteins of these phages are still functional and capable of infecting the bacterial host despite the histidine tag. It was confirmed that the 2nd generation phage was viable and its production yield was comparable to the 1st generation His-tagged phage. Looking at the western blot in Fig. 3.11, both 1st and 2nd generation phages expressed the His-tag motif – on both lanes, a band is visible at ~ 60 kDa, which is known to be the size at which p3 protein runs on a gel [35]. These are useful observations as it suggests it may not be necessary to repeat molecular cloning

steps to replenish the stocks of His-tagged phage. A carefully stored aliquot of the parental His-tagged phage could be enough to propagate another generation.

After successfully confirming the p3 proteins were modified with His-tag motifs, it was necessary to check whether these His-tags were actually exposed and capable to interact with nickel ions-coated surfaces. Nickel-chelating magnetic beads were used for a pull-down assay, aiming at testing the binding of His-tagged phage to nickel. Initially, an ELISA was designed to detect if this binding occurred. However, it was observed that probably the nickel ions from the magnetic beads react with the horseradish peroxidase (HRP) conjugated to antibodies, giving a green coloration even without the presence of the analyte of interest (and hence, giving false positive results). Consequently, a protein gel was used instead to assess for the interaction between the His-tagged phage and the nickel-coated beads.

An illustration of a pull-down assay, using nickel-chelating magnetic beads to capture His-tag phage, is given in Fig. 3.12. Protocols for the pull-down assay and the protein gel are given in Chapter 2 (method 2.10.1; method 2.7.4). Four samples were separately handled – two His-tagged phage samples and two controls. His-tagged phage and untagged phage (control) were mixed with nickel coated-magnetic beads in phosphate buffer. With the use of a magnet, the magnetic beads were pelleted to the bottom of the eppendorf and the supernatant carefully discarded and kept to later run on a gel (Fig. 3.12, Lane 2-5). 250 mM imidazole elution buffer was added to the magnetic beads. The magnetic beads were again precipitated using the magnet, and the elution samples were collected to run on a gel (Fig. 3.12, Lane 6-9).

The gel shows fewer bands on the elution samples, implying that a considerable fraction of the phage did not bind to the beads and was therefore washed away. Nonetheless, a characteristic band is visible in these lanes corresponding to the p8 proteins, suggesting the presence of phage. One of the control samples (untagged phage, on lane 8) also shows a fainter band for p8, however this was

considered to be due to non-specific interactions to the beads. The presence of this band on lane 8 could be explained by the higher initial concentration of phage on this control sample (especially visible by the brighter 10 kDa band on lane 4 in comparison with the other lanes), which could have further promoted unspecific binding to the magnetic bead.

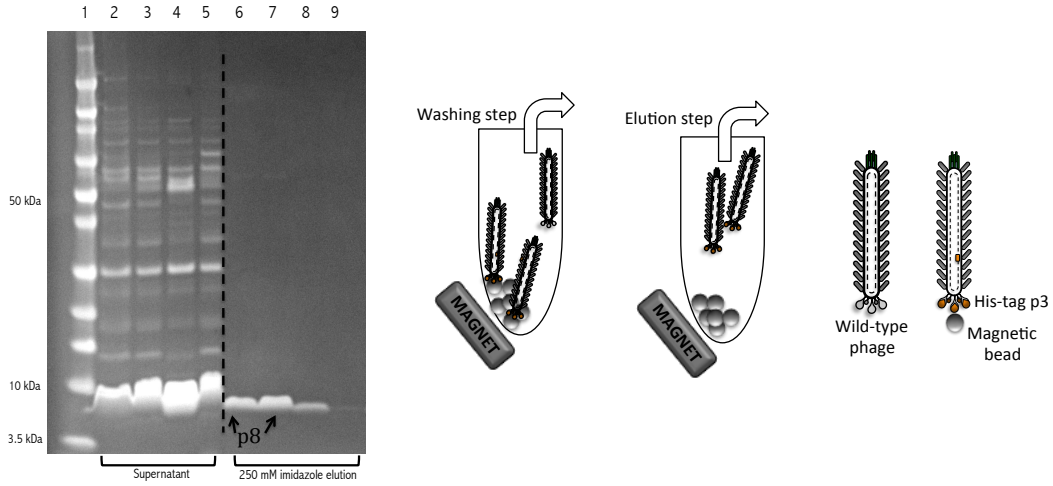

Figure 3.12: Pull-down assay using nickel-chelating magnetic beads. (Left) Precast (4-12%) Bis-Tris gel of nickel-chelating magnetic beads assay. Lane 1 - protein ladder. Lane 2,3 and 6, 7 respectively – 2 samples of His-tag modified phage (1st and 2nd generation) after incubation with beads, and the samples of His-tag modified phage (1st and 2nd generation) after elution with imidazole. Lane 4, 5 and 8, 9 respectively – 2 control samples (untagged phage) after incubation with beads, and the control samples (wild-type phage) after elution with imidazole. (Right) Pull-down assay design using nickel-chelating magnetic beads. In the illustrated example, the sample is a mixture of untagged phage and His-tagged phage. Ideally, the beads would capture only the tagged phages, which could then be eluted. In the experiments demonstrated by the gel however, the tagged and untagged phage samples were handled separately.

The resulting protein gel from the pull-down assay using the magnetic beads provided a good indication that the His-tag motifs on the p3 proteins are exposed and capable of binding to nickel-chelating surfaces. Therefore, the His-tag motif could be used as a simple and affordable alternative to immobilise phage particles by one-end onto appropriate surfaces. Featuring the His-tagged phage in the microfluidics biosensor design has great interest, as the genetically introduced His-tag could serve as an anchoring point to surfaces, which could

then be "turned off" by using low pH or imidazole elution buffers, releasing the phage particles from the surface. We consider it is possible to integrate this anchoring functionality with the spectroscopy-based biosensor described in Chapter 5, similarly to how other His-tagged proteins are immobilised to the surface of chips [36]. However, this was not pursued further as the biosensor platform was not developed to the point that this could be tested. The His-tag moieties could also be explored as a method to separate phage particles from a reaction mixture containing other biomolecules – for example, after chemically modifying the phage surface (as explored in section 3.2.2), the modified phages could be captured using nickel-chelating surfaces of magnetic beads or columns, ensuring a standardised purification method for functionalised phage particles.

3.2.2 Modifying the phage surface

The p8 protein is the most abundant of the phage proteins, with 2700 copies around its long axis, and it is smaller (~ 5 kDa) than the p3 protein. It seems intuitive to think any modifications to p8 will make the biggest impact on the phage. However, care must be taken on chemically and genetically modifying the p8 proteins, as the overall structural change to the phage could be too drastic to keep it viable. In this section, we describe three functional modifications to the p8 proteins: labelling with TRITC dye for the imaging work on Chapter 4, bioconjugation with an antibody as a probe for the biosensor platform described in Chapter 5, and decorating the phage surface with DNA molecules using a novel protocol. Genetic engineering techniques to mutate the p8 protein were also explored, and documented in Chapter 5. These include the expression of a *Salmonella*-binding peptide in some of the p8 proteins of the phage, the design of a mutant phage with a cysteine residue in every p8 protein, a mutant phage with an extra tryptophan residue in every p8 protein, and a longer version of the phage by encapsulation of a larger genome.

3.2.2.1 TRITC dye conjugation

Tetramethylrhodamine isothiocyanate (TRITC) is an amine-reactive dye, which can be conjugated to the lysine residues (position 8) and to the N-terminal of the p8 proteins of the phage capsid (Chapter 2, method 2.4.2.1). Others fluorophores and near-infrared fluorescent dyes have been previously conjugated to the phage [20]. TRITC is commonly used in bioimaging protocols [37] because of its photostability and reasonable price. Therefore, it was considered to be suitable for labelling the phage for the microscopy imaging done in Chapter 4. Because imaging quality directly depends on the quality of labelling, an experiment was designed to test which pH would favor the labelling of the primary amines on the p8 protein. UV-Vis measurements were used to estimate the dye per phage particle ratio. As shown in Fig. 3.13, considering there are 2700 copies of p8 proteins per phage, using a pH 7.6 buffer results in a ~ 15% labelling of the phage surface. A more alkaline buffer promotes a more efficient conjugation, resulting in more than 500 molecules of TRITC dye per phage. At a pH higher than 8.7, it appears the labelling efficiency is reaching a plateau. This is consistent with the literature [38] and believed to be caused by steric hindrance and contact quenching between the dye molecules.

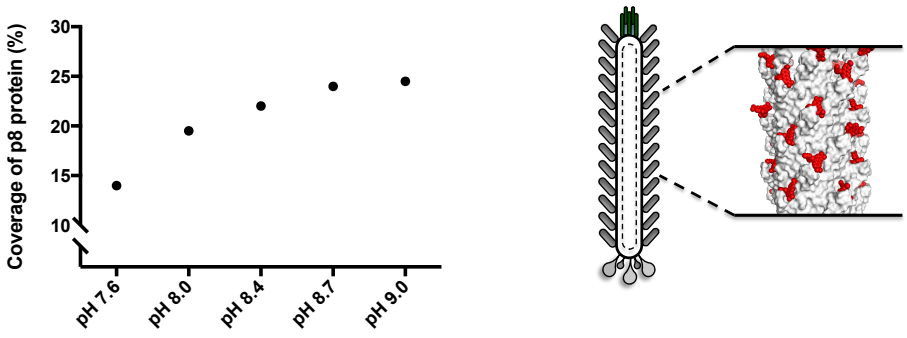

Figure 3.13: Labelling the phage surface with TRITC. (Left) Plot of the total percentage coverage of the phage surface with TRITC in 100 mM borate buffer at a range of pH values. (Right) Illustration of TRITC dye molecule conjugated to the N-terminal of p8 proteins of the M13 bacteriophage. Molecular docking was done on Chimera (PDB entry: 2MJZ) by Dr. Shirin Jamshidi.

The labelling of the phage with TRITC was confirmed by LD, in which a characteristic dye peak can be observed in samples conjugated in buffers at pH 8 and pH 9 (Fig. 3.14).

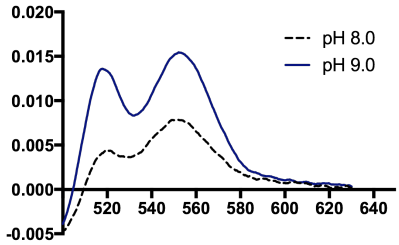

Figure 3.14: LD spectra of phage decorated with TRITC in buffer at pH 8 and pH 9. LD signal zoomed at TRITC dye peak, showing that the signal is more intense at higher pH (which translates into having more dye molecules per phage particle).

Labelling the surface of the phage with TRITC was an important step for the microscopy-based platform described in Chapter 4, ensuring an adequate fluorescence signal to image the phage constructs. Other fluorophores, such as Alexa Fluor and coumarin dyes, were also successfully conjugated to the phage to decorate its capsid, and explored as probes in spectroscopy-based platforms (Chapter 5). Indeed, the aptitude of the phage to accommodate chemoselective dual-modifications (*i.e.* with a dye molecule plus another biomolecule, such as an antibody) endows it with great versatility for the development of multifunctional biomaterials, which can be integrated with biosensors.

3.2.2.2 Antibody conjugation

Linear Diagnostics Ltd. developed a LD-based biosensor using the phage as a scaffold. This diagnostic technology is further explored in Chapter 5. Illustrated in Fig. 3.15 is the protocol developed by Linear Diagnostics to chemically conjugate antibodies and dye molecules to the p8 protein for the LD-based biosensor. This method employs the use of p8 protein's primary amines and, by converting them to thiol groups using SATA (N-succinimidyl S-acetylthioacetate), it is possible to conjugate maleimide-derivatised antibodies. One of the strategic attributes of this platform is that it can simultaneously detect

a variety of targets in a sample (*i.e.* multiplexing). This is achieved by conjugating a readily maleimide-modified dye to the remaining thiol groups on the surface of the phage. A detailed method is given in Chapter 2 (method 2.4.2.2.1).

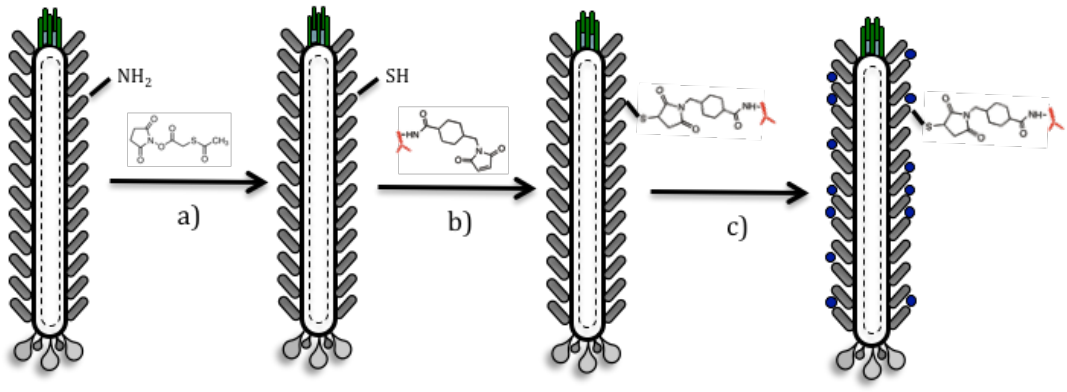

Figure 3.15: Scheme of the bioconjugation protocol developed by Linear Diagnostics Ltd. for the LD-based immunoassay. All steps carried out at room temperature. a) SATA converts primary amines (-NH_2) of the p8 protein to thiol groups (-SH). A de-protection step is also required (with hydroxylamine) to expose the thiol group from the reagent. b) Conjugation with the maleimide-derivatised antibody (modified with SMCC). c) Conjugation with a maleimide-modified Alexa Fluor 647 dye (shown as blue dots) required for the multiplexing modality of the assay. Figure not drawn to scale.

Despite the indisputable value of Linear Diagnostics' biosensing platform, it was discussed that several aspects of the technology could be improved and alternative methods could be explored. For this, a number of modifications to the biosensor were considered, as described in Chapter 5. An example is the alternative bioconjugation protocol we explored to conjugate antibodies to the p8 proteins of the phage, using an aldehyde-hydrazine reaction (Fig. 3.16).

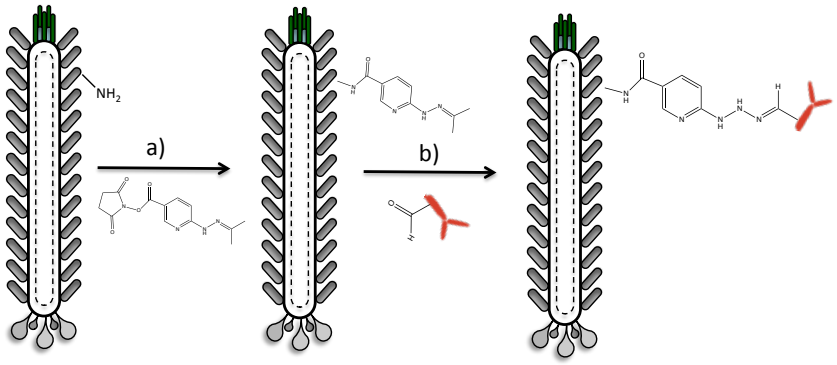

Figure 3.16: Scheme illustrating the 2-steps hydrazine-aldehyde chemical reaction, to conjugate antibodies to the phage surface. a) Treatment with SANH to incorporate hydrazine moieties to the primary amines of the p8 proteins; b) Conjugation of $NaIO_4$ treated-antibody to the hydrazines.

The bioconjugation method from Fig. 3.16 explores the modification of the p8 protein's primary amines with hydrazine groups, upon treatment with SANH (succinimidyl 6-hydrazinonicotinamide acetone hydrazine) reagent. The aldehyde groups of a $NaIO_4$-treated antibody, can then be reacted with the hydrazine groups of the phage, producing a phage-antibody conjugate. The advantage of using this type of chemical modification instead of the one proposed by Linear Diagnostics lays on the ability to control the directionality of the antibodies conjugated to the phage. A full explanation and details on the outcome of this bioconjugation protocol are given in Chapter 5 (section 5.2.5).

3.2.2.3 DNA strands conjugation

As detection elements, DNA molecules have the advantage of being cheaper to synthesise and, reportedly, more stable than antibodies. Maybe for that reason, there has been an increasing interest on chemically conjugating DNA to the filamentous phage [15,39,40]. In here, we explored the conjugation of DNAzymes to the phage surface, envisioning a LD-based assay for the detection of lead ions (Pb^{2+}).

3.2.2.3.1 DNAzymes for a Pb^{2+} detection assay

Heavy metal ions are common pollutants of the soil and water, and present a public health concern [41]. Lead ions (Pb^{2+}) are a widespread metal pollutant that can cause serious health damage because of its known adverse effects in humans – lead is a potential neurotoxin that can accumulate in the bones and kidneys [42]. Recent news, exposing Michigan's environmental scandal, covered the toxicity of lead to humans by consuming contaminated water [43,44]. In this incident, several children were critically sick which was believed to have been caused by lead poisoning.

DNAzymes [45, 46], also termed catalytic DNA or deoxyribozymes, are attractive molecules for heavy metal detection because of their metal-dependent activity. DNAzymes have already been explored for metal ions biosensors [47-53] and are composed of two almost complementary DNA strands, the enzyme and the substrate strand. Pb^{2+}-specific DNAzymes, known as "8-17" DNAzymes, are made of a substrate strand (17DS) and an enzyme strand (17E). Both strands are made of DNA, except for a RNA (riboadenosine, rA) residue on the 17DS strand. This rA is the cleavage site – the substrate strand gets cleaved by the enzyme strand in the presence of Pb^{2+} ions [50]. To integrate a DNAzyme system in a phage-based biosensor, it is necessary to attach DNA probes to the phage surface. Labelling of the phage surface with DNA strands has been explored before, using different conjugation methods [15,39,40]. However, to our knowledge, this application was not yet considered. The metal selectivity of the "8-17" DNAzyme joined with the phage properties could be harnessed in an assay for lead detection, exploring the phenomenon of LD.

The phage-DNAzyme system described here was inspired by the work of Yi Lu and colleagues [51-53] on DNAzymes and gold nanoparticles. The sequences of the constructed DNA structures are given on Table 3.2. To conjugate the DNAzyme to the phage, its substrate strand was extended at both the 3' and 5' ends. These 12-mer extensions are complementary to the DNA strands conjugated to the phage (termed as DNA probe 1 and DNA probe 2),

consequently hybridising the DNAzyme with the phage. This was expected to cause aggregation between the phages, and hence less alignment, resulting in an overall decrease on LD signal. However, when lead ions (Pb^{2+}) are added to the system, the DNAzyme collapses. The hypothesis was this breakage would result in less aggregation between the phages, which would result in an increase on the LD signal. Fig. 3.17 illustrates the principle of a LD-based Pb^{2+} detection biosensor.

Name	DNA sequence
DNA Probe 1	5′ I-link – CACGAGTTGACA 3′
DNA Probe 2	5′ TCACAGATGAGT – NH_2 3′
17DS substrate strand	5′ ACTCATCTGTGAACTCACTAT**rA**GGAAGAGATGTGTCAACTCGTG 3′
17E enzyme strand	5′ CATCTCTTCTCCGAGCCGGTCGAAATAGTGAGT 3′

Table 3.2: DNA probes and DNAzyme sequences. Sequence of the "8-17" DNAzyme 17DS substrate strand with 12 bases extension on its ends, 17E enzyme strand, DNA probe 1 with a 5' modification, and DNA probe 2 with a 3' modification.

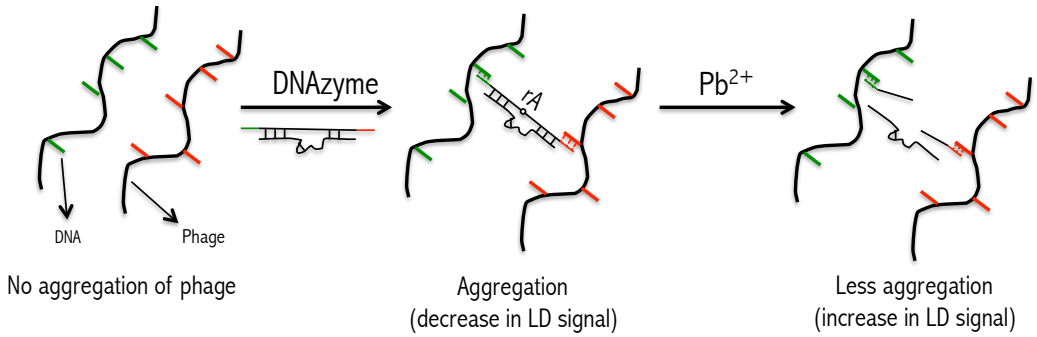

Figure 3.17: Integrating a DNAzyme with phage probes. Two types of chemically modified phages, each containing different DNA probes (red, DNA probe 1; green, DNA probe 2), were designed. These DNA probes are complementary to the extremities of the substrate strand of the Pb^{2+}-DNAzyme. When the DNAzyme binds to the DNA probes on the phages, this was expected to cause aggregation between the phages, and hence less alignment, resulting in an overall decrease on LD signal. When lead (Pb^{2+}) is present however, the DNAzyme collapses. The hypothesis was this breakage would result in less aggregation between the phages, which would result in an increase on the LD signal.

3.2.2.3.2 Bioconjugation and gel characterisation

The bioconjugation protocol to conjugate the DNA probes to the chemically modified p8 proteins of the phage was developed with Dr. Dylan Domaille, at University of Boulder Colorado. A detailed protocol is given in Chapter 2 (method 2.4.2.3).

DNA probe 1 and DNA probe 2 were purchased from IDT with chemical modifications on its ends – DNA probe 1 had a hydrazine (I-link) group on its 5' end, and DNA probe 2 had an amine modification on its 3' end. Firstly, the amines on the p8 proteins of the phage were modified to aldehyde moieties. The phage-aldehyde was conjugated to the I-link of the DNA probe 1. A crosslinking reagent was used to conjugate the amine groups of the DNA probe 2 to the aldehydes of the phage. This bioconjugation protocol generated two types of phage-probes, here denominated as phage-DNA probe 1 and phage-DNA probe 2. As illustrated in Fig. 3.17, the idea was that the DNAzyme would link phage-DNA probe 1 to phage-DNA probe 2, by complementary pairing between the DNA probes conjugated to the phage and the extensions at the ends of the DNAzyme substrate strand. The success of the chemical conjugation between the phage and the DNA probes was confirmed by gel (Chapter 2, method 2.7.4). Fig. 3.18 illustrates the built phage-probes and the characterisation of the constructs on a protein gel. A similar conjugation protocol between an I-link modified DNA strand to an aldehyde-phage has been explored [39], but, to the best of our knowledge, this is the first report of conjugation between an amine modified DNA strand and an aldehyde-phage.

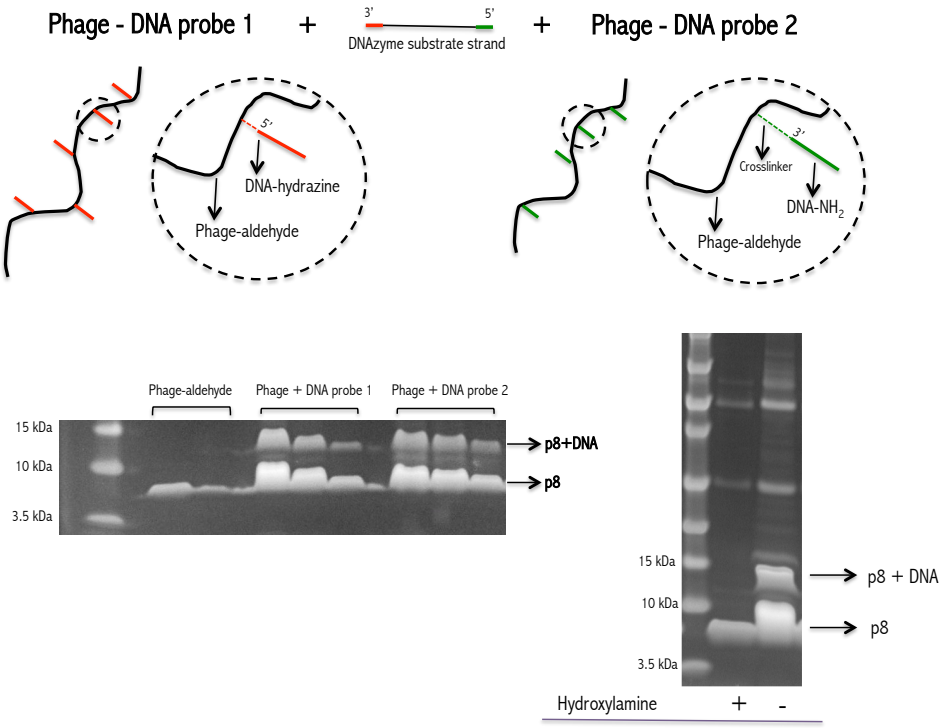

Figure 3.18: Labelling the phage with DNA strands and characterisation by gel. (Top) Scheme of the conjugation of DNA to the p8 protein of the phage modified with aldehyde groups. DNA probe 1 is a hydrazine modified 12-mer strand of DNA, conjugated to the modified phage-aldehyde. DNA probe 2 is an amine modified 12-mer strand of DNA, conjugated via a crosslinker to the modified phage-aldehyde. (Bottom left) Precast (4-12%) Bis-Tris gel. From left to right: protein ladder; 1.3× and 4× dilution of phage-aldehyde; 2×, 4× and 10× dilution of phage-aldehyde conjugated with DNA probe 1; 1.3×, 2× and 4× dilution of phage-aldehyde conjugated with DNA probe 2. All samples in PBS buffer. (Bottom right) Precast (4-12%) Bis-Tris gel. Left to right: protein ladder; phage-DNA probe 1 reacted for 6 hours with 25 mM hydroxylamine (pH 6); Phage-DNA probe 1 without hydroxylamine. Hydroxylamine dissociates the conjugated DNA strands from the p8 proteins, and hence the p8+DNA band is no longer visible on the gel. This confirms the band is a result of the conjugated DNA.

3.2.2.3.3 Preliminary LD studies

Simple LD experiments were set to explore the properties of the newly constructed phage-DNA probes. Unfortunately, due to time restrictions, the full potential of this phage-based biosensor could not be investigated.

An interesting observation from the preliminary experiments was the phage-DNA probe 1 LD signal, which was inverted compared with naked phage, as

shown in Fig. 3.19. This result was replicated with another independently constructed phage-DNA probe 1 conjugate, in which the same peculiarity was noted. A literature search revealed that this phenomenon has been previously observed by Carr-Smith and colleagues [15]. They reported that by loading a phage particle with several DNA strands, the LD signal of the phage is mirrored, probably due to hydrodynamic properties changes to the filamentous structure of the phage.

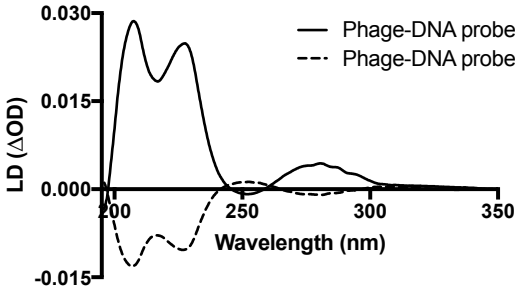

Figure 3.19: LD of the phage-DNA probes. LD spectra from the phage-DNA probe 1 (solid line) and phage-DNA probe 2 (dashed line) constructs, in PBS buffer.

To further investigate this phenomenon, a non-conventional LD experiment was designed. In these experiments, a circular quartz window was used instead of a Couette flow cell, and, contrary to standard LD measurement that induce alignment by spinning the phage solution, a manual motion was applied to force the filamentous phage particles to align. A drop of wild-type phage stock was pipetted onto the surface of a quartz window and induced to align. This was achieved by horizontally dragging the drop with a pipette tip, from left to right, in parallel strokes over the surface, until completely dry (Chapter 2, method 2.8.2.3). Next, the quartz window was attached to the front of the LD detector and the resulting LD spectrum from the aligned phage was collected. The window was then manually rotated 90 ° with respect to the previous position, as illustrated in Fig. 3.20, and LD was measured again.

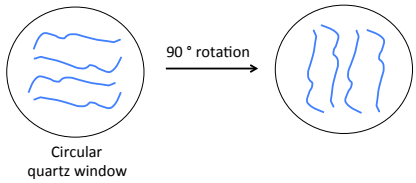

Figure 3.20: Alignment of phage on a quartz window. Illustration of the circular quartz window with aligned phage (shown as blue lines) dried onto its surface. By rotating the quartz window by 90 °, the phage particles will be perpendicularly oriented in respect to their original alignment.

Fig. 3.21 shows the resulting LD spectra collected from the physically aligned wild-type phage onto the quartz window. As expected, the LD spectrum is characteristic for filamentous phage particles, with the fingerprint peaks at the near-UV (aromatic side chains) and far-UV regions (peptide backbone). By manually rotating the quartz window by 90 °, the aligned phage particles take a perpendicular orientation with respect to the original alignment, resulting in an almost exact inversion of the phage LD spectrum.

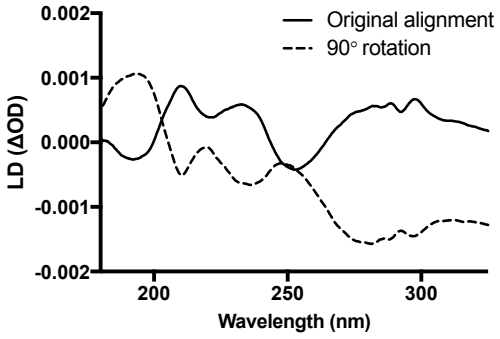

Figure 3.21: LD from the induced aligned wild-type phage on the surface of a quartz window. The resulting spectrum shows all the expected characteristic peaks from filamentous phage particles. By rotating the quartz window by 90 ° in respect to its original position, the phage LD spectra gets inverted (dashed line).

This experiment, along with the observations from [15], suggested the inversion of the LD spectra of the phage-DNA probe 1 sample resulted from a difference in the overall orientation of the phage particles, probably induced by the

conjugated DNA strands. Strangely however, this behavior was not observed in the phage-DNA probe 2 sample. This was thought to be due to the differences in the bioconjugation protocol, which resulted in a lower yield of conjugation of DNA probe 2 to the phage surface, and therefore there was a minor contribution to the overall phage alignment.

The described LD spectrum inversion was also observed in subsequent experiments. Fig. 3.22 illustrates the LD spectra of the phage constructs, phage-DNA probe 1 and phage-DNA probe 2, mixed together with the DNAzyme. Typically, 0.05 mg/mL of phage-DNA probe 1 and phage-DNA probe 2 were mixed in PBS buffer, followed by adding the enzyme and substrate strands, in a total of 100 µL. The phage-DNA probes and the DNAzyme were incubated for one hour at room temperature prior to LD measurements.

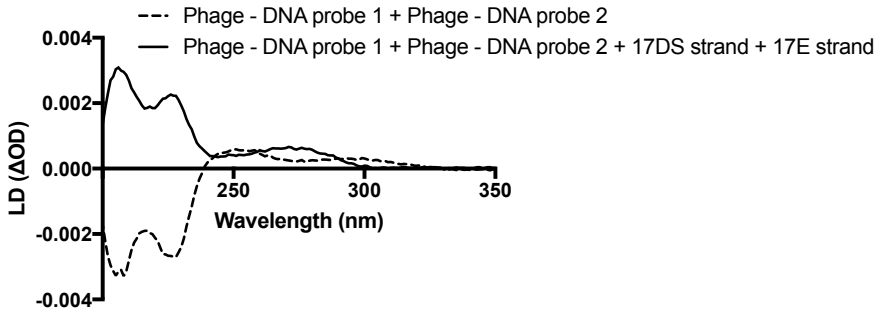

Figure 3.22: LD of the phage-DNA probes and DNAzyme. LD spectrum of phage-DNA probe 1 and phage-DNA probe 2 in PBS buffer (dashed line). LD spectrum of phage-DNA probe 1, phage-DNA probe 2, 1 µM substrate strand (17DS) and 1 µM enzyme strand (17E) in PBS buffer (solid line).

The effect on LD signal inversion, believed to be caused by the phage-DNA probe 1, seemed to predominate when phage-DNA probe 1 and phage-DNA probe 2 were mixed together. Interestingly however, the signal flipped when the DNAzyme (substrate (17DS) and enzyme (17E) strands) was added to the system. This effect seemed to be reproducible as it was observed in following LD measurements, using independent batches of the constructed phage-DNA

probes. To further investigate whether the DNAzyme had an effect on the observed LD signal inversion, LD measurements were made in which only the substrate (17DS) strand was added to the system, because this strand is physically responsible for linking the phage-DNA probes (Fig. 3.23).

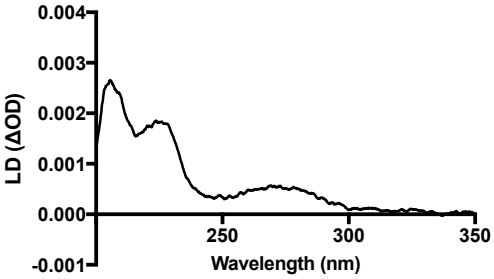

Figure 3.23: LD of the phage-DNA probes, mixed with the substrate strand of the DNAzyme. LD spectrum of phage-DNA probe 1, phage-DNA probe 2 and 1 μM substrate strand (17DS) in PBS buffer (dashed line).

As observed in Fig. 3.22, when the DNAzyme was added to the phage-DNA probes, the LD signal reverted back to the "standard" LD spectrum. From the data on Fig. 3.23, it seemed the substrate strand (17DS) played a role on that flip. When the enzyme strand (17E) is added to the phage-DNA conjugates, the overall LD signal remained inverted on the negative quadrant of the spectrum (data not shown). When the 17DS strand (which has complementary extensions at both its ends to hybridise with the DNA on the phage) was added to the phage-DNA probes, the LD signal reverted back to the positive quadrant of the spectrum.

The previously described experiments were thought to be important to demonstrate the unpredictability of newly designed phage-based probes, in this case the phage-DNA probes/DNAzyme system, on an LD-based assay. For a throughout analysis, it was obvious the number of variables and possible conditions to test were large. These experiments provided limited insight on the LD-related aspects of the phage-DNA probes. In order to fully understand the behaviour of the phage-DNA constructs and its interaction with the lead-specific

DNAzyme, several experiments needed to be conducted, testing, for example, a range of concentrations of phage-DNA probes, and 17DS and 17E strands ratios. It would also be necessary to determine which factors interfere with DNAzymes kinetics – Lu and colleagues found that optimal conditions of temperature and salt ions are important aspects to consider when designing a lead sensor [53]. Other experiments should confirm and clarify on the interaction between the phage-DNA probes and the DNAzyme strands. An example of this could be to set up a FRET (Förster Resonance Energy Transfer) experiment. A FRET system would be in place by labelling the DNA probes conjugated to the phage with a chromophore molecule (FRET acceptor), and the ends of the DNAzyme substrate strand with a different chromophore (FRET donor) – when at a certain distance from each other, a light of specific wavelength would be emitted. This distance-dependent fluorescence would suggest on the proximity between the substrate strand and the DNA probes, indicating if hybridisation did occur and potentially also providing some insight on the stability of this interaction.

3.3 Conclusion

Filamentous bacteriophages have a number of features that make them an ideal choice as a programmable scaffold for nanotechnology applications. In this chapter, chemical and biological approaches for manipulation of the bacteriophages structure were explored. The goal of this work was to experiment on modifications to the phage structure that could be integrated into biosensing platforms. M13 bacteriophages are good scaffolds for biosensing platforms because they are simple and stable macromolecules that can be easily grown in large amounts, tolerating both chemical and genetic modifications. Phage surface functionalisation can be achieved by genetic engineering; however, excessive mutation may interfere with the life cycle of the phage, and does not allow for incorporation of synthetic compounds. Strategic chemoselective modifications tackle these limitations, and expand the potential applications of phage-based biomaterials. In here, it was shown to be possible to anchor and functionalise the

surface of the filamentous phage by modifying its proteins. To immobilise phages onto surfaces, antibodies, magnetic beads, and polyhistidine tags were conjugated to the p3 proteins and serve as anchoring points. The phage capsid, made of 2700 copies of p8 protein, comprises a large area for multivalent modifications, allowing for conjugation of fluorophores, antibodies and DNA molecules. We also exploited one of the phage's simplest features – being a long, thin molecule that can be aligned under flow. Combining this principle with phage surface functionalisation, two optical-based biosensing platforms were designed, as described in Chapter 4 and Chapter 5.

3.4 References

1. Chung, W., Lee, D., Yoo, S. Chemical modulation of M13 bacteriophage and its functional opportunities for nanomedicine. *International Journal of Nanomedicine* **9**, 5825–5836 (2014).
2. Rakonjac, J., Bennett, N., Spagnuolo, J., Gagic, D., Russel, M. Filamentous bacteriophage: biology, phage display and nanotechnology applications. *Curr. Issues Mol. Biol.* **13,** 51–76 (2011).
3. Sidhu, S. *Phage display in Biotechnology and Drug Discovery.* (CRC Press, 2005). ISBN: 9780824754662
4. Russel, M., Model, P. *The Bacteriophages*. (Oxford University Press, 2006). ISBN: 9780195148503
5. Specthrie, L., Bullitt E., Horiuchi, K., Model, P., Russel, M., Makowski, L. Construction of a microphage variant of filamentous bacteriophage. *J Mol Biol* **228**, 720–724 (1992).
6. Brasino, M., Cha, J. Isothermal rolling circle amplification of virus genomes for rapid antigen detection and typing. **140,** 5138–5144 (2015).
7. Branston, S. An investigation of the properties of bacteriophage M13 and the implications for its large-scale bioprocessing. PhD thesis, University College London (2009).
8. Finnigan, T. *et al.* Virus-based toolkit for the directed synthesis of magnetic and semiconducting nanowires. **303,** 213–218 (2004).
9. Murugesan, M., Abbineni, G., Nimmo, S., Cao, B. & Mao, C. Virus-based photo-responsive nanowires formed by linking site-directed mutagenesis and chemical reaction. **3,** 1–7 (2013).
10. Niu, Z., Bruckman, M., Harp, B., Mello, C. Bacteriophage M13 as a scaffold for preparing conductive polymeric composite fibers. *Nano Research* **1**, 235–241 (2008).
11. Ghosh, D. *et al.* M13-templated magnetic nanoparticles for targeted in vivo imaging of prostate cancer. *Nat. Nanotechnol.* **7,** 677–682 (2012).
12. Suthiwangcharoen, N. *et al.* M13 bacteriophage–polymer nanoassemblies as drug delivery vehicles. *Nano Research* **4,** 483–493(2011).

13. Carrico, Z. *et al.* N-terminal labelling of filamentous phage to create cancer marker imaging agents. *ACS Nano* **6**, 6675–6680 (2012).
14. Li, S. *et al.* Direct detection of *Salmonella typhimurium* on fresh produce using phage-based magnetoelastic biosensors. *Biosens. Bioelectron.* **26,** 1313–1319 (2010).
15. Pacheco-Gomez, R. *et al.* Detection of pathogenic bacteria using a homogenous immunoassay based on shear alignment of virus particles and linear dichroism. *Anal. Chem.* **84,** 91–97 (2012).
16. Khalil, A. *et al.* Single M13 bacteriophage tethering and stretching. *Proc Natl Acad Sci.* **12**, 4892–4897 (2007).
17. Carr-Smith, J. *et al.* Polymerase chain reaction on a viral nanoparticle. *ACS Synthetic Biology* **4**, 1316-1325 (2015).
18. Rodger, A., Nordén, B., Dafforn, T. Linear Dichroism and Circular Dichroism (Royal Society of Chemistry, 2010). ISBN: 9781847559029
19. Clack, B., Gray, D. Flow Linear Dichroism Spectra of Four Filamentous Bacteriophages : DNA and Coat Protein Contributions. *Biopolymers* **32,** 795–810 (1992).
20. Lakowicz, J. *Principles of fluorescence spectroscopy*. (Springer US, 2006). ISBN: 9780387312781
21. Wemyss, A. The development of experimental and analytical techniques for the study of aligned fluorophores. PhD thesis, University of Warwick (2016).
22. Arévalo, F., González-Techera, A., Zon, M., González-Sapienza, G., Fernández, H. Ultra-sensitive electrochemical immunosensor using analyte peptidomimetics selected from phage display peptide libraries. *Biosens. Bioelectron.* **32,** 231–237 (2012).
23. Lang, Q. *et al.* Specific probe selection from landscape phage display library and its application in enzyme-linked immunosorbent assay of free prostate-specific antigen. *Anal. Chem.* **5**, 2767–2774 (2014).
24. Li, S. *et al.* Direct detection of *Salmonella typhimurium* on fresh produce using phage-based magnetoelastic biosensors. *Biosens. Bioelectron.* **26,** 1313–1319 (2010).
25. Mao, C., Liu, A., Cao, B. Virus-based chemical and biological sensing. *Angew. Chemie - Int. Ed.* **48,** 6790–6810 (2009).
26. Kather, I., Bippes, C., Schmid, F. A stable disulfide-free gene-3-protein of phage fd generated by in vitro evolution. *J. Mol. Biol.* **354,** 666–678 (2005).
27. Langone, J. Protein A of *Staphylococcus aureus* and related immunoglobulin receptors produced by Streptococci and Pneumococci. *Adv. Immunol.* **32,** 157-252 (1982).
28. Moks, T. *et al.* Staphylococcal protein A consists of five IgG-binding domains. *Eur. J. Biochem* **156,** 637-643 (1986).
29. Miltenyi, S., Muller, W., Weichel, W., Radbruch, A. High gradient magnetic cell separation with MACS. **238,** 231–238 (1990).
30. Walt, D. Optical methods for single molecule detection and analysis. *Anal. Chem.* **3**, 1258–1263 (2013).
31. Fuh, G., Sidhu, S. Efficient phage display of polypeptides fused to the carboxy-terminus of the M13 gene-3 minor coat protein. *FEBS Lett.* **480,** 231–234 (2000).

32. Hochuli, E. *et al.* Genetic approach to facilitate purification of recombinant proteins with a novel metal chelate adsorbent. *Nat. Biotechnol.* **6,** 1321–1325 (1988).
33. Bornhorst, J., Falke, J. *Purification of proteins using polyhistidine affinity tags*, in *Methods in Enzymology* **326**, 245-254 (2000).
34. Howarth, M., Fairhead, M. Site-specific biotinylation of purified proteins using BirA, in *Methods in Molecular Biology* book series *(Springer, 2014)* ISBN: 9781493922727
35. Steiner, D., Forrer, P., Stumpp, M., Plu, A. Signal sequences directing cotranslational translocation expand the range of proteins amenable to phage display. **24,** 823–831 (2006).
36. Kimple, A., Muller, R., Siderovski, D., Willard, F. *A capture coupling method for the covalent immobilization of hexahistidine tagged proteins for surface plasmon resonance,* in *Methods in Molecular Biology* book series (Springer, 2010). ISBN: 9781607616702
37. Chan, J., Dodani, S., Chang, C. Reaction-based small-molecule fluorescent probes for chemoselective bioimaging. *Nat. Chem.* **4,** 973–984 (2012).
38. Li, K. *et al.* Chemical modification of M13 bacteriophage and its application in cancer cell imaging. *Bioconjugate Chem*. **21**, 1369–1377 (2010).
39. Domaille, D., Lee, J., Cha, J. High density DNA loading on the M13 bacteriophage provides access to colorimetric and fluorescent protein microarray biosensors. *Chem. Commun.* **49,** 1759–1761 (2013).
40. Lee, J., Domaille, D., Cha. J. Amplified protein detection and identification through DNA-Conjugated M13 bacteriophage. *ACS Nano* **6,** 5621–5626 (2012).
41. World Health Organization (WHO). *Exposure to lead: a major public health concern* (2010).
42. World Health Organization (WHO). *Lead poisoning and health*. (Media centre fact sheet, 2016).
43. Ganim, S., Tran, L. from CNN (2016). *How tap water became toxic in Flint, Michigan.* Available at: http://edition.cnn.com/2016/01/11/health/toxic-tap-water-flint-michigan/index.html [Accessed: 10th February 2017].
44. Milman, O., Felton, R. from The guardian (2016). *Flint water crisis: Michigan officials ignored EPA warnings about toxicity.* Available at: https://www.theguardian.com/us-news/2016/feb/03/flint-water-crisis-congress-michigan-officials-ignored-epa-warnings-lead [Accessed: 10th February 2017].
45. Beaker, R. DNA enzymes. *Nat. Biotechnol.* **15,** (1997).
46. Ponce-Salvatierra, A. *et al.* Crystal structure of a DNA catalyst. *Nature* **529,** (2016).
47. Mazumdar, D. *et al.* Easy-to-use dipstick tests for detection of lead in paints using non-cross-linked gold nanoparticle-DNAzyme conjugates. *Chem. Comm*. **46**, 1416–1418 (2010).
48. Zhu, X. *et al.* A sensitive and specific electrochemiluminescent sensor for lead based on DNAzyme. *Chem. Comm*. **40**, 6050–6052 (2009).

49. Wang, B. Z., Lee, J. H., Lu, Y. Label-free colorimetric detection of lead ions with a nanomolar detection limit and tunable dynamic range by using gold nanoparticles and DNAzyme. *Adv. Mater*. 20, 3263–3267 (2008).
50. Lan, T., Lu, Y. *Metal ion-dependent DNAzymes and their applications as biosensors*, in *Metal Ions in Life Sciences* book series (Springer, 2011). ISBN: 9789400721715
51. Li, J., Lu, Y. A highly sensitive and selective catalytic DNA biosensor for lead ions. *J. Am. Chem. Soc.* **122**, 10466–10467 (2000).
52. Liu, J., Lu, Y. A colorimetric lead biosensor using DNAzyme-directed assembly of gold nanoparticles. *J. Am. Chem. Soc.* **125**, 6642–6643 (2003).
53. Liu, J., Lu, Y. Accelerated color change of gold nanoparticles assembled by DNAzymes for simple and fast colorimetric Pb^{2+} detection. *J. Am. Chem. Soc*. **126**, 12298–12305 (2004).

CHAPTER 4 – Imaging wall shear stress using the M13 bacteriophage as a nanosensor

This chapter was adapted from the published work in Nano Research (2015) [1].

4.1 Introduction

It is well-established that wall shear stress (WSS) - defined as the force exerted by blood flowing over the surface of an arterial wall - is involved in many normal biological phenomena, but also plays a key role in vascular disorders. WSS profiles are abnormal, for example, when atherosclerotic plaque builds up and obstructs a vessel, changing the surrounding blood shear flow and therefore indicating an unhealthy vasculature. Although WSS is of paramount importance in vascular biology, there is currently no method to measure it accurately in physiological systems. Understanding vascular dysfunctions and how to diagnose it, treat it and even prevent it, can not be clearly elucidated without knowledge on the WSS dynamics.

In this work, a strategy for immobilisation of a phage nanosensor was developed, enabling a successful integration of a biological scaffold with a microfluidic biosensor. A fluorescent phage nanosensor was constructed to detect changes in shear flow, in real-time, intended for applications in vascular flow imaging in cardiovascular diseases and therapeutics. We show that these nanosensors can be tracked using standard optical tools. The versatility of our nanosensors was further demonstrated by adapting it for *in vitro* experiments, imaging WSS in the micro-domains of endothelial cells. At a later stage, this phage-based construct could help better understand how blood vessels change *in vivo*, how they become wider or tighten up, and how they respond to cardiovascular drugs.

4.1.1 M13 bacteriophage and wall shear stress

Wall shear stress (WSS) is defined as the force that a moving fluid exerts parallel to a surface, such as that of blood flowing across the surface of the endothelial cells lining blood vessels [2,3]. WSS affects cellular and biochemical reactions and plays a crucial role in normal vascular physiology. Abnormal WSS has been linked to medical conditions, such as atherosclerosis, diabetes, and angiogenesis-dependent cancers, and it is therefore an important parameter in understanding, preventing and diagnosing vascular disorders [4-11].

In the vasculature, the velocity gradient near the wall is often measured using bulk flow techniques, such as particle image velocimetry (PIV) [12]. PIV methods struggle with the complex dynamics of WSS, which might not only lead to missing valuable data but also introducing interferences to the results. One problem with PIV technique is that of the concentration of tracer particles along the vessel – the lumen of the vessel will contain a larger number of tracer particles, which decrease as the surface of the wall is approached. Fewer particles reach the wall surface and therefore less data on this region of the vessel can be collected. Another challenge of this method is that it makes assumptions on the uniformity of the flow and the surfaces the fluid crosses [13]. Such an average measurement may hide variability critical to the understanding of vascular disease states in dynamic systems, as of a blood vessel.

As described in Chapter 1, the M13 phage has been explored to create novel biomaterials and used as a scaffold for nanowires, biosensors, and in bioimaging. The M13 bacteriophage, having a filamentous structure, is an adequate candidate for the experiments described in this chapter. Moreover, it has other inherent properties that are advantageous – it is biologically and mechanically stable, inexpensive to produce using simple microbiology techniques, and it has several available functional groups on its surface for the necessary chemical modifications [14]. As investigated in Chapter 3, it is possible to tether one end of the phage to a surface. The nanosensor construct designed for the work developed in this chapter is a chemically modified phage with a specific binding

element (*e.g.* an antibody) conjugated to the p3 proteins, and a fluorophore dye labelling the p8 proteins (Fig. 3.6, Chapter 3). The nanosensor is anchored to the surface of a microfluidic slide by one-end only, and its behaviour under various shear flow conditions is visualised. Subsequent data analysis allows determining the WSS applied to the surface of the microfluidic slide. The result is a biological flow nanosensor that is potentially usable *in vivo* in the vessel-blood interface.

4.1.2 Glycocalyx – the endothelial gatekeeper

Wall shear stress (WSS) regulates several vascular parameters, as it acts on and is sensed by the endothelial cells. More specifically, it is sensed by the glycocalyx. The endothelial glycocalyx is a thin layer of polysaccharide matrix covering the apical surface of endothelial cells lining the vessel walls [15,16]. It acts as a barrier between the vascular lining and the blood stream (Fig. 4.1). This mesh-like structure is composed of a network of proteoglycans, glycoproteins and plasma proteins, and has an important role in maintaining the integrity of the vascular walls. An example of *in vitro* imaging of the glycocalyx on endothelial cells is shown in Fig. 4.2 (Chapter 2, method 2.5.5).

It is widely accepted that the glycocalyx plays a physiological role as a mechanotransducer (*i.e.* translation of biomechanical forces into biochemical signals), on vascular permeability (as it limits the access of certain molecules to the endothelial cell membranes), and participates on protein-cell interactions (for example, in the leucocyte-vessel wall interaction and the adhesion of the leucocytes to the surface of endothelial cells). The glycocalyx is crucial in normal vascular physiology (*e.g.* angiogenesis) but also in vascular disease – degradation to this layer is thought to be associated with several pathophysiological conditions, such as diabetes, atherosclerosis and cancer [16,17].

The components making up the glycocalyx are continuously synthesised and shed from the endothelial cells surface, in a dynamic process driven by the flow forces of circulating blood. Since the glycocalyx is located in the interface

between blood and the endothelium, it mediates flow-induced shear stress on the endothelial cells. It is in here, a few hundred nanometers above the cell surface, the phage nanosensor was designed to detect and measure shear stress.

Although experimental data strongly suggests the vasculoprotective role of glycocalyx and its overall functional importance [16], research on this subject lacks techniques to properly detect and measure the mechanical forces applied on this layer. Understanding the mechanical properties of the glycocalyx and, therefore, measuring wall shear stress at the surface of blood vessels, is essential to many biological functions and could be crucial to study blood vessels function in health and vascular disease.

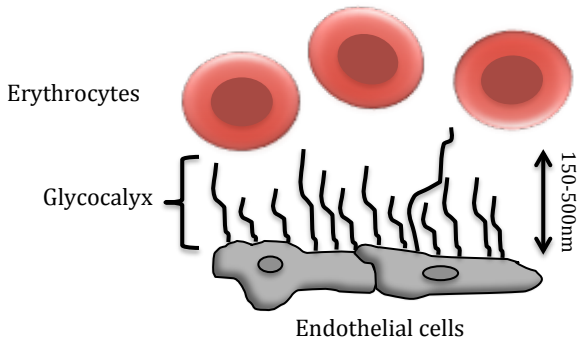

Figure 4.1: Schematic representation of the endothelial glycocalyx. The glycocalyx is a carbohydrate-rich brush-like structure lining the vascular endothelium, and can extend 150–500 nm from the endothelial cell surface. Not drawn to scale.

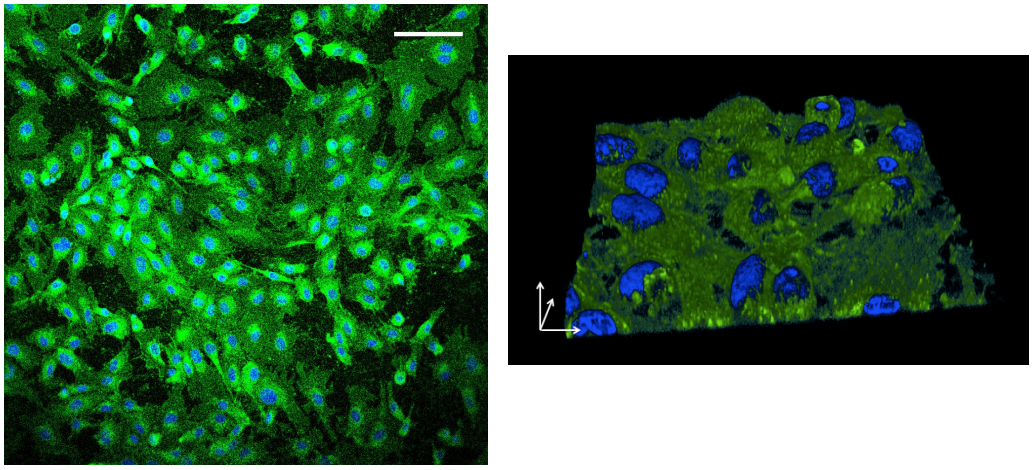

Figure 4.2: Visualisation of the glycocalyx on 5-days cultured human umbilical vein endothelial cells (HUVECs). (Left) Confocal microscopy image of labelled HUVECs. DAPI (blue) - nucleus; WGA-FITC lectin (green) - glycocalyx. Wheat germ agglutinin (WGA) binds to sugar residues, and therefore the green labelling suggests expression of heavily glycosylated glycoproteins, which are present in the glycocalyx. Scale bar: 100 µm. (Right) 3D reconstruction of a series of Z stacks obtained with confocal microscopy. Arrows indicate the direction of the X, Y and Z axis.

4.1.3 Imaging wall shear stress using a chemically modified phage

The method described here, developed to study WSS, anchors a filamentous structure by one-end to a surface and tracks changes in its orientation in response to flow. An illustrative metaphor could be how, in a similar way, a windsock gives information about the wind strength and direction.

The *in vitro* experiments, described in Fig. 4.9, show the behaviour of the phage nanosensor under various flow conditions. The basic principle is the following – the nanosensor, in the absence of flow, oscillates randomly due to Brownian motion, not preferring any specific position. However, when flow is applied, the movement of the nanosensor becomes restricted. The nanosensor lines up with the direction of the flow and it is sensitive to the flow intensity. An illustration of this concept is given in Fig. 4.3. In a system were the direction and/or intensity of flow are unknown, this platform could give valuable information. The chemically modified phage can be adapted to study the flow in the vasculature, in which knowing what alters the blood flow and how it changes in diseases and

therapeutics, can be of great medical importance.

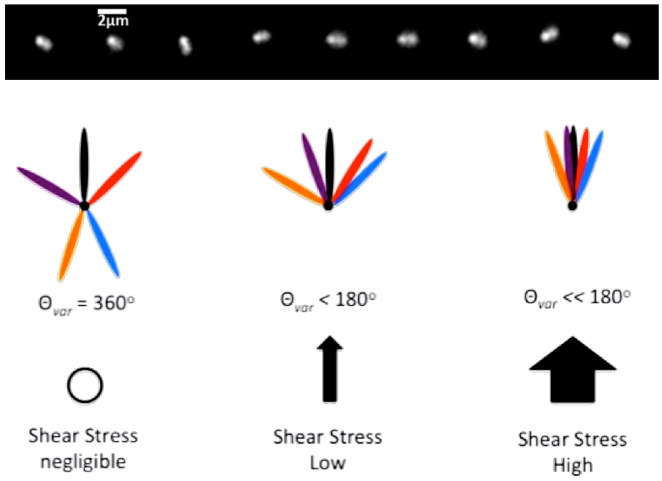

Figure 4.3: Schematic of the concept for measuring WSS developed in this work. The top banner is a microscope film-strip of images of an anchored fluorescent M13 phage responding to flow. The bottom scheme represents the concept of using the bacteriophage as a nanosensor for mapping flow. The black dot represents the anchoring point of the bacteriophage; colourful elliptical shapes illustrate the bacteriophage at different positions in space at different time points. From left to the right: increasing shear flow (black arrow) induces bacteriophage to align in the direction of flow, resulting in a smaller variation of the orientation angle.

4.2 Results and discussion

4.2.1 Building the M13 bacteriophage nanosensor

An overview of the 2-step chemical modification used is given in Chapter 3 (Fig. 3.6). Detailed bioconjugation protocols and purification methods are given in Chapter 2. Firstly, we developed a method to anchor the bacteriophage by one end to a surface. As explored in Chapter 3, a possible approach is to modify the cysteines present on the p3 protein of the phage, by reducing its disulfide bridges to sulfhydryl groups. These thiols are exposed and available to conjugate with the maleimide groups previously inserted on an antibody of choice. Next, fluorophore molecules were chemically attached to the p8 protein of the phage, decorating its capsid. TRITC (tetramethylrhodamine isothiocyanate) is a red-orange dye for chemical labelling of amines. An illustration of the dye-coated phage capsid may be seen in Chapter 3 (Fig. 3.14). This latter step is crucial for

the imaging component of this work, which is required to observe the dynamic behavior of the bacteriophage under a microscope. Since the labelling of the amines on the p8 proteins with TRITC is pH-dependent, an optimal pH for this reaction was investigated (Fig. 3.14, Chapter 3). A buffer of pH 8 was chosen as a compromise, to avoid interfering with the stability of the antibody. The final constructs were purified by size exclusion chromatography (SEC) (Chapter 2, method 2.2.3). The SEC chromatogram on Fig. 4.4 shows that the reaction mixture contained the M13-Antibody-TRITC conjugates and other small molecules, possibly PEG, unreacted reagents and proteinaceous material. As expected, the M13 conjugates have the largest mass, eluting first from the column, at approximately 40 mL. The fractions from this peak were collected, concentrated by PEG precipitation, and run on the LD to confirm for presence of bacteriophage. Moreover, since the filamentous structure of the M13 is crucial for the proposed imaging platform, TEM images were collected to confirm the M13 conjugates were intact following the bioconjugation protocols. A LD spectrum (Chapter 2, method 2.8.2) and a transmission electron microscopy (TEM) image (Chapter 2, method 2.5.7) of the purified M13-Antibody-TRITC are shown in Fig. 4.5, suggesting chemically modifying the surface of the bacteriophage has no observable negative effects on the phage filamentous structure and its overall alignment under flow.

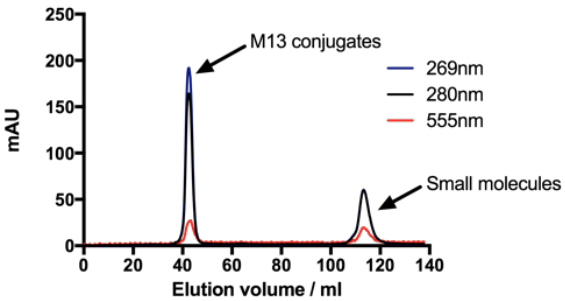

Figure 4.4: Size exclusion chromatogram of M13-Antibody-TRITC conjugates. Multiple absorbance wavelengths monitored: 269 nm (blue) for M13 bacteriophage, 280 nm (black) proteins, 555 nm (red) TRITC dye. The fractions were collected, concentrated and run on LD to confirm for the presence of bacteriophage. The fractions corresponding to the first peak were used for the following experiments. Eluted in 100 mM potassium phosphate buffer, 150 mM NaCl, pH 7.2.

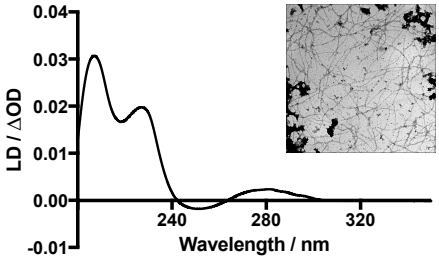

Figure 4.5: LD spectrum and TEM image of the M13-Antibody-TRITC construct, after purification with size exclusion chromatography. Black marks on the TEM image are unwashed stain.

The first stage of experiments for this work was done using collagen-coated microfluidic slides, in which the phage was attached to this surface by an antibody specifically against the collagen (anti-collagen antibody). Although this system was suitable for proof-of-concept, it is a rather artificial and generally not a good representation of what happens *in vivo*. Therefore, a second experimental set-up was designed in which the microfluidic slides were coated with endothelial cells, GEnC (glomerular endothelial cells), as a closer model for the physiological vascular lining. To anchor the phage nanosensor to the endothelial cells' surface, a carbohydrate-binding protein (wheat germ agglutinin, WGA) was used. WGA is a ~ 36 kDa protein that binds to glycoproteins in the membrane of endothelial cells, more specifically to the N-acetyl-D-glucosamine and sialic acid of the glycocalyx expressed by the endothelial cells [18]. This lectin, which can be conjugated to fluorescent dyes such as fluorescein (FITC), has been used for imaging of the glycocalyx [18-20], as shown in Fig. 4.2. The bioconjugation protocol and purification steps were similar to the first set of experiments (Chapter 2, method 2.4.1.2). Schematics of these two set-ups are illustrated in Fig. 4.8.

With most proteins, interfering with its structure could result in loss of function; in this case, the bioconjugation protocol could result in the inability of WGA to recognise and bind to the surface of the glycocalyx. To check the bioconjugation protocol did not substantially affect the WGA structure, a circular dichroism

(CD) spectrum (Chapter 2, method 2.8.3) was collected from the lectin before and after the crosslinking reaction step (with SMCC). As shown in Fig. 4.6, no significant alteration to the WGA structure could be observed on the CD spectrum after treatment with SMCC and purification on a PD-10 column. There is no guarantee, however, the protein kept its function, but it was expected that if the structure was not drastically modified, WGA would still be able bind to the components on the membrane of cells.

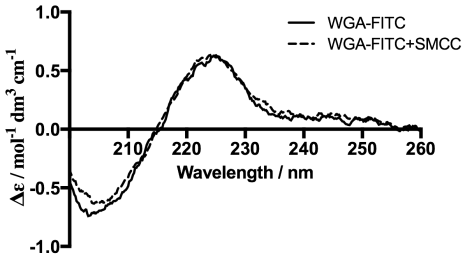

Figure 4.6: CD spectra of WGA-FITC. These spectra were collected to check whether WGA-FITC (solid line) suffers any major conformation change after reacting with SMCC and being purified on a PD-10 column (dashed line).

The FITC molecules conjugated to WGA were used to characterise the success of the bioconjugation of WGA to the bacteriophage. The UV-Vis spectra of WGA-FITC, M13+WGA-FITC and M13+WGA-FITC+TRITC samples were collected (Fig. 4.7). The peak at 490 nm, corresponding to FITC, is present in the M13+WGA-FITC sample, suggesting WGA is present in the phage sample. However, this experiment alone does not prove the FITC dye is attached to the phage – it only informs about the presence of FITC in the sample. For this reason, another experiment was carried out, in which the M13+WGA-FITC+TRITC was observed under a microscope with a double-beam filter, looking for the fluorescence of FITC and TRICT (Chapter 2, method 2.5.6). As shown in Fig. 4.7, a green blob at the end of a red rod-shaped figure seems to indicate the presence of FITC molecules at the end of what one can imagine being the phage coated with TRITC dye. These data suggested the conjugation of WGA to the p3 proteins of the phage was successful.

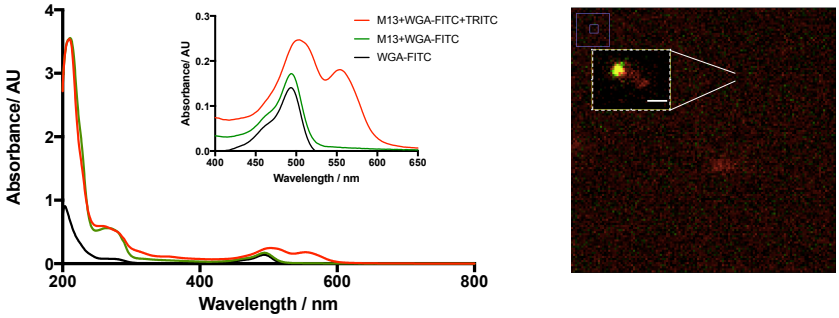

Figure 4.7: UV-Vis spectra and microscopy image of the M13+WGA-FITC+TRITC conjugate. (Left) UV-Vis of the lectin conjugated to a FITC dye molecule (WGA-FITC, black line); of the product of reaction between the M13 phage and the lectin (M13+WGA-FITC, green line) after being purified through a PD-10 column and PEG/NaCl precipitation; and of the product of the final step of the bioconjugation between the phage-lectin and the TRITC dye (M13+WGA-FITC+TRITC, red line) after being purified. Inset - zoom of the dye absorbance regions on the spectra. (Right) Double-beam (red-TRICT, green-FITC) confocal microscopy image of the TRITC+WGA-FITC modified phage. Scale bar: 1 μm.

4.2.2 Experimental set-up and analysis overview

M13 were grown, purified [21] and labelled as outlined in Chapter 2. M13 was derivatised with the anchor-molecule attached to the p3 protein and its p8 proteins fluorescently decorated. The nanosensor construct anchored to a microfluidic slide is schematically illustrated in Fig. 4.8. Microfluidic slides (μ-Slide I Luer, ibidi) were assembled into a controlled flow system by using a peristaltic pump (ibidi). It has been previously shown that ibidi systems are able to orient semi-rigid molecular systems [22]. The M13 construct was bound to the surface of the microfluidic slide (coated with collagen for the first set of experiments, and coated with endothelial cells for the second set of experiments) and unbound M13 was rinsed off. A nominal WSS (0–3.5 dyn/cm^2) was applied. The fluorescent images of the derivatised and labelled phage constructs in flow were measured by using either a spinning disk confocal microscope or a wide-field inverted microscope. Flow experiments and imaging details are described in Chapter 2. Recorded time-lapses images were post-analysed using a function in MATLAB scripted by Dr. Alan Wemyss [23], who also plotted the data shown

on Fig. 4.9, 4.11, 4.12 and 4.13.

From imaging analysis, the orientation angle and approximate length and width of the M13 sensor in each frame was determined. Using MATLAB, the region that the M13 occupies on each frame was first defined by finding a threshold pixel intensity below which all pixels were set to zero and above which they were set to one (Otsu method, [24]). The pixels with value one, whose nearest neighbour also had value one, were defined as regions of interest (ROI). The largest of these was assumed to be the M13. An image stack with the largest ROI subtracted out was created to be the background and was subtracted from the original binary image, leaving only the M13 sensor in each image. The major axis was then defined as the longest possible straight line that could be drawn within the ROI, and its angle, determined relative to the horizontal axis of the image, defined the phage's orientation.

The tethered nanoparticle motion under Brownian effects and flow was also modeled phenomenologically by Dr. David Smith, from University of Birmingham. Although crucial to take conclusions from the experimental data, the modeling component of this work falls out of the scope of this thesis – further details are described in the supplementary information of [1].

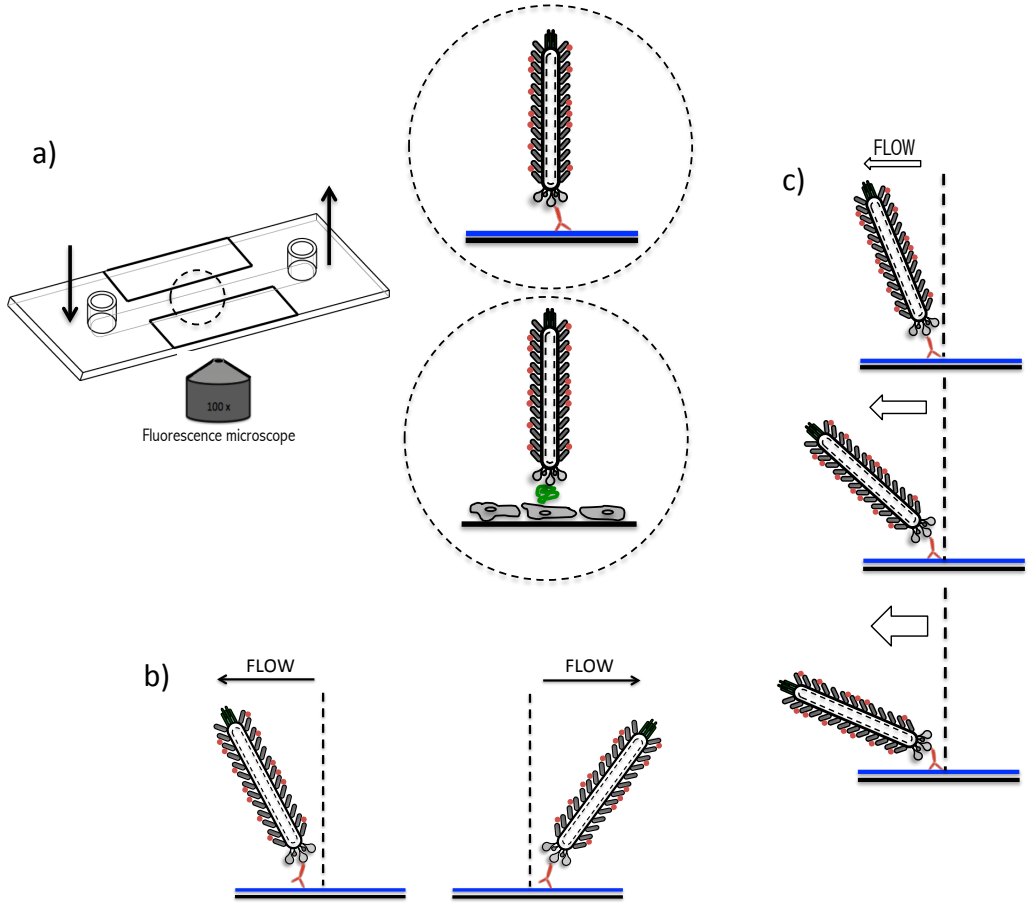

Figure 4.8: Scheme of the microfluidic design using the anchored phage to study flow variations. a) (Top circle) An ibidi slide flow chamber coated with collagen (blue line) with a phage attached via an anti-collagen antibody. (Bottom circle) An ibidi slide flow chamber coated with endothelial cells with an anchored phage via WGA (green blob). The two arrows illustrate the in/out of the microfluidic slide chamber. The microfluidic slide is observed under a microscope. The dynamic behavior of the chemically modified phage anchored by one-end to a surface b) orients to the right or to the left depending on the direction of the flow, and c) differentiates between flow intensities – less intense flow allows for a wider angle between the phage and the microfluidic slide surface; stronger flow forces the phage to align more parallel to the surface.

4.2.3 Imaging wall shear stress

To image WSS, two systems were developed using the novel M13 nanosensor:

i) Fluorescent M13 constructs derivatised with anti-collagen antibodies (M13-Antibody-TRITC) anchored to a collagen coated microfluidic slide. The collagen was designed to act as a relatively flat surface to test the principles of the constructed nanosensor.

ii) Fluorescent M13 constructs derivatised with WGA (M13-WGA-TRITC) anchored to cultured endothelial cells (via the glycocalyx) on a microfluidic slide. The endothelial cells were considered to act as a closer model to a blood vessel.

4.2.3.1 Imaging wall shear stress on collagen-coated slides

Spinning disc images of M13-Antibody-TRITC exposed to a range of nominal WSS (0–3.5 dyn/cm^2) were collected. The data from these experiments take the form of time-lapse images of individual M13-Antibody-TRITC constructs on the surface. The constructs could be recognised under the microscope as bright points, agitating in the buffer. Once under high digital magnification, the M13-Antibody-TRITC constructs appears as elliptical shapes that adopt different angles as a function of time (Fig. 4.9). Once an M13-Antibody-TRITC construct was in focus, the flow was induced to test if the construct was bound. Images of the flow slide with no shear flow applied suggested that the M13-Antibody-TRITC construct is on the surface and randomly oriented (in response to Brownian motion). The reaction to flow-induced shear is obvious by eye – the fluorescent ellipse orients, seemingly instantaneously, with its long axis preferentially aligned with the shear flow direction. The degree of orientation increases with flow rate. The microscope focus typically required adjustment to achieve optimal imaging, once flow was applied. The signal-to-noise decrease over time as would be expected if bleaching was occurring; however, more than 10 minutes of continuous imaging was possible without compromising the quality of the data collected.

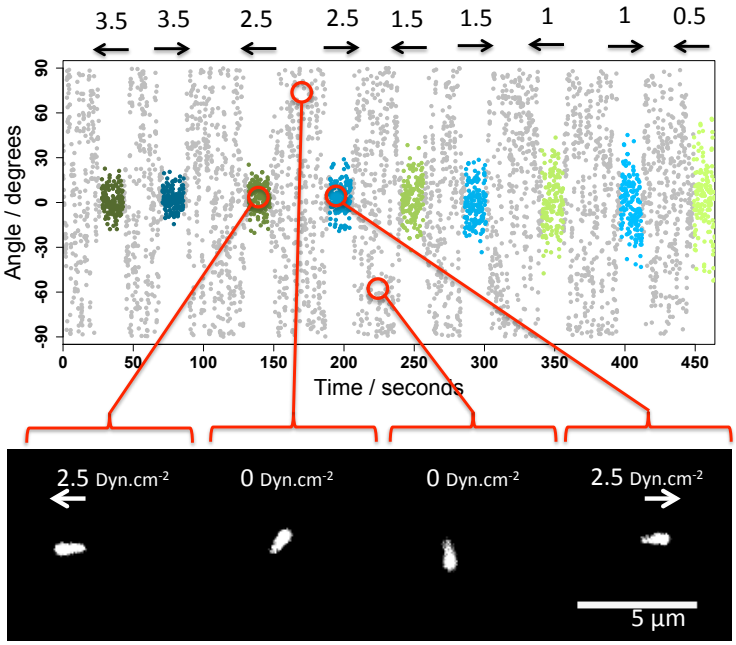

Figure 4.9: Example of wall shear stress visualised by M13-Antibody-TRITC bound to a collagen-coated flow slide. The plot illustrates the functionalised M13 orientation versus time in a typical experiment. The nominal wall shear stress (assuming a linear relationship between bulk fluid flow and WSS) is indicated at the top in dyn·cm^{-2}. The flow direction and magnitude at each time point are indicated by the arrows and by the color and intensities of the overlays (negative (green), positive (blue), and zero (grey)). Example of bacteriophage images at time points corresponding to the red circles in background subtracted spinning disk confocal image frames are shown below.

4.2.3.2 Imaging wall shear stress on endothelial cells-coated slides

Glomerular endothelial cells (GEnC), typically used as a model capillary system for kidney disease [25], were seeded onto sterile flow slides. These kidney-derived cells provide an intellectual bridge to future work in how complications of diabetes (*e.g.* nephropathy) affect flow in kidneys. WGA conjugated to the p3 protein of M13 (M13-WGA-TRITC) made a nanosensor that was visualised by using a wide-field fluorescent microscope showing that the bacteriophage had successfully adhered to a confluent layer of cells on the flow slide surface. A picture of a phage nanosensor anchored to the surface of an endothelial cell is given in Fig. 4.10.

Time-lapse images show that in the absence of flow the conjugates move fairly randomly in response to Brownian motion in a manner consistent with the attachment to the cellular surface by only one-end. The angle space it explores is reduced compared with the collagen-coated slides. This suggested the phage nanosensor is responding to a non-uniform surface.

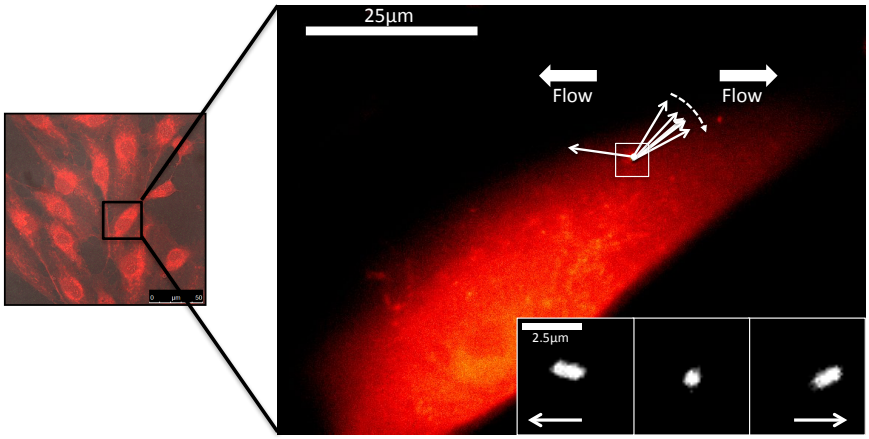

Figure 4.10: Microscope image of a M13-WGA-TRITC construct on the surface of an endothelial cell. Modified phage (white dot on top of the cell) is bound to the surface of the cultured cell, and various flows are passed over it. In the box area are examples of images from the modified phage under -3.5, 0.5 and 3.5 dyn/cm^2 (from left to right).

4.2.4 Response of M13-Antibody-TRITC and M13-WGA-TRITC constructs to flow

To use the data to quantify WSS, a robust data analysis methodology was required. This has two parts: turning the videos into orientation data of the type summarized in Fig. 4.9, and the development of a theoretical model of how the phage orientation relates to the flow.

MATLAB code was written to extract the phage orientation and major axis length data. Its angle relative to the horizontal axis of the image defined the bacteriophage's orientation. The MATLAB segmentation code was found to be accurate by eye and gave similar results to a Fiji/ImageJ directionality plugin [26]. Videos of these time-lapses are available. The mathematical model gave

insight on how to judge the relationship between WSS and the behaviour of the nanosensor under various flow rates, on two different surfaces.

The data collected from M13-Antibody-TRITC on the collagen-coated slides were used as a simplistic model to demonstrate that WSS can be predicted from the behavior of the nanosensor in flow, using David Smith's proposed mathematical model. In the collagen-coated slides experiments, the movement of the anchored M13-Antibody-TRITC nanosensor was unrestricted in all directions. The nanosensor has a similar response to positive and negative flow direction, being likely to take any orientation ranging from –90° to +90°. This symmetry in response to flow, regardless of its direction, is illustrated in the top plot of Fig. 4.11. This plot illustrates the behaviour of the nanosensor in various flow rates. When no flow is applied, the anchored nanosensor moves freely taking any random orientation from –90° to +90°. Increasing flow rates constrain the movement of the nanosensor - higher flow rates result in a smaller variation in the nanosensor orientation, which is shown by the size of the red error bars on the plot.

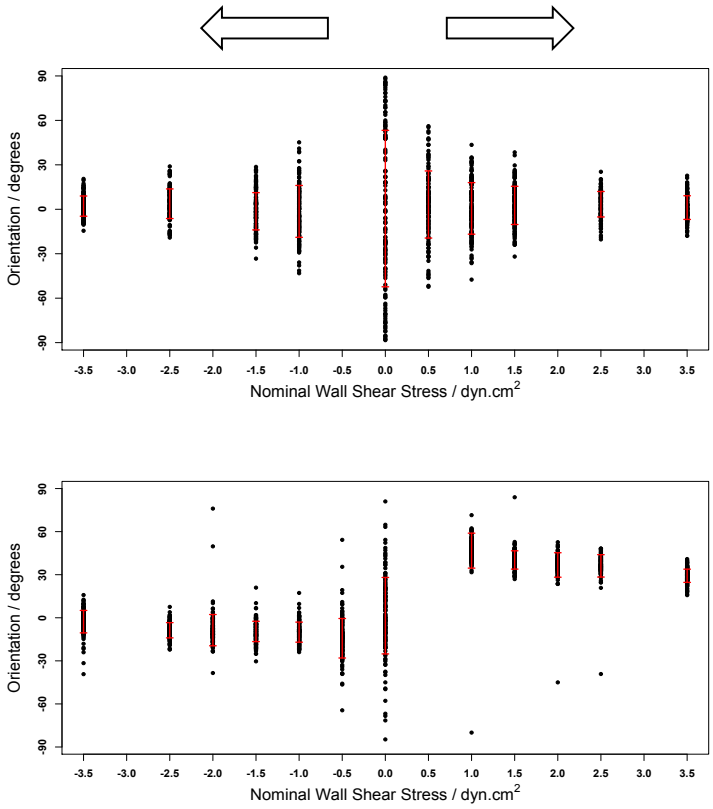

Figure 4.11. Tracking the orientation of the anchored phage construct. Orientation vs. nominal WSS for an M13 anchored to collagen (top) and GEnC endothelial cells-coated slides (bottom), representing negative flow (arrow to the left) and positive flow (arrow to the right). σ is denoted by the red bars for each flow around the mean value.

The bottom plot of Fig. 4.11 shows the processed data from the collected time-lapses of the M13-WGA-TRITC nanosensor anchored to an endothelial cells-coated slide. This plot clearly illustrates the difference in behaviour of the nanosensor on a flat collagen-coated microfluidics slide and on a non-uniform GEnC-coated microfluidics slide. This plot shows that in the negative flow direction, the average orientation adopted by the nanosensor is around 0, whereas the average variance in orientation of the nanosensor is reduced when flow is applied in the positive direction. This illustrates that the nanosensor is not moving freely, which is probably due to its location on the surface of the cell. Protruding endothelial cells have been shown to interfere with local wall shear stress [27,28]. In the specific example of this data, the M13-WGA-TRITC nanosensor was observed to be anchored on top of the nucleus of the endothelial cell, which may have hindered its movement.

The mathematical model predicted that a plot of ln(σ) versus ln(nominal WSS) will have a slope of –0.5 and that the nominal WSS is proportional to the inverse square of the standard deviation of the particle's adopted orientation at a given flow rate. This was confirmed to be accurate for the collagen-coated slides experiments, as shown in Fig. 4.12. Plotting the ln(σ) versus ln(nominal WSS) for the M13-WGA-TRITC nanosensor anchored to an endothelial cell, would make it easier to visualise the effect of the non-uniformity of the surface on the WSS. These data are illustrated in Fig. 4.12.

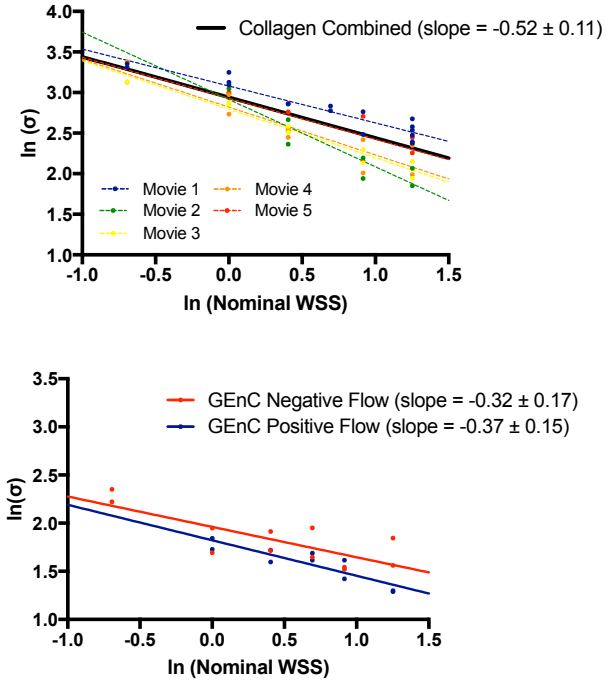

Figure 4.12: ln(σ) versus ln(nominal WSS) on collagen- and endothelial cell-coated surfaces. (Top) ln(σ) versus ln(nominal WSS) of 5 movies of the M13-Antibody-TRITC nanosensor anchored to a collagen-coated microfluidics slide. (Bottom) ln(σ) versus ln(nominal WSS) of 1 movie of the M13-WGA-TRITC nanosensor anchored to an endothelial cells-coated microfluidics slide, under positive and negative direction flow.

Although the slopes of the data of Fig. 4.12 for the M13-WGA-TRITC nanosensor are smaller than the predicted –0.5 from the model, this was considered to still be in agreement within the large error of the experiment. In

order to reduce the error from these experiments, it would be necessary to collect and analyse more data points using the M13-WGA-TRITC nanosensor on flow experiments. Nominal WSS is the value of the WSS if the bulk flow is a correct predictor of the flow at the surface. We expect this to be accurate for the uniform collagen coated-slides experiments. By way of contrast, endothelial cells-coated slides are non-uniform surfaces. These data suggest that the bulk flow-determined nominal WSS from the collagen-coated slide is not a good estimate of WSS at a cell surface. This is clearer in Fig. 4.13.

From the equations of the mathematical model we could derive that the nominal WSS is proportional to the inverse variance of the phage's orientation. Therefore, a plot of $1/\sigma^2$ versus the nominal WSS could demonstrate what is the effect of the endothelial cells on the WSS. Fig. 4.13 illustrates these data for the nanosensor anchored to the collagen and endothelial cells slide.

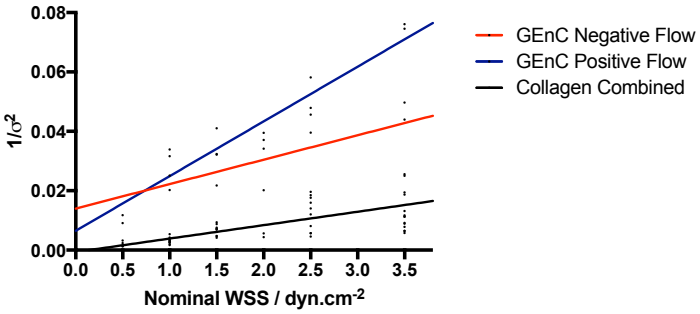

Figure 4.13. Relationship between WSS and the topography of a surface. Plot of the inverse variance ($1/\sigma^2$) versus nominal WSS from Fig. 4.12 and the combined collected data from M13-Antibody-TRITC anchored to a collagen-coated slide.

From analysing Fig. 4.13, it seems clear the endothelial cells are altering the WSS, which is locally sensed by the phage nanosensor. The slopes of the two GEnC lines in Fig. 4.13 are larger than those of the collagen-coated slides. For example, for a 3.5 dyn/cm^2 nominal WSS, the nanosensor anchored to the collagen uniform surface senses the equivalent to an inverse variance of 0.015; the nanosensor anchored to the surface of an endothelial cell surface however senses

higher values – the inverse variance was calculated to be 0.071 for positive flow direction and 0.043 for negative flow direction. This indicates that the observed movement of the nanosensor, free or restricted, depends on the surface topography and the direction of flow. This data further suggested that averaging shear stress over a surface, as commonly used methods tend to do, might lead to erroneous estimations of the local wall shear stress.

4.3 Conclusion

Reported in this chapter is a strategy for imaging and detecting WSS by using a chemically modified version of the M13 phage as a nanosensor. M13 phage naturally possesses different chemical groups on its structure, which were explored to anchor it to surfaces. The bioconjugation protocols to modify the surface of the phage, together with the observation of the behaviour of the phage nanosensor in flow, produced a system that can be used to study flow dynamics applied to a surface. It resulted in a simple, novel, and scalable method for imaging WSS on a micron scale level, using fluorescent microscopy.

WSS is usually calculated by using flow velocity gradients measured close to the wall, which are often unreliable approximations. We have shown that by anchoring one end of a fluorescent M13 bacteriophage onto a surface, the free body of the nanosensor particle repositions itself in response to the direction and intensity of shear flow, depending on the topography of the surface of attachment.

This method relied on the construction of two nanosensors, the M13-Antibody-TRITC and the M13-WGA-TRITC, which have been tested on two types of surfaces, respectively: relatively flat collagen-coated slides, which compare well with bulk flow expectations, and endothelial cell-coated slides. It was demonstrated that the relationship between the nanosensor particle flow behavior and WSS could be predicted by using a simple theoretical model. Measurement of the local WSS on the irregular surface of a slide coated with

endothelial cells was possible, further demonstrating the validity of the concept. The collected data and the mathematical model suggested that WSS in physiological systems is likely to deviate significantly from that expect on bulk flow estimates.

The nanosensor construct is adaptable and can, in principle, be used in *in vivo* systems. There are several key areas to develop before the technique can be used *in vivo* to explore how differences in cell surfaces are affected by local flow effects. The biophysical properties of the phage nanosensor, in particular its binding to different surfaces, may require an improvement to the modulation of the p3 proteins. Possible alternatives to the current WGA anchoring system are genetically inserting binding peptides specific for the surface of endothelial cells [29] or chemically conjugating adhesion anti-CD31 antibodies.

In summary, we developed a microscopy-based biosensing platform for tracking differences in flow, using a chemically modified phage. Although further nanosensor and data-quality developments are needed, this phage construct, with low manufacturing costs and high adaptability, suggests a way to map flow and WSS in biological systems, thus opening up a wide range of potential applications in fundamental research and medicine.

4.4 References

1. Lobo, D. *et al.* Direct detection and measurement of wall shear stress using a filamentous bio-nanoparticle. *Nano Res.* **8,** 3307–3315 (2015).
2. Katritsis, D. *et al.* Wall shear stress: theoretical considerations and methods of measurement. *Prog. Cardiovasc. Dis.* **49,** 307–29 (2007).
3. Papaioannou, T., Stefanadis, C. Vascular wall shear stress: basic principles and methods. *Hellenic J. Cardiol.* **46,** 9–15 (2005).
4. Zarins, C. K. *et al.* Carotid bifurcation atherosclerosis quantitative correlation of plaque localization with flow velocity profiles and wall shear stress. *Circ. Research* **53**, 502–515 (1975).
5. Tarbell, J. Shear stress and the endothelial transport barrier. *Cardiovasc. Res.* **87,** 320–30 (2010).
6. Slager, C. *et al.* The role of shear stress in the generation of rupture-prone vulnerable plaques. *Nat. Clin. Pract. Cardiovasc. Med.* **2,** 401–407 (2005).

7. Slager, C. *et al.* The role of shear stress in the destabilization of vulnerable plaques and related therapeutic implications. *Nat. Clin. Pract. Cardiovasc. Med.* **2,** 456–464 (2005).
8. Shaaban, M., Duerinckx, J. Wall shear stress and early atherosclerosis: a review. *AJR. Am. J. Roentgenol.* **174,** 1657–65 (2000).
9. Reneman, R., Arts, T., Hoeks, A. Wall shear stress – an important determinant of endothelial cell function and structure in the arterial system in vivo. *J. Vasc. Res.* **43,** 251–69 (2006).
10. Moore, J., Xu, C., Glagov, S., Zarins, C., Ku, D. Fluid wall shear stress measurements in a model of the human abdominal aorta: oscillatory behavior and relationship to atherosclerosis. *Atherosclerosis* **110,** 225–40 (1994).
11. Chatzizisis, Y. *et al.* Role of endothelial shear stress in the natural history of coronary atherosclerosis and vascular remodeling: molecular, cellular, and vascular behavior. *J. Am. Coll. Cardiol.* **49,** 2379–93 (2007).
12. Smith, M., Long, D., Damiano, E., Ley, K. Near-wall μ-PIV reveals a hydrodynamically relevant endothelial surface layer in venules in vivo. *Biophysical Journal* **85,** (2003).
13. Scharnowski, S., Cierpka, C. On the uncertainty of digital PIV and PTV near walls. *Experiments in Fluids* **52**, 1641–1656 (2012).
14. Chung, W., Lee, D., Yoo, S. Chemical modulation of M13 bacteriophage and its functional opportunities for nanomedicine. *International Journal of Nanomedicine* **9**, 5825–5836 (2014).
15. Alphonsus, C., Rodseth, R. The endothelial glycocalyx: a review of the vascular barrier. *Anaesthesia* **69**, 777–784 (2014).
16. Reitsma, S., Slaaf, D., Vink, H. The endothelial glycocalyx: composition, functions, and visualization. *Eur. J. Physiol.* **454**, 345–359 (2007).
17. Mitchell, M., King, M. The role of cell glycocalyx in vascular transport of circulating tumor cells. *American Journal of Physiology* **306**, 89-97 (2014).
18. Kataoka, H. *et al.* Fluorescent imaging of endothelial glycocalyx layer with wheat germ agglutinin using intravital microscopy. *Microscopy research and technique* **37,** 31–37 (2016).
19. Mochizuki, H. et al. Evaluation of ocular surface glycocalyx using lectin-conjugated fluorescein. *Clin. Ophthalmol.* **4,** 925–930 (2010).
20. Singh, A. *et al.* Glomerular endothelial glycocalyx constitutes a barrier to protein permeability. J. *Am. Soc, Nephrology* **18**, 2885–2893 (2007).
21. Pacheco-Gomez, R. *et al.* Detection of pathogenic bacteria using a homogenous immunoassay based on shear alignment of virus particles and linear dichroism. *Anal. Chem.* **84,** 91–97 (2012).
22. Cheng, X. *et al.* Continuous-channel flow linear dichroism. *Anal. Methods* **4**, 3169–3173 (2012).
23. Wemyss, A. The development of experimental and analytical techniques for the study of aligned fluorophores. PhD thesis, University of Warwick (2016).
24. Otsu, N. A threshold selection method from gray-level histogram. *IEEE Trans. Syst. Man Cybernetics*. **9**, 62–66 (1979).

25. Satchell, S. *et al.* Conditionally immortalized human glomerular endothelial cells expressing fenestrations in response to VEGF. *Kidney Int.* **69**, 1633–1640 (2006).
26. Schindelin, J *et al.* Fiji: An open-source platform for biological-image analysis. Nat. Methods **9**, 676–682 (2012).
27. Barbee, K. *et al.* Subcellular distribution of shear stress at the surface of flow-aligned and nonaligned endothelial monolayers. *American Journal of Physiology - Heart and Circulatory Physiology* **268**, 1765–1772 (1995).
28. Pozrikidis, C. Shear flow over a protuberance on a plane wall. *Journal of Engineering Mathematics* **31**, 29–42 (1997).
29. Hardy, B. *et al.* Angiogenesis induced by novel peptides selected from a phage display library by screening human vascular endothelial cells under different physiological conditions. *Peptides* **28,** 691–701 (2007).

CHAPTER 5 – Expanding on the original design of a linear dichroism-based biosensor

5.1 Introduction

As illustrated in Chapter 3, phages are good scaffolds for biosensing platforms because of their simplicity, versatility, and robustness, tolerating both chemical and genetic modifications. This, for instance, allowed for a controlled anchoring of the phage particles to a surface (which was then explored for building a microscopy-based biosensing platform, as shown in Chapter 4). In Chapter 5 the main focus is on genetic and chemical alterations to the phage surface specifically aimed at optimising an existing spectroscopy-based biosensor. Linear Diagnostics Ltd., a biotech startup that spun from University of Birmingham, developed a biosensing diagnostic platform that exploits the phenomenon of linear dichroism (LD), based on the work of Pacheco-Gomez and colleagues [1]. During the course of this work, a collaboration with Linear Diagnostics led to the design of new protocols to expand on the existing immunoassay. This chapter describes the proposed biological and chemical engineered modifications to the phage, particularly interested on simplifying the current immunoassay, reducing its costs and improving its sensitivity.

5.1.1 The principle of the LD-based biosensor

Antibody-based detection methods, collectively named immunoassays [2], are one of the major biomolecular diagnostic platforms. Traditional microbial culture methods, which are slow, time consuming and have limited applicability, have been evolved to sophisticated immunoassays, such as enzyme-linked immunosorbent assays (ELISA) and lateral flow assays (LFA). Complexity, cost and time are the main three pillars of diagnostic platforms. One of the main limitations of most immunoassays tends to be on multiplexing: the capacity of detecting, simultaneously, several different antigens in the same sample.

Therefore, an inexpensive, simple, multiplexed and fast immunoassay are valuable in diagnostics. Linear Diagnostics' LD-based biosensor aims at integrating these features through the use of a phage scaffold.

Linear Diagnostics' biosensor platform uses a chemically modified version of the M13 bacteriophage capable of binding to a target of interest (*e.g.* pathogenic bacteria) by the conjugated antibodies on its surface (*i.e.* on its p8 proteins). These modified phages were constructed using the bioconjugation protocol described in Chapter 3. When the target is present in a sample, the modified phage interacts with it, perturbing the phage overall alignment. That changes the phage spectroscopic LD signal, allowing for detection and quantification of the target. An illustration of this principle is given in Fig. 5.1.

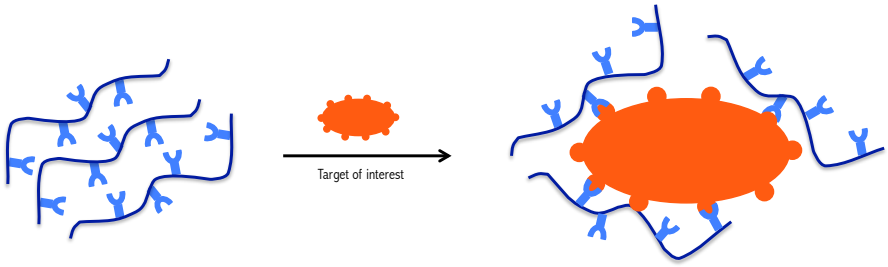

Figure 5.1: Illustration of the concept behind the LD-based biosensor immunoassay. Chemically functionalised M13 bacteriophages (blue lines) with antibodies (light blue Y-shapes) naturally align under flow, giving an expected phage LD signal. When a target of interest (orange shape) is added, the antibody-functionalised phage interacts with it. This results in an overall reduced phage LD signal because, in the presence of the target, the phage aggregates. Ultimately, the biosensor assay exploits the principle that functionalised M13 bacteriophages have a more intense LD signal than the aggregated mesh of phage-target.

A bench-top LD spectrometer is a heavy (> 100 kg) and expensive piece of equipment, and can only be used by trained scientists. Thus, Linear Diagnostics, in partnership with Molecular Vision, designed and built a portable, handheld device to use as the reader for the biosensor (Fig. 5.2). This reader, which is easy to use and can give results in less than 10 minutes, is expected to be a versatile tool to be utilised *in situ* in a wide range of sectors, including medical,

environmental, defence and security, food safety and agriculture.

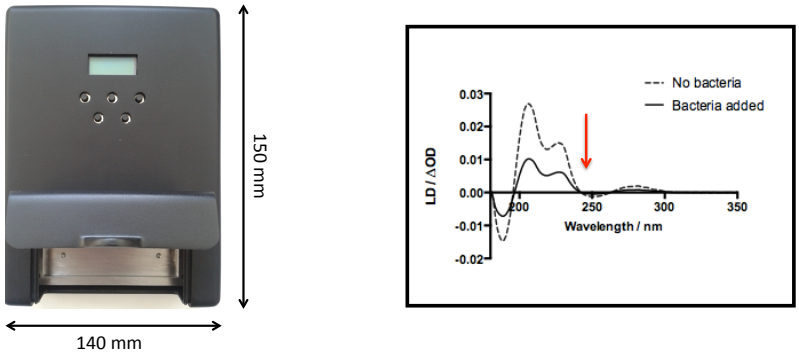

Figure 5.2: Linear Diagnostics' biosensing platform. (Left) Prototype of the biosensor reader, designed by Linear Diagnostics Ltd. In contrast to the bench-top LD machine, this miniaturised LD device is a light, handheld and portable platform. (Right) Example of a LD spectrum illustrating the drop in the phage LD signal upon addition of a target of interest (*e.g.* bacteria) to the functionalised phage.

As illustrated by the LD plot in Fig. 5.2, when target bacteria are added to the functionalised phage, this interaction perturbs the overall alignment of the filamentous phage, resulting in a decrease of its LD signal. This LD-based immunoassay has been tested and the proof-of-concept is now well-established. However, there are features of the technology that were considered as significant aspects to improve. The major drawback of the current biosensor is its limit of detection (LOD). The biosensor was presented as capable of detecting up to 10^5 cells per milliliter, but it struggles to detect bacteria below that threshold. The sensitivity of the current immunoassay is considered to be insufficient for most medical diagnostics, where a two or three order of magnitude lower LOD would be desirable. Other downsides are the associated costs, time and complexity of the chemical approaches used to modify the phage scaffold.

5.1.2 Proposed modifications to the biosensor by genetic and chemical modulation of the phage surface

The goal of the work reported in this chapter was to explore alternatives to the existing biosensing platform. Linear Diagnostics continuously optimised their immunoassay, but adjustments to the current bioconjugation protocol (see Chapter 3, Fig. 3.6) seemed not to produce significant improvements. Therefore, it was concluded that more radical changes to the phage scaffold might be necessary. Our main focus was on exploring genetic and chemical modifications to modulate the phage surface, hoping to enhance the sensitivity and the simplicity of the biosensor. Among the possible changes, these were the ones considered and developed in this work: increase to the overall surface of the phage by increasing its length (section 5.2.1), introducing an extra tryptophan on each p8 protein (section 5.2.2), introducing a cysteine on the p8 proteins (section 5.2.3), expression of a *Salmonella*-binding peptide (section 5.2.4), directional conjugation antibodies by aldehyde-hydrazine chemistry (section 5.2.5), purification of the biosensor samples using magnetic beads (section 5.2.6). A brief background to the biological and chemical approaches is given in each section, prior to describing and discussing the results obtained in this work. For clarity, each of the sections exploring the modifications to the phage scaffold has been divided in two main sub-sections, "context" and "results and discussion".

5.2 Results and discussion

Firstly, the assumption that the phage LD signal decreases upon binding of the functionalised phage to the target of interest, creating a mesh-like structure of phage-target, was challenged. For this, a replication of the LD-based biosensor assay was set on a microscope slide. Chemically modified phage, with anti-*Salmonella* antibodies conjugated to the p8 proteins, was used for this experiment. Three independent samples were set - modified phage on its own, modified phage plus *E. coli*, and modified phage plus *Salmonella*. *E. coli* bacteria were used as a control - since the antibodies on this sample were *Salmonella*-

specific, no interaction was expected. After a short incubation time between the modified phage and the bacteria, an aliquot of the samples was dropped on a microscope slide and immediately observed under a microscope. Snapshots of the collected microscopy images can be seen in Fig. 5.3.

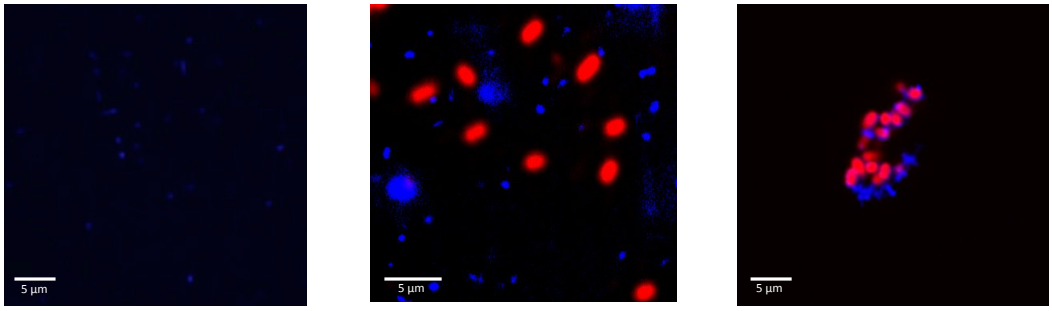

Figure 5.3: Testing the immunoassay principle on a microscope. In this experiment, a sample of chemically modified phage (with anti-*Salmonella* antibodies and a fluorescent blue dye) is used. The bacteria (*E. coli* and *Salmonella*) were previously conjugated with a red dye. Three samples were prepared: modified phage on its own; modified phage and *E. coli* bacteria (as a control); modified phage and *Salmonella* bacteria. The modified phage and the bacteria were mixed together and left to interact for 10 minutes prior to visualisation under a microscope (Leica SP8), immobilised under a 5% agarose pad. (Left) Microscopy image of the chemically modified phage, which can be seen as blue dots and blobs. (Middle) Microscopy image of the interaction between *E. coli* bacteria (red) and the chemically modified phage (blue). (Right) Microscopy image of the interaction between *Salmonella* bacteria (red) and the chemically modified phage (blue).

As observed in Fig. 5.3, the modified phage (with anti-*Salmonella* antibodies on its surface) does not seem to interact with *E. coli*; however, when *Salmonella* is in the sample, the phage binds to the bacteria creating an aggregate composed of several phages and bacteria interlocking together. This was the first time the immunoassay was visualised under a microscope, and provided proof that the detected drop in the phage LD signal upon addition of bacteria, is due to the formation of aggregates between the phage and the bacteria.

5.2.1 Mutation to increase the length of the bacteriophage

5.2.1.1 Context

An interesting line of investigation was to test whether an increase in the phage length would result in a substantially different LD signal, as it was expected a longer phage would orient better. More importantly, it was speculated if using a longer phage on the LD-based biosensor would enhance the sensitivity of the current immunoassay. An extension on the length of the phage (by increasing the number of p8 proteins) would result in an increased available surface area, which could translate into more antibodies being conjugated to the phage. This section describes the method to construct mutant phages that are physically longer, the characterisation of these mutants and the collected spectroscopic results.

5.2.1.2 Results and discussion

The rationale behind engineering longer bacteriophages comes from knowing that the p8 protein that encapsulates the genome of the M13 bacteriophage can accommodate larger or smaller genomes [3]. An increase in the length of the viral particle by cloning extra DNA into the genome is, therefore, expected. Making use of that knowledge, in collaboration with Henry de Malmanche from University College London, a set of mutant bacteriophages with different lengths were designed and successfully grown. In the work reported in this thesis, only two of these mutants were fully explored – phages that were estimated to be ~ 1150 nm and ~ 1575 nm in length, which corresponds to an approximate 250 nm (28%) and 675 nm (75%) increase in length, comparing to the wild-type phage of 900 nm. These two mutants will be addressed as "+ 1kb phage" and "+ 4kb phage", respectively, because this represents the approximate amount of kilobase pair (kb) DNA added to the phage genome.

5.2.1.2.1 Genetically engineering longer bacteriophages

The molecular cloning method for engineering longer bacteriophages is given in Chapter 2 (method 2.11.5) and described with more detail in [4]. Briefly, a fragment of DNA of specific length (1 or 4 kb) was cut from a plasmid using

restriction enzymes. A phage plasmid (M13mp18 plasmid, NEB) was also cut using the same restriction enzymes. After an overnight ligation, the M13mp18 plasmid with the inserted fragment of DNA was transformed into competent cells and plated on a LB/agar plate. After an overnight incubation, a single phage plaque was picked. The mutant phages were then grown and purified by standard PEG/NaCl protocols. Phage plaque assays (Chapter 2, method 2.3.1) were performed to confirm the engineered mutant phages were infective against the bacterial host, *E. coli* (Fig. 5.4).

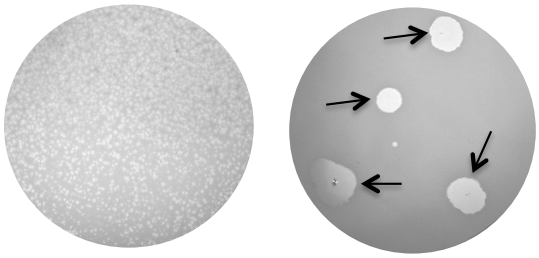

Figure 5.4: Plate pictures of the mutant phage plaque assay. (Left) The double agar overlay method. The mutant phage was spread over a LB/agar plate lawn with *E. coli* bacteria. The visible turbid plaques are in fact the areas where the *E. coli* did not grow efficiently because of being infected with the phage. (Right) The droplet method. Small drops of the mutant phage were pipetted over a LB/agar plate lawn with *E. coli* bacteria, confirming its infectivity.

Commonly, phage concentration is given in mass (mg per mL), molarity (number of virion particles per mL) or by plaque forming units (pfu per mL). Phage concentration, in mg/mL and number of virions/mL, rely on UV-Vis spectroscopy measurements and the absorbance registered at 269 nm, arising from a combination of peptide and DNA absorbance [5] (Chapter 2, method 2.3.2). Throughout this work, the phage concentration will be mainly given in number of virions/mL, as it was thought to be simpler to convey. Pfu/mL is a common way to express the concentration of a phage sample, and it is typically estimated from the double agar overlay method [6]. Pfu/mL is correlated with the ability of a phage to infect a bacterial host on a bacterial lawn. Both "+ 1kb" and "+ 4kb" mutant phages consistently showed lower pfu/mL than the wild-type phage (*i.e.* over the same period of incubation, the mutant phages

consistently produce fewer plaques over a lawn of bacteria on a plate than the wild-type phage). This may be related to the mutant phages' structure, which could have hampered the phage diffusion over the lawn of bacteria to neighboring bacteria cells, resulting in a lower number of bacteria being infected [4]. Moreover, although the plaque assay experiments confirmed the mutant phages are able to infect *E. coli,* this was noticed to be a slower and less efficient process, which was observed on the plaque morphology – longer phage mutants gave rise to smaller diameter plaques comparing to the wild-type phage. It was assumed mutant phages are either hindered in their capacity of infecting the bacterial host, or take more time to assemble and get released from the bacteria.

After verifying the mutant phages were capable of infecting the bacterial host, the phage plasmids were analysed. To confirm the 1 kb and 4 kb DNA fragments were inserted into the M13mp18 plasmid, resulting in the "+ 1kb" and "+ 4kb" phages, respectively, a diagnostic gel was carried out (Fig. 5.5). Plasmids of the phage mutants were digested with the corresponding restriction enzymes and resolved on an agarose gel (Chapter 2, method 2.7.1).

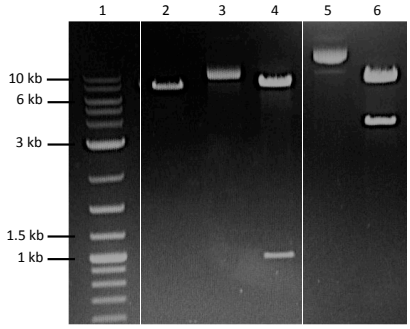

Figure 5.5: Diagnostic digest of the mutant phages on an agarose gel. The plasmids of the "+1kb" and "+4kb" phages were analysed to confirm the extra DNA fragment was inserted into the M13mp18 plasmid. Lane 1 – DNA marker (2-Log ladder). Lane 2 – uncut 7.2 kb M13mp18 plasmid, with no DNA insert. Lane 3 – uncut "+ 1kb" phage plasmid. Lane 4 – restriction enzyme digest of the "+ 1kb" phage plasmid, showing a band for the M13mp18 plasmid and a band for the 1 kb DNA insert. Lane 5 – uncut "+ 4kb" phage plasmid. Lane 6 – restriction enzyme digest of the "+ 4kb" phage plasmid, showing a band for the M13mp18 plasmid and a band for the 4 kb DNA insert.

Distinctive bands corresponding to the inserted DNA fragments can be seen – the gel on Fig. 5.5 suggests the mutation to the phage plasmid was successful. The plasmid of the "+ 1kb" mutant phage (lane 3), when cut with the appropriate restriction enzyme, gave rise to two bands, one at around 7.2 kb from the M13mp18 original plasmid and another band at around 1 kb from the inserted DNA fragment (lane 4). Similarly, the plasmid of the "+ 4kb" mutant phage (lane 5), when cut with the corresponding restriction enzyme, gave rise to two bands, one at around 7.2 kb from the M13mp18 original plasmid and another band at 4 kb from the inserted DNA fragment (lane 6).

The diagnostic digest of the mutant phage plasmids and DNA sequencing [4] confirmed successful cloning of the extra fragment of DNA into the M13mp18 plasmid. However, this does not guarantee the phage grown from these recombinant plasmid constructs will be with the expected length. To confirm a population of longer viral particles was created, transmission electron microscopy (TEM) images (Chapter 2, method 2.5.7) of the mutant and wild-type phages were collected and processed using ImageJ, to measure their length. Fig. 5.6 shows the general distribution in size/length of 40 phages of each population (wild-type phage (WT), "+1 kb" and "+4 kb" mutant phages).

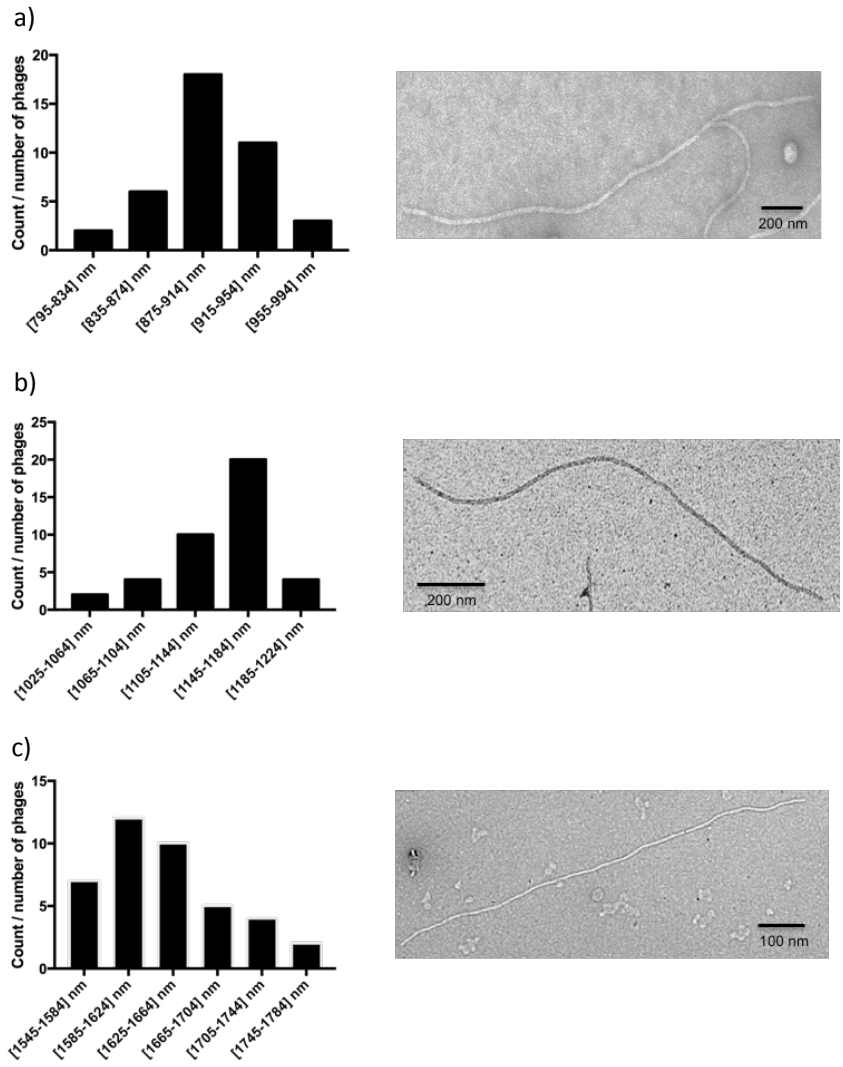

Figure 5.6: Plot of the length distribution of each phage population, measured using TEM images. a) WT phage, 904 nm ± 5 nm; b) "+ 1kb" longer phage, 1155 nm ± 6 nm; c) "+ 4kb" longer phage, 1635 nm ± 12 nm. Measurements were done using ImageJ (n=40, for each). Magnification was 25000× for WT phage, and 15000× for the longer phages. ± represents standard error of the mean.

The average measured length of each phage population was similar to the theoretically calculated length of the filaments (from simply assuming their length will scale linearly with genome size). Since a wild-type M13 phage has a 6.4 kb genome and is around 900 nm in length, the "+ 1kb" longer phage, which has a genome of ~ 8.2 kb, should be around 1150 nm and the "+ 4kb" longer phage, which has a genome of ~ 11.2 kb, should be around 1575 nm. The

average length of the wild-type, "+ 1kb" and "+ 4kb" mutant phages was 904 nm ± 5 nm, 1155 nm ± 6 nm, and 1635 nm ± 12 nm, respectively. Therefore, it was thought to be reasonable to conclude the mutated phage plasmid, with the extra DNA inserts, originates longer versions of the filamentous phage.

5.2.1.2.2 LD and FDLD profile of the mutant phages

Since the ability of the filamentous phage to align under flow is a major component of the previously described LD-based biosensor, the next step was to test the mutant phages on a LD system. The thermostability of the mutant phages was also considered an important characteristic, as it was envisioned that some of the features of the LD-based biosensor might later involve polymerase chain reaction (PCR) protocols [7]. Since the LD signal of the phage is linked to its filamentous nature, this spectroscopy technique can be used to evaluate the structural integrity of the phage particles when exposed to elevated temperatures [8].

The effect of temperature on the mutant phages was tested by incubating an aliquot of phage sample for 5 minutes at a range of temperatures, and then measure its LD signal (Chapter 2, method 2.8.2.1). The results are clearer by looking at the change of LD at a single wavelength, 225 nm – for all the three phage populations, as the temperature reaches 80 °C, the overall LD signal decreases, suggesting the phage fiber conformation is compromised, not aligning properly under flow (Fig. 5.7). These results suggest that the mutant phages are as thermally stable as the wild-type, and that temperatures above 80 °C destroy the phage filamentous structure.

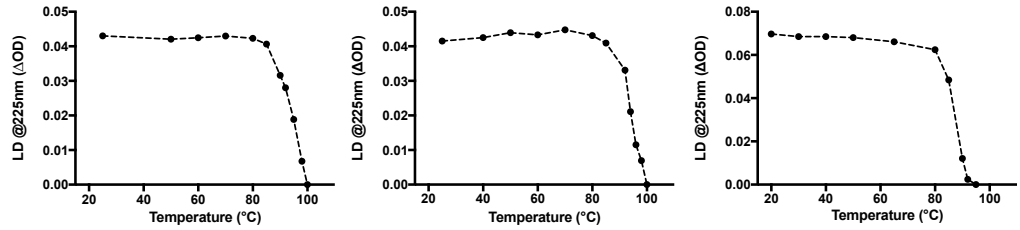

Figure 5.7: Effect of temperature on the stability of the wild-type, "+ 1kb" and "+ 4kb" phages (left to right). For all three samples, the LD phage signal at 225 nm remains fairly constant up to 80 °C. Above that temperature, the LD signal intensity decreases abruptly.

LD experiments, such as the one shown in Fig. 5.7, give information on the mutant phages structural integrity. It was also speculated that, due to their length, the mutant phages might be less resistant to mechanical forces and need to be handled more carefully. Shredding, often caused by repetitive pipetting of filamentous particles, could present a problem. However, after repeated cycles of vortex and pipetting the mutant phage stock solutions, it was observable that the phage LD signal from several aliquots (derived from the same phage stock) was comparable across samples. This suggested there is no substantial alteration to the filamentous structure of the phages after standard laboratory procedures. Knowing this, it was assumed the mutant phages could be handled as the wild-type phage, with no extraordinary precautions.

An interesting question is to determine whether there is a relationship between the phage length and its LD spectrum (specifically, its magnitude). Intuitively, it was expected that longer filaments would have more intense LD signals when compared with the LD spectra of shorter filaments. However, it is known that the degree of alignment of a filamentous particle, such as the phage, is not a straightforward property [9]. The persistence length of the phage is related to its flexibility. The wild-type phage is considered to be a semi-flexible filament, which is the property explored by LD [10], and on the creation of phage nanorings [11]. An engineered increase in the phage length could result in either a more rigid or flexible particle, which could, in any case, result in changes to the

LD spectrum [12]. LD spectra of mutant phages are shown in Fig. 5.8 (Chapter 2, method 2.8.2).

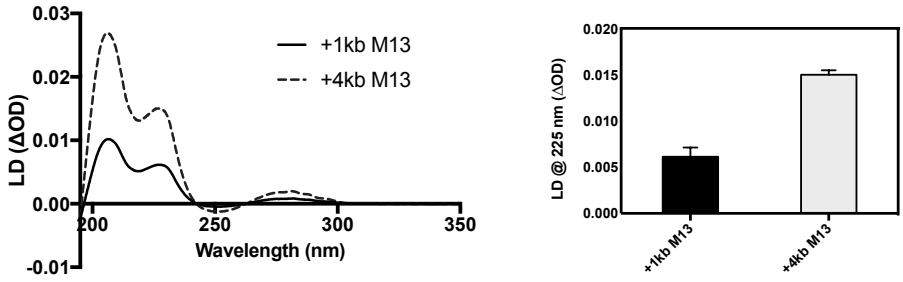

Figure 5.8: LD spectra of the "+ 1kb" and "+ 4kb" mutant phages. The column plot shows LD signal at 225 nm. Data are mean values and error bars represent the standard deviation from three LD measurements. Phages in PBS buffer at concentration of 10^{12} virions/mL.

Based on Fig. 5.8, there seems to be a relationship between the length of the mutant phage and its LD spectrum – the ~ 1575 nm phage ("+ 4kb" phage) has a greater LD signal than the ~ 1150 nm phage ("+ 1kb" phage). However, these data on their own do not facilitate determining the correlation between length and molecular alignment. Assuming proportionality, if the wild-type phage has 2700 copies of p8 proteins, the "+ 1kb" and "+ 4kb" phage will have around 3450 and 4800 copies, respectively. An equal number of phage particles of the mutant and wild-type phage, means that the mutant phage will have more p8 proteins, which translates into more molecules capable of absorbing light contributing to the LD signal. Therefore, the longer mutant will naturally have a higher intensity LD signal, without necessarily meaning it aligns better under flow. Section 5.2.1.2.4 explores this topic in greater detail.

As explored in Chapter 3, the major coat protein of the phage, the p8 protein, has one tryptophan amino acid in its sequence. Tryptophan fluorescence has been extensively used to study protein structure and function, and because of its sensitivity to the local surrounding environment, conformational changes to the protein are generally reflected in the tryptophan spectra. Although a complex

phenomenon, it also appears tryptophan is uniquely sensitive to quenching by nearby residues within the protein [13].

In the case of the mutant phage constructs, a more fluorescent phage could indicate a higher amount of tryptophans in its surface (which would be expected, given that longer phages have more p8 proteins to encapsulate the viral genome). To test this, FDLD measurements of the wild-type and mutant phages were taken. FDLD is a similar technique to LD, differing in the fact that FDLD detects fluorescence. The fluorescence derived from the aromatic residues of the aligned phages can be measured. Since the phage major proteic component is from the p8 protein, the spectroscopic detected peaks correspond to the amino acids (mainly, tryptophans) on this protein. The resulting FDLD spectrum from wild-type and mutant phage samples is plotted in Fig. 5.9 (Chapter 2, method 2.8.2).

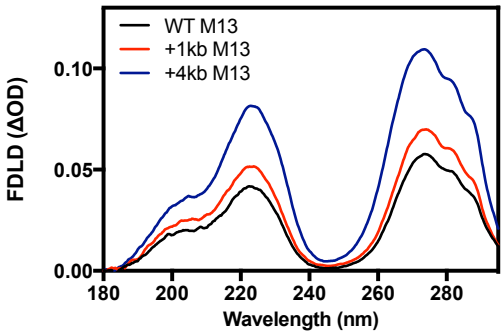

Figure 5.9: FDLD spectra of 10^{12} virions/mL wild-type and mutant M13 phages. A 300 nm cut-off filter was introduced in front of the LD machine detector. Parameters used as per Table 3.1 (Chapter 3).

The peak observed between 260 and 280 nm corresponds to the side chains of the aromatic amino acids, deriving mainly from tryptophan residues. Looking at Fig. 5.9, it is apparent that the "+ 4kb" phage has a more intense peak at this wavelength range, suggesting there are more tryptophans in this phage in comparison with the wild-type and "+ 1kb" phage. This finding supports the idea that a longer phage has greater intrinsic fluorescence.

5.2.1.2.3 Mutant phages as scaffolds for the LD-based biosensor

The motivation for building a longer phage particle came mainly from the assumption that a mutant phage would have more points of attachment on its surface for recognition elements – more p8 proteins could be modified by the bioconjugation protocol (illustrated in Chapter 3, Fig. 3.15), possibility resulting in more antibodies and dye molecules per phage. Theoretically, this could improve the sensitivity of the LD-based biosensor.

An essential step of the bioconjugation protocol is the conjugation of maleimide molecules to the phage surface. Therefore, an experiment was designed to test the ability of the p8 proteins of the mutant phages to be conjugated to maleimide groups. The mutant phages were labelled with AF647, a maleimide-derivatised dye (Chapter 2, method 2.4.2.1), and the LD of the dye-labelled phages was measured. The phage LD signal at the dye wavelength is plotted in Fig. 5.10.

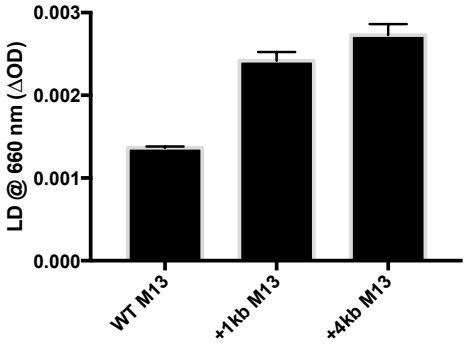

Figure 5.10: LD signal at 660 nm illustrating AF647 maleimide-derivatised dye conjugation to wild-type and mutant phages. LD spectra normalised at 225 nm. Data are the mean values of three LD measurements, and error bars represent standard deviation.

The experiment on Fig. 5.10 confirmed the p8 proteins on the mutant phages are maleimide-reactive. It is also noticeable that an increase in p8 proteins seemed to correspond to an increase in amount of conjugated maleimide-derivatised molecules. This suggests that a longer mutant phage can accommodate more dye molecules on its surface than a wild-type phage.

Building on these results, the mutant phages were chemically conjugated with maleimide-derivatised anti-*Salmonella* antibodies (Chapter 3, Fig. 3.15), and tested in Linear Diagnostics' LD-based biosensor (Chapter 2, method 2.8.2.2). The immunoassay results were plotted in Fig. 5.11.

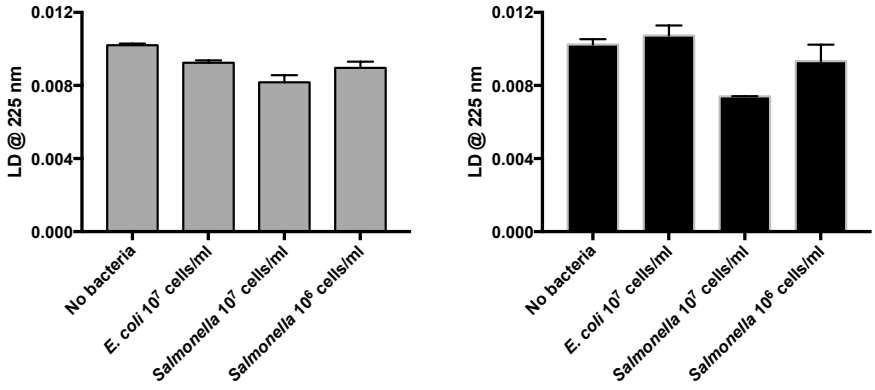

Figure 5.11: LD-based immunoassay using the "+ 1kb" and "+ 4kb" mutant phages as scaffolds for the detection of bacteria. Mutant phages were conjugated with anti-*Salmonella* antibodies, and *E. coli* bacteria were used as control. The variation of LD signal at 225 nm was tracked, as it relates to the overall alignment of the long axis of the phage particles. The initial amount of mutant phage on each immunoassay was so that $LD_{225} \sim 0.01$. Data are the mean values and error bars represent standard deviation on LD measurements of three independent immunoassays using the same phage conjugate sample. (Left, grey bars) LD signal resultant from the interaction between the anti-*Salmonella* "+ 1kb" mutant phage and *Salmonella* bacteria. Anti-*Salmonella* mutant phage detects 10^7 *Salmonella* cells per mL. (Right, black bars) LD signal resultant from the interaction between the anti-*Salmonella* "+ 4kb" mutant phage and *Salmonella* bacteria. Anti-*Salmonella* mutant phage detects 10^6 *Salmonella* cells per mL.

As illustrated in Fig. 5.11, both anti-*Salmonella* mutant phages were sensitive to the presence of *Salmonella,* which is indicated by the drop in LD signal when this bacterium was added. Furthermore, it is interesting to note that the anti-*Salmonella* "+ 4kb" mutant phage was sensitive to 10^6 bacterial cells, while it took 10^7 bacterial cells to perturb the "+ 1kb" mutant phage LD signal. Although these results seem to suggest the longer phage particles can be successfully integrated with the LD-based immunoassay, no apparent improvement to the sensitivity of the current biosensor (10^5 bacterial cells per mL) was achieved.

Further experiments needed to be conducted to expand on these findings. However, this line of investigation was not continued, as it was realised these mutant phages might not be an ideal biological scaffold, as discussed below.

5.2.1.2.4 Unresolved challenges

- **Comparing the LD alignment of the mutant phages**

Both concentration and degree of alignment of the mutant phage are variables that contribute to the LD data collected. The major challenge in assessing the LD spectrum of the mutant phages was on how to compare them with the wild-type phage and between themselves. The chosen phage concentration unit depends greatly on the research question. An interesting line of investigation would be to investigate whether a longer phage particle aligns better than a wild-type phage. As previously noted, directly comparing the LD spectra of 10^{12} longer phage particles with the spectra of 10^{12} shorter phage, in a 1-to-1 ratio, may not be a fair comparison, because there are substantial differences in the number of p8 proteins contributing to the LD signal. Instead, by keeping the concentration of the phage populations constant in mg/mL, the number of p8 proteins will be similar between different samples. For perspective, one can imagine comparing the LD signal of the following two phages – a phage of length A and a phage of length 2A (that is exactly double the length of phage A). To keep the mass proportionality, two phages A would have to be compared to one phage 2A, in a 2-to-1 ratio. Comparing the LD of longer phage particles by mass means that any observable change in the spectra will be largely due to differences in the overall phage structure. An LD spectrum of the mutant and wild-type phages at 0.2 mg/mL was plotted in Fig. 5.12. By normalising to mass units, it was expected that the structural changes of the mutant phages would be evident, as it was assumed that longer filamentous particles would orient better and give higher LD signals. However, as shown, the differences between the LD spectra of the three phage populations were unremarkable. From looking at these LD data, it seemed the ability of the mutant phages to align under flow was not enhanced by its increase in length.

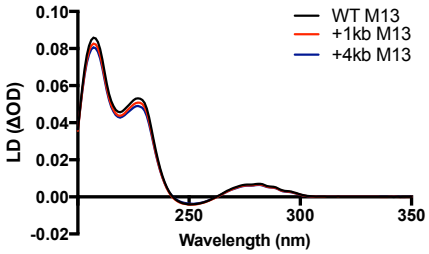

Figure 5.12: LD spectra of wild-type (WT) and mutant phages at 0.2 mg/mL.

As mentioned above, the degree of alignment of a filamentous particle is not a straightforward characteristic, and it depends greatly on the flexibility of the filament. This is found to be true, for example, for calf thymus DNA molecules, where it was shown that an overall increase in DNA flexibility (caused by factors such as elevated temperature, reduced viscosity and increased ionic strength) resulted in a reduction of the orientation of the molecules in flow which ultimately reduced the LD signal magnitude [14]. It is likely that longer phage particles have increased bending flexibility, which could result in a reduced ability to align, and hence a reduced LD signal, so we concluded that the wild-type phage was already maximised the degree of orientation possible for a given stiffness particle.

- **Instability of the mutant phage**

Although it was demonstrated it is possible to construct and grow phages longer in length, the benefit from doing so does not seem to counterweigh the shortcomings. The yields obtained from growing the mutant phages were considerably lower (< 2 mg per milliliter of culture) than the titers typically obtained with the wild-type phage (> 8 mg per milliliter of culture). Perhaps, this could be improved by optimising the culture conditions used to grow these mutants. Almost intuitively, it is not difficult to imagine why the mutant phage would be harder to grow in the laboratory. A longer phage would require more energy to assemble and pack the viral proteins, and more resources to keep up with that need. From a purely Darwinian point of view, if there were a benefit for the M13 bacteriophage to be longer, would it not have evolved and already

exist in nature? It was observed that in successive propagations, the phages had a tendency to go back to its wild-type original size. It is possible this is due to cross-contamination, in which a small population of wild-type phage (*i.e.* M13mp18 phage plasmid with no insert) thrives and grows more successfully, becoming the dominant population in subsequent generations, which ultimately led to batch-to-batch variability between bacteriophage preparations. Perhaps, this could be due to genetic instability of the constructed phage plasmids – diagnostic gels and sequencing data showed that the plasmids engineered for the production of longer phages could delete out the inserted fragment of DNA. This could be a result of the specific sequence of DNA inserted, and also the size of the DNA fragment – large inserts are thought to be more likely to get deleted from the original plasmid [15,16]. One way to improve the method would be to acquire synthetic DNA instead of cutting it out of a plasmid, to ensure the entire inserted DNA is junk (*i.e.* does not code for genetic elements) and it does not interfere with the phage life cycle or pose a metabolic burden to the bacteria.

Although it was disappointing that the work to create the longer phage did not increase sensitivity, in the long run for the biosensor, the much easier to produce wild-type phage can be concluded to provide an optimal signal per its length, so the result was appreciated by the Linear Diagnostics team.

5.2.2 Mutation to introduce an extra tryptophan to the p8 proteins of the phage

5.2.2.1 Context

Another method to increase the number of tryptophans in the phage capsid could be by simply adding the amino acid to the sequence of every p8 protein (Chapter 2, method 2.11.4). In comparison with the wild-type phage, this would result in a mutant phage with double the amount of tryptophan in its surface (*i.e.* the mutant phage would have two tryptophan residues per p8 protein). This would create the possibility of easily probing the phage LD signal in the aromatic region, at 280 nm.

5.2.2.2 Results and discussion

This genetic mutation can not be inserted at random as certain changes to the p8 protein sequence lead to dysfunction of the assembly of the phage during its life cycle, compromising its viability [17]. An extra tryptophan was added to the N-terminal of the wild-type p8, as it is generally considered the least likely region to negatively affect the p8 structure. Additionally, two glycines were introduced to act as a linker between the p8 protein helix and the added tryptophan. Mutagenesis on the phage was confirmed to be successful by DNA sequencing analysis and matrix-assisted laser desorption/ionisation time-of-flight mass spectrometry (MALDI-TOF MS) (Fig. 5.13) (Chapter 2, method 2.8.1).

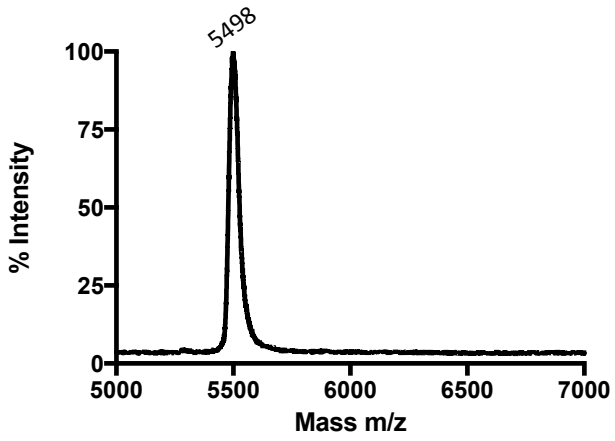

Figure 5.13: MALDI-TOF MS spectrum of the mutant phage with an extra tryptophan on p8 protein. Expected Mw ~ 5496 Da.

Assuming independent effect from both tryptophan molecules, adding an extra tryptophan to every p8 protein was thought to enhance the overall fluorescence of the phage, having a similar effect to what was observed on the mutant longer phage particle – increased number of p8 proteins translated into a more intense intrinsic fluorescence profile. Unexpectedly, this was not the case.

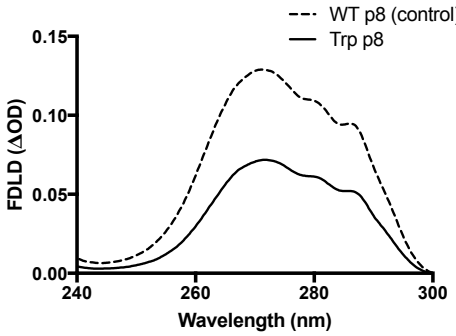

Figure 5.14: Intrinsic fluorescence of the mutant phage with an extra tryptophan on p8 protein. FDLD spectra of 10^{12} virions/mL wild-type p8 phage (WT p8, dashed line) and mutated p8 phage (Trp p8, solid line) zoomed on the aromatic (260-280 nm) region. Average spectra of three independent measurements using the parameters given in Table 3.1 (Chapter 3).

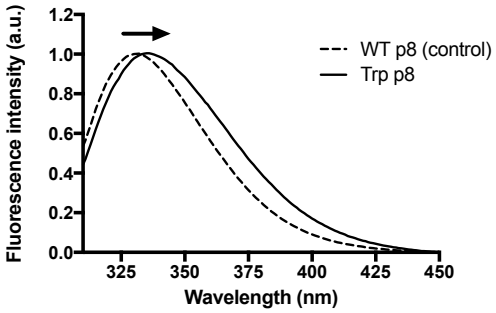

Figure 5.15: Normalised emission fluorescence spectra of the mutant phage with an extra tryptophan on p8 protein. Emission fluorescence spectra of 10^{12} virions/mL wild-type p8 phage (WT p8, dashed line) and mutated p8 phage (Trp p8, solid line). Spectra were normalised at maximum intensity peak (330 nm) to compare the shape of the curves. A 4-nm red-shift relative to the wild-type phage is indicated with a black arrow. Excitation wavelength was set at 280 nm. Average spectra of three independent measurements are shown. Data collected on a Jasco FP-6500 spectrofluorimeter.

It was expected that, by doubling the amount of tryptophan residues on the phage capsid, this would be evident by FDLD, with a distinct amplification in signal. As shown in Fig. 5.14, this was not observed – the wild-type phage has a more intense intrinsic fluorescence than the mutated phage with an extra tryptophan residue. The emission spectra (Fig. 5.15) emphasises changes in spectral shape, displaying a 4-nm shift to a longer wavelength, of the mutant phage

spectra relative to the wild-type phage spectra. This red-shift assigns the tryptophans to a polar environment, which implies the added residues are more likely to be solvent-exposed. It was speculated that the extra trytophan would be more disordered on the phage surface as a result of the increased flexibility, which could retrospectively affect its spectroscopic signal. Molecular dynamics simulations, conducted by Dale Ang from Western Sydney University, gave a possible explanation for the results. It was observed that, contrary to the native tryptophan (position 26), which is exposed on the surface and generally maintains an orientation perpendicular to the long axis of the phage, the added extra tryptophan residue (attached to the flexible glycine linker) is able to interact with adjacent peptide chains. In doing so, there is the possibility of fluorescence quenching by the phenol group of the aromatic tyrosine residue, at position 24 [18,19]. Additionally, the added tryptophan could be contact quenching the native tryptophan. These events could not only cancel any effect the added tryptophan could potentially have, but also interfere with the already existing intrinsic fluorescence of the phage.

The determined concentration of the mutant phage was an inaccuracy only noticed upon later analysis of the collected data. In the experiments presented here, the extinction coefficient of the mutant phage was assumed to be the same as for the wild-type phage. However, this is an inadequate approach – the mutant phage, having one more tryptophan constituting its capsid, would have an increased overall extinction coefficient. By using the same extinction coefficient for the wild-type and mutant phage, the concentration of the latter was underestimated. Ultimately, inaccurate estimation of phage concentration would have had a considerable effect on the FDLD measurements.

The extinction coefficient of the mutant phage could have been empirically determined. For example, one could freeze-dry a solution of the mutant phage, weight the resulting solid pellet, dissolve it in a precise amount of buffer, and measure this phage sample of known concentration on the UV-Vis to derive its extinction coefficient. Another approach could be to denature the phage and

extract its DNA, and compare samples using gel densitometry: 1) run several samples of known concentration of wild-type phage through an agarose gel and establish a relationship between the concentration of the wild-type phage and the density of the DNA bands; 2) run the unknown sample of mutant phage on the same gel; 3) based on the calibration curve built from 1), estimate the concentration of the mutant phage. An approximation of the mutant phage extinction coefficient could also be theoretically determined, by adding the molar extinction coefficient of tryptophan at 269 nm multiplied by 2700 (the number of p8 proteins on the phage) to the molar extinction coefficient of the wild-type phage. By doing so, it was estimated that the mutant phage concentration was underestimated by less than 20% (note that most of the contribution at 269 nm derives from the viral DNA). The expected outcome from adding an extra tryptophan to the phage capsid was that its FDLD signal intensity would double. Correcting for the miscalculation of the extinction coefficient of the mutant phage would nevertheless result in a spectroscopic signal less intense than expected, supporting that the conclusions and reasoning underlined above are possibly still valid.

5.2.3 Introducing of a cysteine to the p8 protein – the V31C mutation

5.2.3.1 Context

As discussed in Chapter 3, the p3 proteins of the wild-type phage have cysteines, but p8 proteins lack this amino acid in its sequence. For this reason, the first step in the bioconjugation protocol (Chapter 3, Fig. 3.15), in which the SATA (N-succinimidyl S-acetylthioacetate) reagent is used to convert the primary amines of the p8 protein to thiol groups, is required in order to conjugate the antibodies. An alternative method to circumvent the necessity for this chemical step is to genetically introduce the cysteine in the p8 sequence.

Initially, a cysteine residue was genetically introduced into the N-terminal of the p8 protein. However, this mutation resulted in very low production yields,

suggesting this mutation interferes with the phage life cycle in the host bacteria or compromises its secretion from the host. Due to cysteine reactivity, not all positions in the p8 protein tolerate the mutation. Hemminga and co-workers have methodically developed all possible mutagenesis combinations to introduce a cysteine onto the p8 protein sequence [20]. From the several mutations proposed in the literature, the V31C mutation, in which the valine in position 31 of the p8 protein is replaced with a cysteine, was chosen for this work as it has been used for different applications by others [21-24]. The method for creating the V31C mutation on the wild-type phage, by site directed mutagenesis, is described in Chapter 2 (section 2.11.4.8).

5.2.3.2 Results and discussion

The success of the mutagenesis was checked by DNA sequencing, which confirmed that the mutant phage (*i.e.* the V31C phage) had 2700 cysteines throughout its capsid. An Ellman's reagent test (Chapter 2, method 2.9.3) suggested these cysteines were exposed to the surface and not yet cross-linked to form disulfide bridges – the sample immediately turned yellow without the need to add any reducing agent, such as TCEP (Fig. 5.16). It was noticed, however, that a transparent gel-like precipitate formed over time, probably due to inter and intra cross-linking interactions between the V31C phages.

The wild-type p8 protein sequence
AEGDDPAKAAFNSLQASATEYIGYAWAMVV<u>V</u>IVGATIGIKLFKKFTSKAS
The V31C phage p8 protein sequence
AEGDDPAKAAFNSLQASATEYIGYAWAMVV<u>C</u>IVGATIGIKLFKKFTSKAS

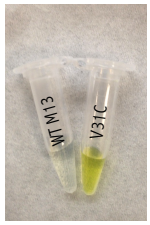

Ellman's reagent test

Figure 5.16: The V31C phage. (Left) Sequence of the wild-type and mutated p8 protein. These phages only differ on one amino acid, in which a valine was swapped for a cysteine, at position 31. (Right) Picture of the reaction between Ellman's reagent and wild-type (WT) and V31C phage, in PBS buffer. The wild-type phage, which contains only an insignificant fraction of cysteines on the p3 proteins, does not react with the Ellman's reagent, and therefore the solution does not turn yellow. The strong yellow coloration of the V31C phage sample indicates the abundant presence of thiols.

5.2.3.2.1 Maleimide-reactivity of the V31C phage

Additional experiments, such as MALDI-TOF mass spectrometry (Fig. 5.17) and protein gels (Fig. 5.18), further confirmed the presence of the cysteines and suggested these were available to conjugate with maleimide moieties. This was essential for this work, as maleimide-derivatised antibodies are used in the bioconjugation protocol (Chapter 3, Fig. 3.15).

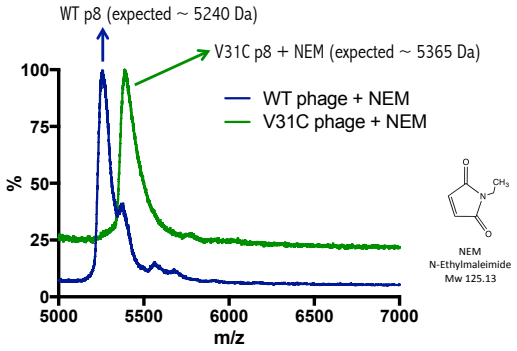

Figure 5.17: MALDI-TOF MS spectra of wild-type phage and V31C phage after an overnight reaction with NEM. (NEM, N-Ethylmaleimide, Mw ~ 125 Da). (Blue spectrum) Wild-type p8. Max. peak at ~ 5246 Da. A small shoulder is also visible, and this was thought to be due to the slower interaction between the maleimides and the primary amines on the p8 proteins. (Green spectrum) V31C p8. Max. peak at ~ 5377 Da.

Wild-type and V31C phage were reacted with a final concentration of 50 mM NEM (N-Ethylmaleimide) overnight at room temperature, purified using Zeba spin columns, and subsequently analysed by MALDI-TOF MS (Chapter 2, method 2.8.1). It was expected that, if the V31C phage capsid had maleimide-reactive cysteines, an increment of the mass of the p8 protein, corresponding to the mass of NEM, should be observable. As shown in Fig. 5.17, since there are no natural occurring cysteines in the wild-type p8 protein that the NEM could conjugate to, the p8 protein mass (~ 5246 Da) did not change. On the other hand, the mass of the p8 protein of the V31C phage increases, with a peak shift corresponding to the mass of the conjugated NEM to the cysteines in the p8 protein. This experiment confirmed the cysteines (*i.e.* thiol groups) on the surface of the V31C phage are reactive with maleimides.

Another experiment was designed to demonstrate the maleimide molecules get conjugated to the p8 proteins of the V31C phage. The V31C phage was conjugated to a maleimide-derived fluorescent dye (AF647) and analysed on a Tris-Tricine gel – prior to Coomassie staining, fluorescence images of the gel were acquired (Chapter 2, method 2.7.3.1) (Fig. 5.18).

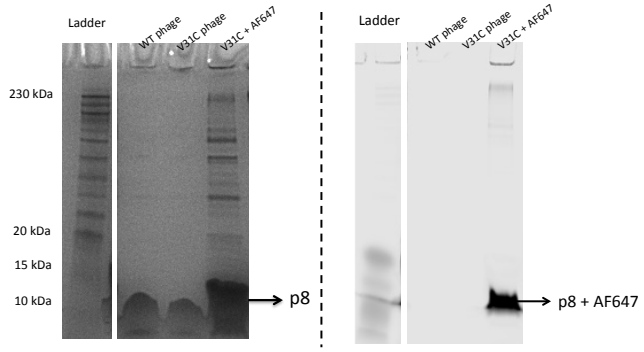

Figure 5.18: Tris-Tricine precast gel of the AF647-V31C phage. (Left) Coomassie blue stained gel. (Right) Fluorescent image of the gel prior to staining.

Fig. 5.18 shows two pictures of the same gel – a stained gel image and a fluorescent image of the gel before being stained. The purpose of this experiment was to confirm that the p8 proteins of the V31C phage are maleimide-reactive. AF647 dye was conjugated to the V31C phage, and after PEG/NaCl precipitation, the conjugate was resolved on a 10–20% precast Tris-Tricine gel. Wild-type and V31C phage, not conjugated to AF647 dye, were also analysed on this gel to guarantee there was no detectable fluorescent bands arising from autofluorescence or detectable intrinsic fluorescence. Prior to staining, fluorescence images of the gel were acquired. Then, the gel was stained with Coomassie blue and imaged again (under white light). The broad band at around 10 kDa visible on the stained gel, on the three samples, was assigned to be from p8 proteins. The fluorescent image of the gel shows a similar broad band, suggesting the p8 proteins of the V31C phage were labelled with AF647 fluorescent dye. There is also a fainter band at the top of the gel, probably from aggregated product. The p8 protein band of the label-free wild-type and V31C phage is not visible in the fluorescent gel.

In summary, the constructed V31C phage was demonstrated to be viable (*i.e.* it was capable of infecting the bacterial host and assembling correctly) and to have one cysteine, and therefore a thiol group, on each p8 protein. These cysteines were confirmed to be reactive against maleimide moieties. The next step would be to adjust the bioconjugation protocol (Chapter 3, Fig. 3.15) to accommodate the use of the V31C phage instead of the wild-type phage. The protocol was followed as usual, but initiated at step b) (since there is no longer the need to use SATA to introduce thiol groups on the p8 proteins) – the V31C phage was conjugated to the maleimide-derivatised antibodies and purified as previously described.

However, despite several attempts, the V31C phage modified with maleimide-derivatised antibodies seemed to be inadequate for the biosensor immunoassay. As described above in this chapter, in order for a modified phage with antibodies to be considered sensitive to the presence of target bacteria, a drop on its LD signal must occur. While running the immunoassay using the modified V31C phage, there was no visible change on the LD signal, as it would be expected when bacteria are added.

These results were puzzling. The protocol conditions were tuned to no avail – bioconjugation steps repeated with lower pH buffers, addition of a reducing agent to break possible disulfide bridges between phages (that would affect thiols accessible to maleimide groups) prior to conjugation with antibody, serial dilution of the concentration of V31C phage and maleimide-derivatised antibody, longer incubation times between V31C phage and antibody, longer interaction time between the target bacteria and the modified V31C phage. The conjugation of the V31C phage capsid with antibodies was considered as the most likely problematic step. It was possible that the conjugation of the maleimide-antibodies to the thiols on the p8 proteins of the V31C phage was not as straightforward as initially thought. Perhaps, the cysteines at position 31 in the p8 proteins are harder to access/less exposed than the chemically introduced thiols at position 8. If so, it is possible that a steric hindrance

phenomenon is disrupting the conjugation of the antibody to the cysteine on the surface of the V31C phage.

5.2.3.2.2 Cysteine (position 31) versus lysine (position 8)

An important line of investigation would be to compare the positions of the thiol groups on the V31C phage and on the SATA-chemically modified wild-type phage (using the bioconjugation protocol described in Chapter 3). From looking at Fig. 5.19, it appears that the genetically introduced cysteines (position 31) on p8 protein are spatially closer to each other than the thiols generated by the SATA reagent on the lysine residues (position 8).

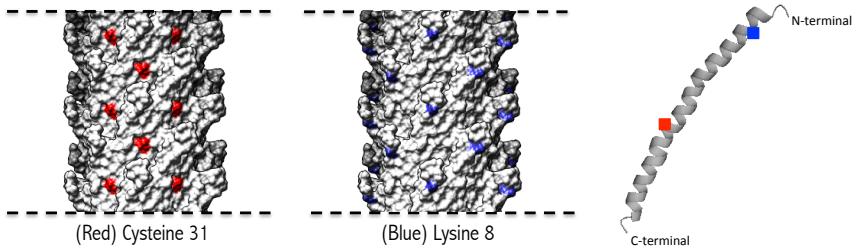

Figure 5.19: Illustration of the partial side-view of the surface of the phage. A single p8 protein helix is also shown. Position 31 of the p8 protein was labelled in red and position 8 of the p8 protein was labelled in blue. Images produced using Chimera (PDB entry: 2MJZ [25]).

To better quantify this observable difference, the distances between adjacent reactive groups on the capsid of the phage were measured using the distance analysis tool on Chimera software.

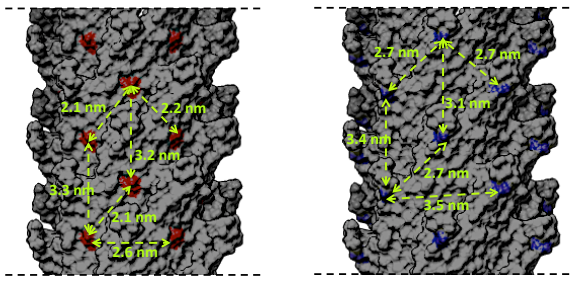

Figure 5.20: Distances between functional groups on the surface of the phage. (Left) Distances between adjacent cysteines at position 31. (Right) Distances between adjacent lysines at position 8. Distances determined using Chimera (PDB entry: 2MJZ [25]).

Fig. 5.20 illustrates the distances between the cysteines of the V31C phage (red), and the distances between the lysines of the wild-type phage (blue). Closest neighbouring thiol groups are diagonally separated by 2.1 nm on the V31C phage, and by 2.7 nm on the wild-type phage. In the azimuthal direction, the distance between the thiol groups on adjacent p8 proteins on the V31C phage and the wild-type phage are 2.6 nm and 3.5 nm, respectively. Overall, these measurements confirm that lysines at position 8 are more sparsely dispersed over the phage surface than cysteines at position 31. At the molecular level, these are significant differences. It is not implausible to speculate that shorter distances between conjugation sites over the surface of the phage may interfere with the conjugation of antibodies (~ 150 kDa).

To get some perspective on this, an experiment using two different dyes was designed, in which their molecular weight was the considering factor. 7-Diethylamino-3-((((2-maleimidyl)ethyl)amino)carbonyl)coumarin (MDCC) and Alexa Fluor 647 (AF647) have a molecular weight of 380 Da and 1250 Da, respectively. Both these dyes are maleimide-derivatives, but their mass differs by more than 3-fold, with MDCC being a smaller, more compact molecule.

2 mg of V31C phage and SATA-modified phage were conjugated with equimolar amounts of MDCC and AF647, and purified by PEG/NaCl precipitation (Chapter 2, method 2.4.2.1). After fully resuspending the phage pellets in PBS buffer, the samples were assessed by LD (Chapter 2, method 2.8.2). Fig. 5.21 shows plots of the LD phage signal zoomed in on the dye peak region (600-700 nm for AF647, and 350-550 nm for MDCC) – free-in-solution dye molecules can not align on their own, and therefore the LD signal collected is only from the dye conjugated to the phage particle.

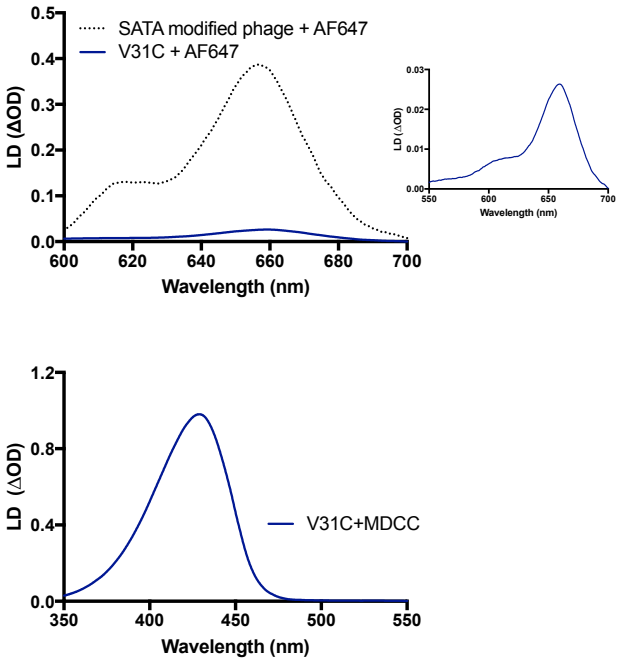

Figure 5.21: LD spectra of the phage zoomed at the dye (MDCC and AF647) absorption region. (Top) LD spectra normalised at 225 nm comparing the AF647 dye peak of a SATA-modified wild-type (WT) phage and a V31C phage. Inset zoomed at the AF647 dye peak on the V31C phage. (Bottom) LD spectra normalised at 225 nm of the MDCC dye peak on the V31C phage.

Fig. 5.21 shows the LD spectra of phage-dye conjugates. The spectral data on the top suggests that AF647 dye labelling of the SATA-modified phage was more efficient than on the V31C phage. Also, illustrated on the spectral data on the bottom, the LD dye peak from the V31C-MDCC conjugate was greater than the LD dye peak derived from the V31C-AF647 conjugate. These data suggest two things – AF647, despite being a large dye molecule, conjugated efficiently to the chemically modified amines but not to the cysteines on the V31C phage; MDCC dye molecules were conjugated to the surface of the V31C phage to a greater extent than the AF647 dye.

Although the two fluorophores, MDCC and AF647, have distinct spectral profiles and chemical properties that have not been considered here, it is possible that the observed differences in labelling of the p8 proteins are due to the size of the dye molecules and the arrangement of the functional groups on the phage surface. Extrapolating this line of thought, it is not unlikely that conjugating

antibodies to V31C phage would be spatially and energetically unfavourable, resulting in a low degree of labelling incompatible with the LD-based immunoassay. Molecular simulations could further clarify on the importance of the distances between adjacent cysteines, and how that could compromise the labelling of the phage surface. Naturally, the reasoning that steric hindrance phenomena disrupted the potential use of the V31C phage on the LD-based biosensor is only valid when assuming conjugation between V31C and antibodies was indeed unsuccessful. To confirm this was the case, ideally one should test the V31C-antibody conjugate, and check for the presence or absence of the antibody on the V31C phage capsid. This could be achieved, for example, by setting up an ELISA. The V31C-antibody conjugate could be attached to a 96-wells plate using anti-p3 antibodies as anchors. Then, an HRP-conjugated antibody, specifically against the antibody conjugated to the V31C phage, could be added, detecting the presence or lack of the antibody on the phage surface. Since the V31C phage was not compatible with the LD-based biosensor, an alternative to include thiols on the phage surface was envisioned. This involved cloning a cyclic-cysteine peptide on the N-terminal of the phage (as discussed in the "conclusion" section), which would create more exposed thiol groups along the phage capsid.

5.2.4. Expression of a *Salmonella*-binding peptide on the surface of the phage

5.2.4.1 Context

Peptide-binding peptides have been used as an alternative to antibodies in diagnostics. Antibodies are expensive and relatively fragile molecules, and although antibody-antigen interactions are much stronger than peptide-peptide interactions, the latter are reported to be sufficient for most immunoassays applications [26]. Theoretically, the antibodies used in the LD-based biosensor could be substituted with a bacteria specific-binding peptide.

Peptide-binding peptides are generated by phage display biopanning [26-28] – an *in vitro* affinity technique for the selection of peptide sequences that bind to a target of interest, as described in Chapter 1. The first step of biopanning involves inserting a DNA fragment derived from a random library into the phage genome, so that the surface of the phage displays the coded peptide. Next, the resulting phage-peptide particles are exposed to a target of interest. The phage-peptides that have affinity for a target will get captured, while the weakly bound phage-peptides will be washed off. The final step of biopanning is the elution of the phage-peptide strongly bound to the target. Typically, several rounds of biopanning are required to select a peptide-binding peptide. Successive rounds ensure increased specificity for the target and reduce library diversity, by highlighting the most essential amino acid sequences for target recognition and binding. The peptide-binding peptide displayed on the phage can then be sequenced and added to a database.

A literature review was conducted to explore possible binding peptides that could replace the anti-*Salmonella* antibodies used in the immunoassay. A *Salmonella*-binding peptide, with sequence NRPDSAQFWLHH, was reported by Morton *et al.* [29], and used for *Salmonella* detection platforms by Wang *et al.* in [30], and by Karoonuthaisiri *et al.* in [31]. According to the authors, the described *Salmonella*-binding peptide (named MSal020417) is specific for *Salmonella spp.*, not interacting with other species, such as *E. coli* and *Listeria monocytogenes*, and it is capable of differentiating between different serovars of a bacteria [30].

5.2.4.2 Results and discussion

We considered genetically inserting the 12 amino acid sequence into the p8 protein of the phage. The underlying problem with introducing large peptides (> 6-mer) [32,33] into the p8 protein (which is a small 50 amino acid residues protein) is that the resulting phage may not be able to complete its life cycle and assemble properly, giving rise to very poor production yields. This challenge is well known among the bacteriophage scientific community, and scientists have designed clever ways to bypass it. The mosaic phage is an example of this - an

engineered biomaterial constructed to facilitate standard molecular biology on phage systems [32-35].

The mosaic phage, also called type 88 phage, is a filamentous fd phage designed by Smith *et al* [36]. The mosaic phage has two types of p8 proteins – 3600 copies of a wild-type p8, and around 300 copies of a synthetic p8. The synthetic p8 gene is controlled by a Tac promoter and is, therefore, inducible by IPTG, as demonstrated in Fig. 5.22 (Chapter 2, method 2.8.1). It has unique HindIII and PstI cloning sites, separated by a 21-bp spacer. Replacing this spacer with a DNA insert of interest may result in the display of several copies of the peptide encoded by the insert, which will be fused to the synthetic p8 and presented on the surface of the phage. The peptide of interest will then only be displayed on the synthetic p8 proteins, and because these are sparsely dispersed along the phage surface, these are less likely to disrupt the overall structure of the phage and compromise its viability.

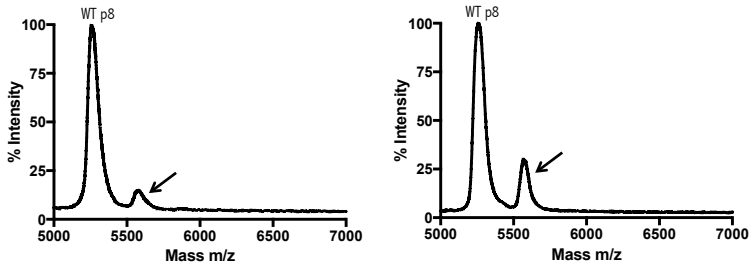

Figure 5.22: MALDI-TOF MS spectra of the mosaic phage. The expression of the synthetic p8 is tunable by IPTG. Both proteins can be assigned on a MALDI-TOF spectrum – a major peak at around 5240 Da from the wild-type p8, and a smaller peak at around 5550 Da from the synthetic p8 (indicated with arrows). (Left) fd mosaic phage induced with 100 μM IPTG. (Right) fd mosaic phage induced with 1 mM IPTG.

The cloning of the *Salmonella*-binding peptide into the synthetic p8 was successful as confirmed by DNA sequencing and MALDI-TOF mass spectrometry (Fig. 5.23). This phage construct is denominated as MSal17 phage in this work.

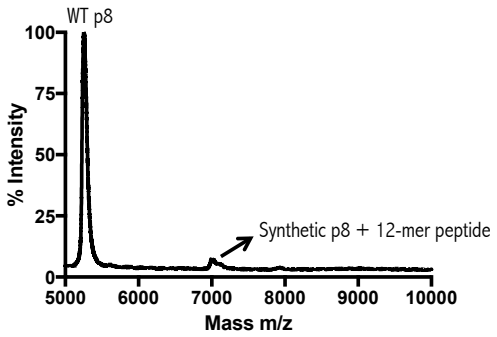

Figure 5.23: MALDI-TOF MS spectrum of the constructed MSal17 phage. The peak assigned to the synthetic p8 (shown in Fig. 5.22) completely shifted with an increase in mass that corresponds to the 12-mer *Salmonella*-binding peptide (roughly 1680 Da). This peak is minor and badly resolved probably due to the low expression levels of the peptide on the phage.

The MSal17 phage had the clear advantage of not needing any further chemical steps to be used in the previously described immunoassay. Therefore, after growing a stock of the MSal17 phage, this construct was readily tested in the LD-based biosensor. Interestingly, although there was an LD response when 10^7 cells/mL were added (*i.e.* there was a drop in the phage LD signal when bacteria was added to the MSal17 phage, suggesting phage and bacteria were interacting), this was observable both with *Salmonella* and *E. coli* bacteria. This is not ideal, as it would mean the immunoassay is unspecific and would be useless with cocktail samples made of several bacterial species. Upon these results, an ELISA was designed to get some insight on the interaction between the constructed MSal17 phage and bacteria.

A scheme of the ELISA is shown in Fig. 5.24, and the method is described in greater detail in Chapter 2 (method 2.6.2). A 96-well microplate was coated with the bacteria – *Salmonella enterica* or *E. coli* – and incubated with MSal17 and wild-type phage. Anti-phage/HRP conjugate antibody was used as the detection element, and ABTS solution was added as the substrate. The absorbance at 410 nm was then measured on a microplate reader.

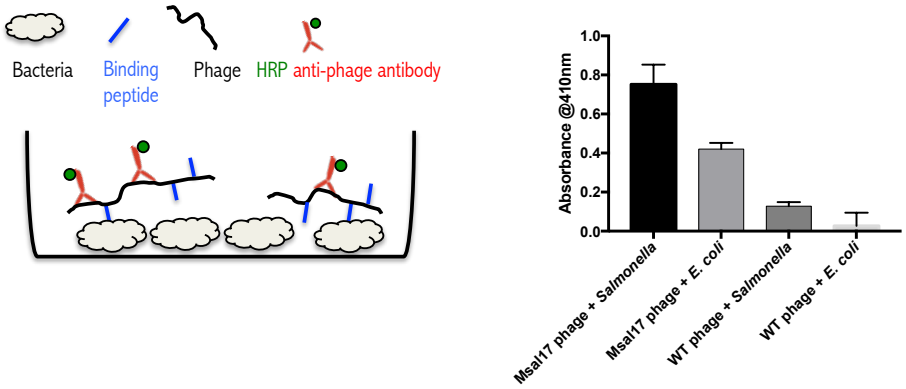

Figure 5.24: Phage-binding ELISA. (Left) Illustration of the ELISA design, of a bacteria-coated well incubated with MSal17 phage. Detection by anti-phage/HRP conjugated antibody. (Right) ELISA suggested wild-type phage had a minor interaction with both bacteria. The MSal17 phage seems to bind to the surface of *Salmonella enterica* Typhimurium, however, it also seems to non-specifically bind to *E. coli*. Data are mean values of three independent wells on the same ELISA plate; error bars represent standard deviation.

As seen in Fig. 5.24, the ELISA suggested the constructed MSal17 phage might not be exclusively specific to *Salmonella enterica*, as it seems to have bound to the surface of *E. coli* bacteria as well. Another ELISA was set using three other *Salmonella enterica* serovars (*Salmonella enterica* Enteritidis, *Salmonella enterica* Infantis and *Salmonella enterica* Senftenberg) and *E. coli*, at a range of concentrations. The data collected are plotted in Fig. 5.25.

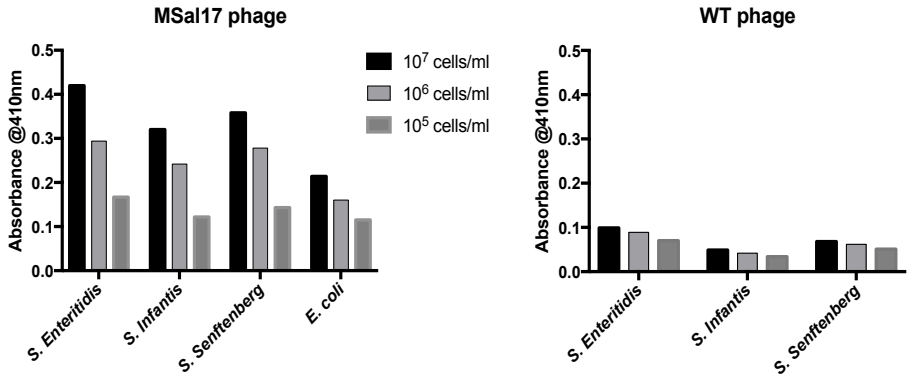

Figure 5.25: Phage-binding ELISA to investigate MSal17 phage interaction with three *Salmonella enterica* serovars and *E. coli*. *Salmonella* serovars tested were *Salmonella enterica* Enteritidis, *Salmonella enterica* Infantis and *Salmonella enterica* Senftenberg, and *E. coli* was used as a control specie, since the *Salmonella*-binding peptide should not bind to it.

As shown in Fig. 5.25, although wild-type phage had some degree of non-specific interaction with *Salmonella enterica* serovars, MSal17 phage substantially cross-reacted with *E. coli* bacteria. These data is consistent with the observed results on Fig. 5.24, further suggesting that the constructed MSal17 phage was not specific for *Salmonella enterica* bacteria.

Replacing antibodies with bacteria-binding peptides would considerably drop the total cost of the existing biosensor, and it would simplify the bioconjugation protocols. Nonetheless, the MSal17 phage construct did not appear to be suitable for the LD-based biosensor (nor for the designed ELISAs). It is possible that the expression levels of the *Salmonella*-binding peptide on the surface of the phage were too low to produce a substantial and measurable difference on the LD-based immunoassay. There are also some fundamental differences between this project and the work described in [30]. The exact sequence referred in [30] includes a flexible spacer followed by the *Salmonella*-binding peptide; this spacer was not included in the Msal17 phage construct. Although the use of the linker seemed to be related to manufacturing specification for phage display rather than for bacterial detection, it is possible this short amino acid linker would be advantageous to include in the MSal17 phage construct. The formulated hypothesis was that the *Salmonella*-binding peptide, cloned in the N-terminal of the synthetic p8, might be partially buried within the phage capsid, meaning some of the amino acids necessary for *Salmonella* recognition are in fact inaccessible. Furthermore, the work reported in [30] makes use of the *Salmonella*-binding peptide on its own, in contrast to have it displayed on the surface of the phage. The 3D conformational differences could have influenced the interaction between the binding-peptide and the *Salmonella* bacteria, and ultimately its affinity.

Synthetic peptides, as the one described here, have been used as probes for microbial detection. There are several other peptide ligands with applications on the fields of food safety, environment monitoring and defense. These binding peptides could be displayed on the phage surface and be tested on the LD-based

assay for the detection of pathogens (*Listeria monocytogenes* [37,38], *Pseudomonas aeroginosa* [39], *Salmonella* spp. [40], *Helicobacter pylori* [41], *Bacillus anthracis* [42-44]). Moreover, biopanning for novel peptide sequences, targeting molecules of interest specifically to Linear Diagnostics' biosensor, could be a relevant line of investigation to evaluate and expand on.

5.2.5 Directional conjugation of antibodies to the surface of the phage by aldehyde-hydrazine chemistry

5.2.5.1 Context

One of the downsides of the protocol presented in Chapter 3 (Fig. 3.15) is the lack of control on the conjugation of the antibody to the phage surface. More specifically, the required step to maleimide-derivatise the antibodies prior to conjugation to the phage – this is achieved by a crosslinking reaction between the maleimide group from the SMCC (succinimidyl 4-(N-maleimidomethyl)cyclohexane-1-carboxylate) reagent to the primary amines of the antibody. Antibodies have several amine groups in its structure, both in the Fab and Fc region (Fig. 5.26). Therefore, it is challenging, using this thiol/maleimide bioconjugation chemistry, to control to which amine on the antibody will the maleimide group get conjugated to, and hence, which direction the antibody will have once conjugated to the phage surface. Ideally, the bioconjugation chemistry will leave the antigen-binding site, essential for antigen recognition, intact. The thiol/maleimide bioconjugation protocol used by Linear Diagnostics does not allow for any control on the orientation of the antibodies on the phage – by not guaranteeing the antigen-binding site is available to interact with the target bacteria, the sensitivity of the biosensor might be compromised. Bearing this particular challenge in mind, an aldehyde-hydrazine chemistry protocol was devised. Aldehyde-hydrazine chemistry allows for directionality control of the conjugated antibody: instead of interacting with the dispersed amines, only the carbohydrates present on the Fc region of the antibody will be modified [45].

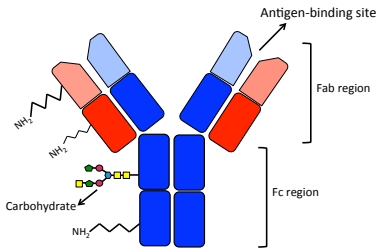

Figure 5.26: Simple illustration of a glycosylated antibody, highlighting some of its chemical groups. Light and heavy chains shown in red and blue, respectively. Amine groups are dispersed both in the Fab and Fc region of the antibody. Carbohydrate chains on glycosylated antibodies are linked only to the Fc region, away from the antigen-binding site.

5.2.5.2 Results and discussion

A detailed protocol of the aldehyde-hydrazine bioconjugation is given in Chapter 2 (method 2.4.2.2.2), and an illustration of this reaction is given in Chapter 3 (Fig. 3.16). Firstly, the phage was treated with SANH (succinimidyl 6-hydrazinonicotinamide acetone hydrazine), which modifies the primary amines of the p8 proteins to hydrazines. Then, the glycosylated antibody (*e.g.* anti-*E. coli*) was treated with sodium meta-periodate ($NaIO_4$), which partially oxidises the Fc-linked carbohydrates, incorporating aldehyde groups. The hydrazine moieties on the phage are then reacted with the aldehyde-modified antibodies, producing a hydrazone conjugate. To our knowledge, this was the first time this bioconjugation method was used to conjugate antibodies to the phage's surface.

Quality control tests were implemented to confirm the successful modification of the phage and the antibody (step a) and step b), respectively, as indicated in Fig. 3.16, Chapter 3). After modification of the phage with SANH, a colorimetric test using 4-nitrobenzaldehyde (p-NBA) confirmed hydrazine moieties were introduced to its surface (Fig. 5.27) (Chapter 2, method 2.9.1). The Purpald test (4-amino-3-hydrazino-5-mercapto-1,2,4-triazole) confirmed the presence of aldehydes on the oxidised antibodies (Fig. 5.28) (Chapter 2, method 2.9.2).

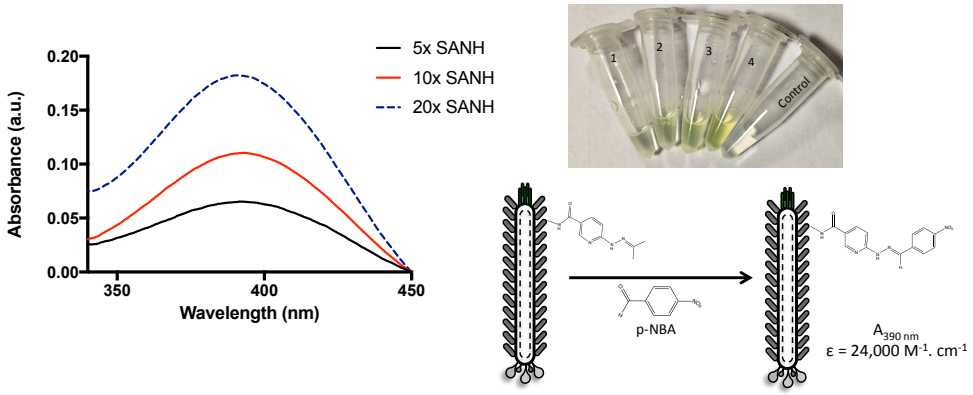

Figure 5.27: The 4-nitrobenzaldehyde (p-NBA) test on the SANH-modified phage. Absorbance was monitored to determine the levels of hydrazine incorporation on the phage. Colorimetric change, to yellow, can be tracked at around 390 nm. 5×, 10× and 20× represent SANH molar excess over p8 proteins of the phage.

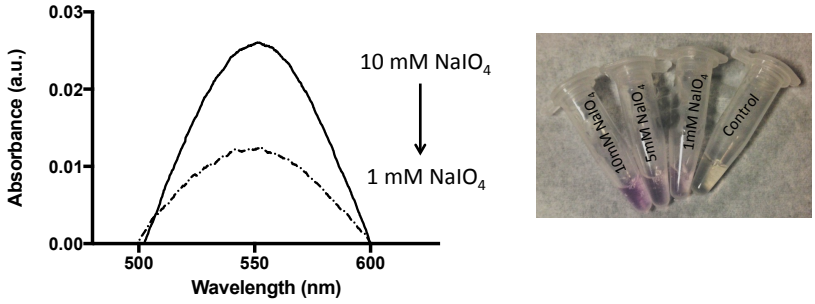

Figure 5.28: Purpald test on glycosylated anti-*E. coli* antibody treated with 10 mM and 1 mM $NaIO_4$. $NaIO_4$ oxidises the carbohydrates of the antibodies to aldehyde groups. The colour purple suggests the presence of aldehydes.

The p-NBA test (Fig. 5.27) confirmed that hydrazine groups have been introduced to the phage capsid. The p-NBA test can be used to determine the amount of hydrazine moieties incorporated on the SANH-modified phage, by estimating the concentration of hydrazines in the sample (Chapter 2, method 2.3.2). Phages modified with 10-fold SANH were estimated to have ~ 140 hydrazine groups on their surface. A word of caution though, it was noticed that calculating phage concentration based on its absorbance at 269 nm could be an inaccurate approach. SANH, which normally absorbs at 320 nm, has its NHS

(*N*-Hydroxysuccinimide) group hydrolysed when conjugated to the phage amines [45]. This produces an absorbance peak shift to 260 nm, closely overlapping with the wavelength used to calculate phage concentration (269 nm) (Fig. 5.29). Therefore, there is a contribution of SANH to the UV-Vis absorbance of the SANH-modified phage, which would lead to an incorrect estimation of the amount of hydrazine groups introduced to the phage surface. The p-NBA test provided only with an approximation of the substitution level of hydrazine groups into the phage, and could be calculated more accurately by mass spectrometry.

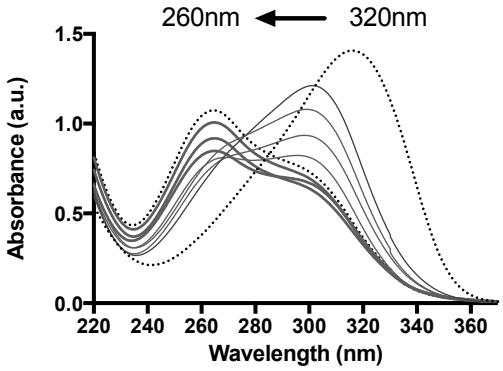

Figure 5.29: Monitoring of the absorbance peak shift of SANH. There is a peak shift, from 320 nm to 260 nm, over a period of 4 days, resultant from the hydrolyses of the NHS group in an aqueous buffer.

5.2.5.2.1 Phage-antibody conjugate as a LD scaffold

Before testing the phage-antibody conjugate on the biosensor assay, the samples were analysed on the LD. Surprisingly however, when comparing the LD spectrum of the SANH-modified phage (*i.e.* still not conjugated with the aldehyde-antibody) with the LD spectrum of the phage-antibody conjugate, a considerable drop in the overall LD phage signal was recorded (Fig. 5.30) (Chapter 2, method 2.8.2).

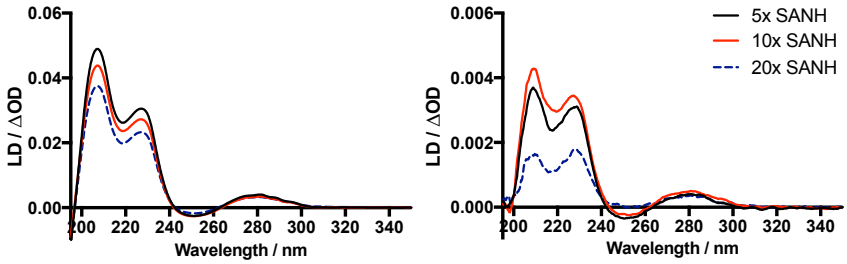

Figure 5.30: LD spectra of the (Left) SANH-modified phage, and of the (Right) phage-antibody conjugate. SANH-modified phage sample was diluted 10-fold prior to LD measurement; phage-antibody conjugate sample was measured without any dilution. 5×, 10× and 20× represent the SANH molar excess over p8 proteins of the phage.

The results in Fig. 5.30 suggest the phage lost its ability to properly align under flow, possibly indicating changes in its filamentous structure. Other experiments illustrated in this chapter demonstrated that changes to the phage high aspect ratio or to its surrounding environment were closely related to its LD signal (section 5.2.1; section 5.2.2). With that in mind, it was determined that the two more likely scenarios that could be linked to the decrease in phage alignment were either shredding of the phage into smaller, shorter particles, or aggregation between phages. Both these phenomena could be promoted by the bioconjugation protocol. Modifying the phage surface with SANH did not seem to negatively perturb its LD signal; however, it was possible the conjugation steps that followed were interfering with the phage structure. A pertinent observation was the formation of a gel-like structure while pelleting the phage-antibody conjugate. A gel precipitate, rather than a white pellet, suggested the hydrodynamic properties of the phage have changed possibly due to intra- and inter-phage associations.

Because of the possibly damaging effect of aniline on the phage structure (personal communication, Dr. Dylan Domaille), an experiment simulating the last step of the bioconjugation protocol (*i.e.* overnight treatment with aniline incubated at 35 °C while mixing at 650 rpm) was replicated and plotted in Fig.

5.31. As shown, neither the incubation conditions nor the use of aniline seemed to have perturbed its LD signal.

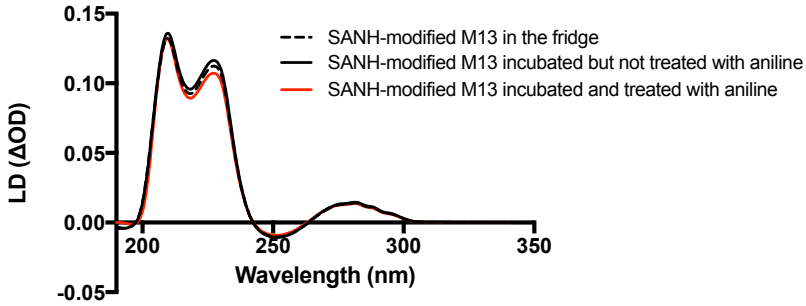

Figure 5.31: LD experiment to check whether aniline or the conditions used during this reaction (pH, temperature, speed of mixing) damaged the filamentous structure of the phage. (dashed black line) 0.5 mg/mL of SANH-modified phage in 0.1 M phosphate buffer pH 6 was left overnight at 4 °C. (solid black line) 0.5 mg/mL of SANH-modified phage in 0.1 M phosphate buffer pH 6 was incubated overnight at 35 °C, 650 rpm on a Thermomixer. (solid red line) 0.5 mg/mL of SANH-modified phage was treated with 10 µl of 1 M aniline stock, in 0.1 M phosphate buffer pH 6 and incubated overnight at 35 °C, 650 rpm on a Thermomixer. The reactions were then PEG/NaCl precipitated; the pellet was ressuspended in PBS buffer and measured on the LD.

It was concluded that the aniline treatment interfered with the phage LD signal. The remaining option was the conjugation between the SANH-modified phage and the $NaIO_4$ treated antibody. The phage-antibody conjugate was measured on the DLS (dynamic light scattering, Chapter 2, method 2.8.4) (Fig. 5.32) to get some insight on the size of the particles present on the samples. These results seemed to support the idea that the phage was aggregating, following conjugation with the treated antibody – there was an observable size shift from ~ 60 nm to ~ 1000 nm, indicating large particles were present on the phage-antibody conjugate sample. To confirm these findings, TEM images were also collected (Chapter 2, method 2.5.7). As shown in Fig. 5.33, it appeared the reaction between the SANH-modified phage and the $NaIO_4$-treated antibody resulted in bulky aggregated conjugates, forming unexpected structures. This

could explain the difference in the LD phage signal, since aggregated phage does not align as well as individual filamentous phage.

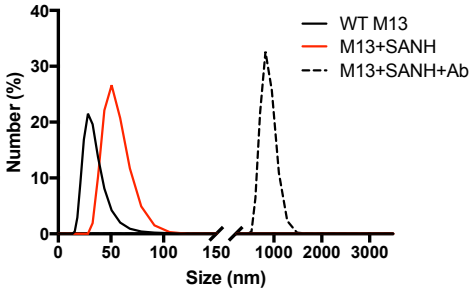

Figure 5.32: DLS spectra of phage samples. Wild-type phage (black), 10-fold molar excess SANH-modified phage (red), phage-antibody conjugate (black dashed).

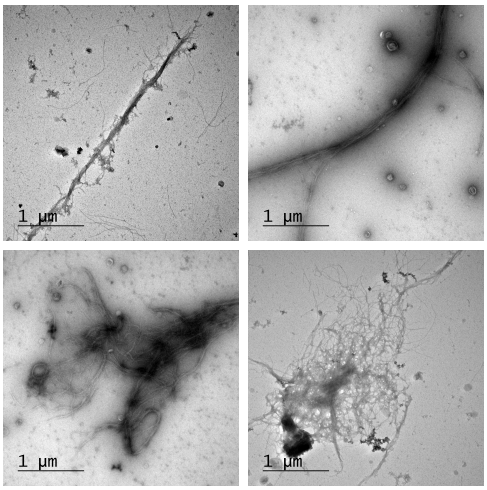

Figure 5.33: TEM images of the phage-antibody conjugate. Phages seemed to be aggregating and assembling along their long axis (forming rope-like structures), or in a disorganised fashion forming bulky aggregates.

The major factor contributing to aggregation and crosslinking between the phage-antibody conjugates was believed to be the conjugation step between the SANH-modified phage and the treated antibody. The conditions of the bioconjugation protocol were tuned – a range of concentrations of phage, antibody, SANH and sodium periodate were explored in independent assays. It was concluded, from LD data, that 1 mg of phage (modified with a ten-fold molar excess of SANH) conjugated to 250 µg of antibody (oxidised with 1 mM

$NaIO_4$) while catalysed with 10 mM aniline, seemly did not promote as much aggregation between phages. The phage pellet was the usual white rather than a gel, suggesting the phages are not significantly aggregating using these conditions. A LD-based immunoassay (Chapter 2, method 2.8.2.2), shown in Fig. 5.34, was set using the constructed phage-antibody conjugate.

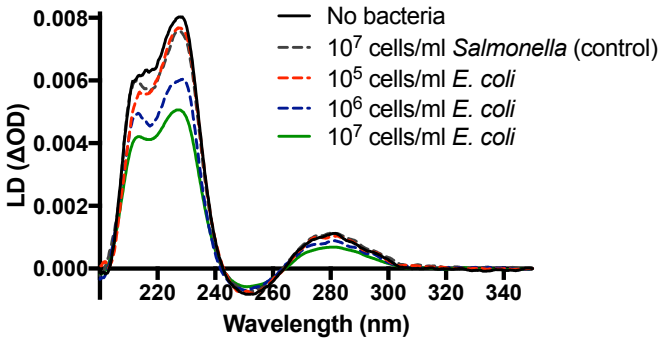

Figure 5.34: LD-based immunoassay using the phage-antibody conjugate sample (*i.e.* oxidised anti-*E. coli* antibody conjugated to SANH-modified phage). Each LD measurement was repeated once, showing a similar trend. The assay was sensitive up to 10^6 cells/mL.

Fig. 5.34 shows an LD-based immunoassay for *E. coli* bacteria. The phage-antibody conjugate (SANH-modified phage conjugated with $NaIO_4$ treated anti-*E. coli* antibody) was sensitive to *E. coli* bacteria, which was illustrated by the drop in the phage LD signal compared with the phage LD signal when no bacteria or *Salmonella* (as a control) is added. Nonetheless, the achieved sensitivity to bacteria was not lower than 10^6 cells/mL, which is not an improvement to Linear Diagnostics' current immunoassay (*i.e.* 10^5 cells/mL).

An interesting behaviour was noticed when adding ethanolamine (25 µL of a 1 M stock, pH 9.6) to the phage-antibody conjugate samples. Ethanolamine blocks unreacted aldehyde sites on the $NaIO_4$ treated antibody. After 3 days, it was observed that the LD signal of a phage-antibody conjugate sample decreased when no ethanolamine was added, perhaps due to continuing crosslinking interactions between the unreacted aldehydes on the antibodies to the phages. Adding ethanolamine seemed to partially prevent this from happening, as the

LD signal of the phage-antibody conjugate with ethanolamine was relatively constant, suggesting these samples were more stable over time. This experiment seems to support the hypothesis that the antibody conjugation to the phage is a critical step on this protocol, and that inter-phage assembly and aggregation are occurring. Interestingly, from the TEM images on Fig, 5.33, it seems the phages are not only cross-linking into disorganised bulk aggregates, but also assembling along their long axis, with several phages interacting side-by-side. Typically, a glycosylated antibody has two carbohydrate chains on its Fc region, one at each side. Perhaps, this side-by-side interaction between several phages could be explained by a cross-linking phenomena occurring between the unreacted aldehyde groups of an antibody (already conjugated to a phage) to a different phage. By blocking the unconjugated aldehyde groups with ethanolamine, the aggregation that happens over time would be avoided. Logically however, using ethanolamine after conjugating the SANH-modified phage to the $NaIO_4$ treated antibody, would only prevent aggregation that is occurring post-conjugation, and does not prevent aggregation that is already happening during the bioconjugation protocol. The above described reaction conditions, used for the immunoassay shown on Fig. 5.34, seemly did not promote aggregation between phages; however, it did not always result in homogeneous samples or successful immunoassays. Therefore, further optimisation of the bioconjugation protocol, more specifically titration of the optimal proportion phage/antibody, needs to be explored. To use the constructed phage-antibody conjugate on the LD-based immunoassay, aggregation (believed to be a consequence of the bioconjugation between the antibody and the phage) needs to be prevented – aggregated samples that are not homogeneous in solution have unknown and unpredictable rheological properties, which would naturally be reflected on their spectroscopic profile.

5.2.6 Magnetic beads purification method

5.2.6.1 Context

A more simplistic approach was to consider the immunoassay as it is (*i.e.* using the protocol described in Chapter 3), and reflect on reasons for the inability to make the immunoassay sensitive to a lower concentration of bacterial cells. Without modifying the chemical protocol established by Linear Diagnostics, one could consider the end product as it is: a chemically modified phage with antibodies conjugated to the p8 proteins.

We hypothesised if there were free antibodies (*i.e.* unconjugated to the phage) in the immunoassay samples that could be compromising the sensitivity of the biosensor. To purify chemically modified bacteriophage samples, PEG precipitation [47] and desalting columns are commonly employed. PEG/NaCl precipitation and PD-10 columns are straightforward methods to purify phage particles without the need for complicated and time consuming techniques, such as dialysis or chromatography. However, it is likely unconjugated antibodies could be co-precipitating/co-eluting with the phage. It was considered that unconjugated antibodies in the immunoassay sample could pose a problem because they would interact with the added bacterial cells, which could compromise the overall sensitivity of the biosensor. To test this idea, a method to further purify the immunoassay sample was considered.

5.2.6.2 Results and discussion

Protein A conjugated magnetic beads have affinity for the Fc region of antibodies, which is a convenient feature for several immunoprecipitation and protein pull-down assays. Protein A immobilised onto surfaces is the commonly used method for purifying monoclonal antibodies from cell culture supernatants [48]. These magnetic beads could be a simple and fast strategy to purify the immunoassay samples from unconjugated antibody. A detailed protocol on how this was done is given in Chapter 2 (method 2.10.2).

The immunoassay samples (*i.e.* p8 proteins of the phage functionalised with antibodies, anti-*Salmonella* or anti-*E. coli,* as illustrated in Chapter 3) were tested on the LD-based biosensor as usual. An aliquot of the magnetic beads was added to each of the immunoassay samples and left mixing on a rotor for about an hour. A magnet was used to precipitate the beads, and the supernatants (*i.e.* the purified immunoassay samples) were collected. Both the magnetic beads and the supernantants were analysed – the supernatants were tested on the LD-based biosensor and the beads were analysed on a silver stained SDS-PAGE.

The purified samples were tested on the LD-based biosensor. The LD results obtained from before and after purifying the immunoassay samples with the magnetic beads were then compared, as shown in Fig. 5.35.

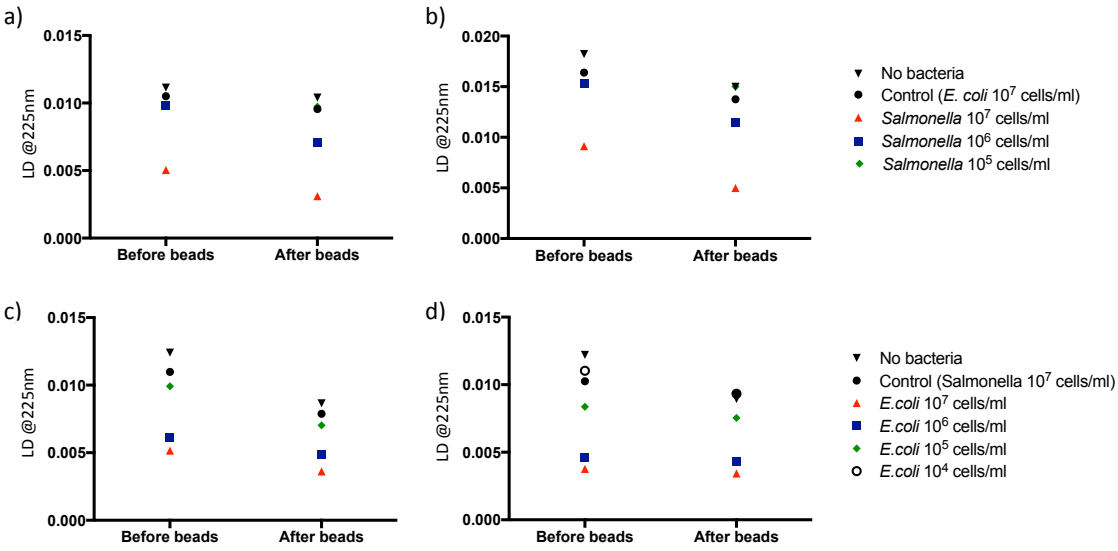

Figure 5.35: Phage-antibody conjugates before and after purification with magnetic beads. Four immunoassay samples (*i.e.* phage conjugated with antibodies along its p8 proteins) were tested on the LD-based biosensor, before and after purification with magnetic beads, at a range of bacterial concentration. a) and b) show the LD signal at 225 nm for two samples of anti-*Salmonella* phage. c) and d) show the LD signal at 225 nm for two samples of anti-*E. coli* phage.

Each data point on the plots of Fig. 5.35 represents the LD phage signal from the immunoassay samples at a range of bacterial concentrations (10^7–10^4

cells/mL). The immunoassay sample is considered to be sensitive to a certain bacterial concentration if the phage LD signal is lower than the phage LD signal when using the control bacteria. The most important observation from these data is that using the magnetic beads to purify the immunoassay samples did not seem to improve the sensitivity of the biosensor (*i.e.* lower concentrations of bacteria did not seem to have any effect on the phage overall alignment, not reducing its LD signal). The tested samples had a sensitivity of 10^5–10^6 cells/mL, which did not change by introducing the magnetic beads. It seemed the extra purification step was rather inconsequential to the performance of the immunoassay samples.

To get some further insight, the magnetic beads used to purify the immunoassay samples were analysed on a SDS–PAGE. For this, the magnetic beads were first exposed to an elution protocol, to release the material that got attached to the beads, following manufacturer's instructions. The magnetic beads were washed in PBS buffer, using a magnet to capture the beads between washes. This washing solution was kept, and analysed on the gel (lanes labelled as "SN sample"). The beads were then soaked in Laemmli buffer and incubated for 20 minutes at 70 °C. The beads were captured using the magnet, and the eluted material was collected. The eluted samples were loaded onto the SDS-PAGE, under denaturing and reducing conditions, and run as usual (Chapter 2, method 2.7.2). The SDS–PAGE was then silver stained (Chapter 2, method 2.7.2.1). Fig. 5.36 shows a picture of the result.

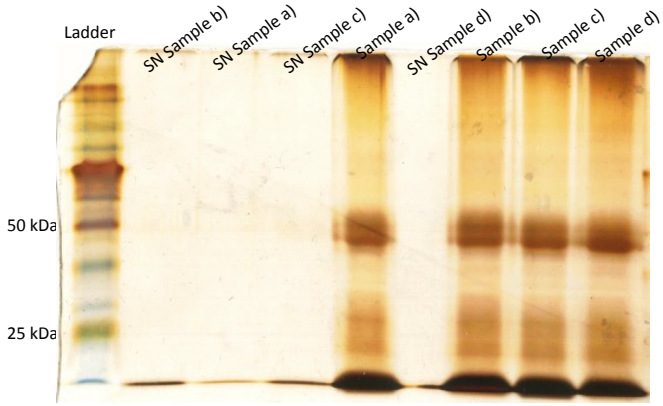

Figure 5.36: Silver stained SDS–PAGE of the eluted magnetic beads. Anti-*Salmonella* phage (sample a) and b); phage chemically conjugated with antibodies against *Salmonella*) and anti-*E. coli* phage (sample c) and d); phage chemically conjugated with antibodies against *E. coli*) were the four immunoassay samples tested on this experiment. The label "SN sample" represents the washing supernatant from the respective samples.

At first glace, looking at the gel in Fig. 5.36, it seemed plausible to assume that the magnetic beads captured unconjugated antibodies in the immunoassay samples. The eluted samples from the beads showed two bands on the gel, at 50 kDa and around 25 kDa, which we thought corresponded to the heavy and light chains of the antibodies, respectively. There was also a band at the bottom of the gel which initially was assigned to be aggregates of unconjugated AF647 dye in the immunoassay samples collected by the beads (which would be consistent with the observed fainter colour of the immunoassay samples after the purification protocol). However, there is the possibility that the bottom band is, in fact, derived from p8 proteins. The beads could have collected the modified phages in the samples, either non-specifically or by interacting with the antibodies conjugated to its surface. The 50 kDa and 25 kDa bands, which were initially assigned to be part of the antibodies, are also visible in gels from phage samples, so it is difficult to assign without a doubt that these bands derive from captured and reduced antibodies. A definite answer could be provided by excising, digesting and analysing the protein bands by mass spectrometry. A simpler option could be to test two control samples: one sample in which the magnetic beads are mixed with unmodified phages, and another sample in which the

magnetic beads are mixed with unconjugated antibody. The magnetic beads would then be handled as before, and the eluted samples would be analysed on a silver stained gel. This should help assign the bands, and clarify on their origin. Furthermore, it would give an indication to whether or not the phage is unspecifically binding to the beads or if this is caused by the antibodies conjugated to its surface. If the latter was observed, this would further confirm there are antibodies conjugated to the phage surface.

This particular magnetic beads purification assay did not provide with a conclusive answer to whether or not unconjugated antibody in the immunoassay samples significantly compromises the sensitivity of the biosensor. The LD-based immunoassay on the tested samples was not improved by adding magnetic beads to the samples, but we are unsure if that was derived from an ineffectively purification method. However, if we were to assume the magnetic beads did not capture antibodies from the immunoassay samples, it would be indicative that only a small amount of unconjugated antibody must be present in the immunoassay samples, suggesting this must not be a factor limiting the sensitivity of the LD-based biosensor. If unconjugated antibodies were proven to be present on the immunoassay samples, there is a strong argument for comprehensive purification methods, which might include size exclusion chromatography. The His-tagged phage (Chapter 3) could be an alternative to circumvent this issue and avoid the need for further purification steps, as it would enable capturing and elution of mostly the His-tagged chemically modified phage particles.

5.3 Conclusion

The startup company Linear Diagnostics Ltd. built a diagnostic platform by incorporating LD spectroscopy with an immunoassay design, using filamentous phage particles as scaffolds. This pathogen detection biosensor explores differences in spectroscopic signal, elucidating on the presence of a given target of interest. One major drawback of the current biosensor is its sensitivity, with

the limit of detection being of the order of the 10^5 bacterial cells per milliliter of sample, making it incompatible for most clinical applications. The development of new methods to modify the phage surface was aimed at cutting on costs and time, and on increasing the sensitivity, simplicity and versatility of Linear Diagnostics' platform.

In this chapter, several examples of genetic and chemical engineering to the phage surface were illustrated, directed at improving an LD-based biosensor. Longer phage particles can be grown by inserting DNA fragments into the viral genome; nonetheless, it seems none of the existing phage-based biomaterials explore this feature. In here, we designed and successfully integrated longer mutant phages with a biosensing platform. However, it was noticed that these particular genetic constructs were unstable and unpredictable. An alternative method that does not require inserting large fragments of DNA could be explored; for example, removing the positively-charged lysines on the phage coat has been shown to result in a less tightly packed viral genome, which in turn originates phages with longer capsids [49]. To enhance the natural intrinsic fluorescence of the filamentous phages and explore it in a biosensor platform set-up, an extra tryptophan was mutated onto the phage surface. This is another example of a rationally designed biological system that shows the genetic engineering of the phage may not be straightforwardly integrated with spectroscopy-based techniques. To simplify the method to label the phage surface with molecular recognition elements (*i.e.* antibodies), a mutant phage with a cysteine on its p8 proteins (V31C phage) and a phage expressing a bacteria-binding peptide (MSal17 phage) were designed. The V31C phage did not seem to respond to bacteria on the LD-based immunoassay, which led us to hypothesise the conjugation of antibodies to the surface of the phage was not efficient and might be compromised due to a steric hindrance effect. Modifications to a more exposed region of the p8 protein (*i.e.* lysine 8) seem to label more efficiently. With that in mind, a different design to include cysteines on the phage surface was envisioned. Although not described in this thesis, we successfully engineered a mutant phage with a cyclic-cysteine on the N-terminal

of its p8 proteins. To avoid excessive reactivity and cross-linking between phages, these cysteines were designed to be "locked" in disulfide bridges until a reducing agent is added. If steric hindrance was in fact the cause for unsuccessful conjugation of antibodies to the V31C phage, we imagined the cyclic-cysteine phage construct could be explored as an alternative. Replacing antibodies with bacteria-binding peptides would primarily decrease the costs of the immunoassay and completely eliminate the need for any bioconjugation protocol to modify the phage surface. Although the chosen *Salmonella*-binding peptide phage construct did not appear to work for our specifications, there are a vast number of other peptide ligand options that could be explored. We also trialled a hydrazine-aldehyde bioconjugation protocol for the oriented immobilisation of antibodies onto the phage surface. Although we showed we could integrate this method with the LD-based immunoassay, we did not observe an improvement to the current sensitivity of the biosensor. Moreover, it was noticed that these phages had the tendency to self-assemble into bulk structures, creating intriguing gel-like materials, which ultimately meant we were dealing with an unpredictable and non-homogeneous system. Other chemical functionalities could be explored by click chemistry [50] (*e.g.* azide-alkyne click chemistry). This approach could facilitate higher yields of conjugation of biomolecules to the phage, possibility positively affecting the sensitivity of the LD-based immunoassay. Another tactic to control the orientation of the antibodies within the phage surface could be to genetically introduce a Z-domain onto the p8 proteins [51-54]. The Z-domain is an immunoglobulin-binding protein that specifically binds to the Fc region of antibodies, facilitating conjugated antibodies with unrestricted antigen-binding regions. Cloning a Z-domain into the p8 protein would create a simple attachment point to antibodies, without the need for bioconjugation protocols. It was also considered that unconjugated antibody present in the immunoassay samples could be compromising the sensitivity of the biosensor. A purification method using magnetic beads was attempted, possibility suggesting free antibodies are not the limiting factor of the immunoassay.

These experiments highlight the importance of carefully choosing how to engineer the filamentous phage, as the modifications may not be practical for the intended application and efficiently integrated with the planned analytical method. Genetic modifications to the phage proteins could replace the need for costly and lengthy chemical protocols; however, care must be taken to ensure the engineered mutations do not interfere with phage stability. Chemoselective approaches are normally simpler to design; on the other hand, batch-to-batch variability between different phage preparations makes it challenging to guarantee and control chemical modifications to the phage capsid. An integration of both systems would be ideal, enabling a plug-and-play phage-based platform, which could be designed for applications on the biosensors field.

5.4 References

1. Pacheco-Gomez, R. *et al.* Detection of pathogenic bacteria using a homogenous immunoassay based on shear alignment of virus particles and linear dichroism. *Anal. Chem.* **84,** 91–97 (2012).
2. Hage, D. Immunoassays. *Anal. Chem.* **71,** 294-304 (1999).
3. Specthrie, L., Bullitt E., Horiuchi, K., Model, P., Russel, M., Makowski, L. Construction of a microphage variant of filamentous bacteriophage. *J Mol Biol* **228**, 720–724 (1992).
4. Malmanche, H. Construction and characterisation of a set of M13 filamentous phages of increasing lengths for applications in linear dichroism-based diagnostic assays. MRes dissertation, University College London (2015).
5. Ikehara, K. *et al.* Studies on the structure of filamentous bacteriophage fd. Physicochemical properties of phage fd and its components. *Bull. Inst. Chem. Res.* **51**, 140-152 (1973).
6. Kropinski, A. *et al.* Enumeration of bacteriophage by double agar overlay plaque assay. *Bacteriophages* in *Method in Molecular Biology* book series (Springer, 2009) ISBN: 9781588296825
7. Carr-Smith, J. *et al.* Polymerase chain reaction on a viral nanoparticle. *ACS Synthetic Biology* **4**, 1316-1325 (2015).
8. Rittman, M., *et al.* Is DNA a worm-like chain in Couette flow? In search of persistence length, a critical review. *Science Progress* **92**, 163-204 (2009).
9. Mclachlan, J. *et al.* Calculations of flow-induced orientation distributions for analysis of linear dichroism spectroscopy. *Soft Matter* **9,** 4977–4984 (2013).
10. Rodger, A., Nordén, B., Dafforn, T. Linear Dichroism and Circular Dichroism (Royal Society of Chemistry, 2010). ISBN: 9781847559029

11. Nam, K., Reelle, B., Lee, S., Belcher, A. Genetically driven assembly of nanorings based on the M13 virus. *Nano Lett.* **4,** 23–27 (2004).
12. Dogic, Z., Fraden, S. Smectic phase in a colloidal suspension of semiflexible virus particles. *Phys Rev Lett* **78**, 2417–2420 (1997).
13. Lakowicz, J. *Principles of fluorescence spectroscopy*. (Springer US, 2006). ISBN: 9780387312781
14. Rittman, M. *et al.* Probing the structure of long DNA molecules in solution using synchrotron radiation linear dichroism. *Phys. Chem. Chem. Phys*. **14**, 353–366 (2012).
15. Enshell-seijffers, D., *et al.* The rational design of a 'type 88' genetically stable peptide display vector in the filamentous bacteriophage fd. Nucleic Acid Research **29**, 1-13 (2001).
16. Sambrook, J., Russel D. *Molecular cloning: A laboratory manual* (CSHL Press, 2001) ISBN: 0879695773
17. Sidhu, S. Engineering M13 for phage display. *Biomolecular Engineering* **18,** 57–63 (2001).
18. Gonnelli, M., Strambini, G. Intramolecular quenching of tryptophan phosphorescence in short peptides and proteins. *Photochem. Photobiol.* **81,** 614–622 (2005).
19. Chen, Y., Barkley, M. Toward understanding tryptophan fluorescence in proteins. *Biochemistry* **2960,** 9976–9982 (1998).
20. Spruijt, R. *et al.* Accessibility and environment probing using cysteineresidues introduced along the putative transmembrane domain ofthe major coat protein of bacteriophage M13. *Biochemistry* **35**, 10383-10391 (1996).
21. Koehorst, R. *et al.* Site-directed fluorescence labeling of a membrane protein with BADAN probing protein topology and local environment. *Biophys* **94**, 3945–3955 (2008).
22. Koehorst R., *et al.* Lipid bilayer topology of the transmembrane alpha-helix of M13 major coat protein and bilayer polarity profile by site-directed fluorescence spectroscopy. *Biophys* **87**, 1445–1455 (2004).
23. Spruijt R., Wolfs C., Hemminga M. Membrane assembly of M13 major coat protein: evidence for structural adaptation in the hinge region and a tilted transmembrane domain. *Biochemistry* **43**, 13972–13980 (2004).
24. Hales, J. Implementing the synthetic biology design cycle to fabricate laser dyes. PhD thesis, University College London (2014).
25. Morag, O., Sgourakis, N., Baker, D., Goldbourt, A. The NMR–Rosetta capsid model of M13 bacteriophage reveals a quadrupled hydrophobic packing epitope. *Proc. Natl. Acad. Sci.* **112,** 971–976 (2015).
26. Zhang, Z., Zhu, W., Kodadek, T. Selection and application of peptide-binding peptides. *Nature Biotechnology* **18**, 71–74 (2000).
27. Huang, J. *et al.* Development of anti-infectives using phage display: biological agents against bacteria, viruses, and parasites. *Antimicrob Agents Chemother*. **9**, 4569-4582 (2012).
28. Rebollo, I. *et al.* Identification of target-binding peptide motifs by high-throughput sequencing of phage-selected peptides. *Nucleic Acids Research* **42,** (2014).

29. Morton, J. *et al.* Production and evaluation of the utility of novel phage display-derived peptide ligands to Salmonella spp. for magnetic separation. *J. Applied Microbiol.* **115**, 271–281 (2013).
30. Wang, J. *et. al.* Rapid detection of pathogenic bacteria and screening of phage-derived peptides using microcantilevers. *Anal. Chem.* **86**, 1671–1678 (2014).
31. Karoonuthaisiri, N. *et al.* Development of a M13 bacteriophage-based SPR detection using Salmonella as a case study. *Sensors Actuators B **190**, 214–220 (2014).*
32. Greenwood, J., Hunter, G., Perham, R. Multiple display of foreign peptides on a filamentous bacteriophage. *J. Mol. Biol.* **220**, 821–827 (1991).
33. Iannolo, G. *et al.* Modifying filamentous phage capsid: limits in the size of the major capsid protein. *J. Mol. Biol.* **248**, 835–844 (1995).
34. Felici, F. *et al.* Selection of antibody ligands from a large library of oligonucleotides expressed on a multivalent exposition vector. *J. Mol. Biol.* **222**, 301–310 (1991).
35. Willis, A., Perham, R., Wraith D. Immunological properties of foreign peptides in multiple display on a filamentous bacteriophage. *Gene* **128**, 78–83 (1993).
36. Smith, G. Surface display and peptide libraries. *Gene* **128**, 1–2 (1993).
37. Nanduri, V., *et al.* SPR biosensor for the detection of L. monocytogenes using phage-displayed antibody. *Biosens. Bioelectron.* **23**, 248 –252 (2007).
38. Carnazza, S., *et al.* Recombinant phage probes for Listeria monocytogenes. *J. Phys. Condens. Matter* **19** (2007).
39. Carnazza S., *et al.* Specific and selective probes for Pseudomonas aeruginosa from phage-displayed random peptide libraries. *Biosens. Bioelectron.* **23**, 1137–1144 (2008).
40. Sorokulova, I., *et al.* Landscape phage probes for Salmonella typhimurium. *J. Microbiol. Methods* **63**, 55–72 (2005).
41. Sabarth, N., *et al.* Identification of Helicobacter pylori surface proteins by selective proteinase K digestion and antibody phage display. *J. Microbiol. Methods* **62**, 345–349 (2005).
42. Zhou, B., Wirsching, P., Janda K. Human antibodies against spores of the genus Bacillus: a model study for detection of and protection against anthrax and the bioterrorist threat. *Proc. Natl. Acad. Sci.* **99**, 5241–5246 (2002).
43. Williams, D., Benedek, O., Turnbough, C. Species-specific peptide ligands for the detection of Bacillus anthracis spores. *Appl. Environ. Microbiol.* **69**, 6288 – 6293 (2003).
44. Turnbough C. Discovery of phage display peptide ligands for species-specific detection of Bacillus spores. *J. Microbiol. Methods* **53**, 263–271 (2003).
45. Hermanson, G. *Bioconjugation techniques* (Academic Press, 2013) ISBN: 9780123822390
46. Grotzky, A., *et al.* Preparation of catalytically active covalent polylysine-enzyme conjugates via UV-Vis quantifiable bis-aryl hydrazone bond formation. Biomacromolecules **11,** 134–144 (2011).

47. Branston, S. *et al.* Precipitation of filamentous bacteriophages for their selective recovery in primary purification. *American Inst. Chem. Engineers* **28,** 129–136 (2011).
48. Shukla, A. *et al.* Downstream processing of monoclonal antibodies – application of platform approaches. *Journal Chromatography* **848,** 28–39 (2007).
49. Greenwood, J., Hunter, G., Perham, R. Regulation of filamentous bacteriophage length by modification of electrostatic interactions between coat protein and DNA. *J Mol Biol* **217,** 223-7 (1991).
50. Hein, C., Liu, X., Wang, D. Click chemistry, a powerful tool for pharmaceutical sciences. *Pharmaceutical Research* **25,** 2216–2230 (2008).
51. Starovasnik, M., Brasited, A., Wells, J. Structural mimicry of a native protein by a minimized. *Proc. Natl. Acad. Sci.* **94,** 10080–10085 (1997).
52. Brasino, M., Cha, J. Real-time femtomolar detection of cancer biomarkers from photoconjugated antibody–phage constructs. *Analyst* **142,** 91–97 (2017).
53. Yu, F., Ja, P. Tailor-making a protein A-derived domain for efficient site-specific photocoupling to Fc of mouse IgG. *PLoS One* **8,** e56597. (2013).
54. Perols, A., Karlström, A. site-specific photoconjugation of antibodies using chemically synthesized IgG-binding domains. *Bioconjug. Chem.* **25,** 481–488 (2014).

CHAPTER 6 – General conclusion

Since it was first discovered, 102 years ago, bacteriophage has been of great interest to the scientific community, due to their remarkable simplicity in an otherwise complex biological environment. Particularly, phages were the seed to understanding key biological phenomena, laying the foundations for pioneering work in molecular biology. The filamentous bacteriophage, named this way because of its ~ 900 nm fibre morphology, became preeminent as a programmable biological entity, creating the possibility for building unique biomaterials with multiple nanotechnology applications. An example is the use of filamentous phages as biorecognition elements and scaffolding templates, in biosensor platforms.

The focus of this work was on exploring phage surface modifications that could be integrated with biosensing platforms. Filamentous phages are a robust and versatile nanomaterial, tolerating both chemical and biological modifications. We made use of these features to tune the phage surface to our purposes, by either chemically and genetically modifying its proteins in a site-specific fashion, without disrupting their functionality. Filamentous phages, such as the M13 and the fd phage, have five structural proteins, but in this thesis only two of these were manipulated – the p8 protein, the major coat protein that covers the length of the phage, and the p3 protein, a minor coat protein at one end of the phage. We explored modifying these proteins in several different ways, as presented in Chapter 3. In this work, the p8 proteins of the phage were labelled with dyes, which is an important step for microscopy and spectroscopy-based techniques. The amine groups of the p8 protein were also modified to conjugate antibodies and to incorporate DNA molecules, which can be integrated into biosensing platforms. The p3 protein was modified to attach phages to surfaces by one-end only. In here, we attempted three methods to anchor phage particles to a surface, which enabled the design of a novel imaging platform, as described in Chapter 4.

The glycocalyx and wall shear stress (WSS) are known to be involved in cardiovascular dynamics, and therefore a better understanding of their physiological role could provide key information on vascular diseases. Chapter 4 proposes a novel method to study the glycocalyx and WSS using a simple microfluidics design. For this, phage particles were fluorescently labelled, anchored to a surface and tracked under a microscope. The modified phage was first observed on a flat collagen-coated surface, and then tested on the surface of an endothelial cell (*i.e.* the cells that line the blood vessels). The data collected using our phage construct allowed us to estimate the local WSS at a non-uniform surface, which is related to cells' topography. To expand on this work, the developed fluorescent phage construct will be anchored to the wall of a blood vessel during *in vivo* experiments.

We have also collaborated with the startup company Linear Diagnostics Ltd., which built a LD-based biosensor for the detection of pathogenic bacteria. This biosensing platform, which was designed as a portable device, is based on the phenomenon of linear dichroism and exploits the filamentous structure of the phage. In Chapter 5 we explored ways to improve and enhance the application of the filamentous phage as a recognition element in a spectroscopy assay. For this, we developed alternative methods to tune the phage surface either by genetic engineering or chemical modifications, envisioning increasing the sensitivity and simplicity of the current biosensing platform. Longer phage mutants were successfully grown and for the first time integrated with fluorescence and absorbance spectroscopic techniques. A phage containing an extra tryptophan was also designed, however we show that the fluorescence of this mutant was not as we expected, probably as a result of contact quenching between neighbouring tryptophan residues. A *Salmonella*-binding peptide was cloned to the surface of the phage as a possible replacement to the use of antibodies and, however we report this phage construct did not seem to be specific to the intended pathogenic bacteria, it illustrates the simplicity of phage cloning. Another example of this was the use of the V31C phage, containing a mutated version of

the p8 protein that includes a cysteine residue, as an alternative to bioconjugation modifications to the phage surface. An aldehyde-hydrazine bioconjugation protocol, for the directional conjugation of antibodies to the phage, was integrated with the LD-based immunoassay. Interestingly, we unintendedly made a gel-like phage material, which we believed was triggered by phage aggregation. We also attempted a purification method, using magnetic beads, which led us to the conclusion that is unlikely for unconjugated antibodies to be the cause for limited sensitivity of the LD-based immunoassay.

Evaluated as a multi-million pound market, biosensors have a range of applications in medicine, pharma, defense and security, food safety, and environmental monitoring. The increased demand for portable and simple point-of-care platforms makes it of paramount importance to explore biological elements that are inexpensive and easy to produce in mass, and that can be integrated with microfluidic devices. As demonstrated in this thesis, filamentous phages are an attractive scaffold for biosensors. By building a toolkit of engineered phages, we hope we will be able to further target this market and contribute for its expansion.

Appendix

Publication: "Direct detection and measurement of wall shear stress using a filamentous bionanoparticle"